STUDIES ON SOME NEW METAL–HYDRAZONE COMPLEXES AND THEIR ZEOLITE ENCAPSULATED ANALOGUES

Thesis submitted to the
Cochin University of Science and Technology
in partial fulfilment of the requirements
for the Degree of

Doctor of Philosophy

in

Chemistry

Under the faculty of science

by

VINEETHA C. P.

DEPARTMENT OF APPLIED CHEMISTRY
COCHIN UNIVERSITY OF SCIENCE AND TECHNOLOGY
KOCHI-682022, KERALA, INDIA

December 2002

30th December 2002

CERTIFICATE

This is to certify that the thesis entitled "***Studies on some new Metal-Hydrazone complexes and their zeolite encapsulated analogues***" submitted for the award of the Degree of Philosophy of Cochin University of Science and Technology, is a record of bonafide research work carried out by Ms. Vineetha C. P., under my supervision in the Department of Applied Chemistry.

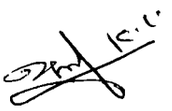

Prof. K. K. Mohammed Yusuff

PREFACE

Transition metal complexes encapsulated in zeolite cavities have been used as heterogeneous catalysts in a variety of reactions. To prepare some new and interesting encapsulated metal complexes, some hydrazone type of ligands were synthesised and complexed with metal ions like Fe(III), Co(II), Ni(II) and Cu(II). Hydrazones are important ligands having triatomic linkage C=N-N- and have been used as ligands in view of their diverse applications in biological, biochemical and non-biological front. However the use of complexes of hydrazones for encapsulation in zeolite cavities has not been attempted much. During the present study three hydrazone type of ligands namely, acetylacetone- 2-hydroxyphenylhydrazone (APAcAc), acetoacetanilide- 2-hydroxyphenylhydrazone (APAcAcA) and acetoacetanilide-3,5-dihydro-2,4-dione pyrimidylhydrazone (AUAcAcA) were synthesized by diazotization of a primary amine and coupling with compounds containing active methylene group. Since the metal complexes of these ligands were hitherto unknown the Fe(III), Co(II), Ni(II) and Cu(II) complexes isolated presently were subjected to detailed molecular structure determination using spectral, magnetic, conductance and TG measurements. These complexes were encapsulated in the cavities of zeolite Y and were characterized. The oxidation of cyclohexanol using *tert*-butyl hydrogen peroxide as oxidant was studied in presence of the pure metal complexes and their encapsulated analogues as catalysts. Parameters like solvent, temperature, oxidant/ substrate ratio were standardized for this reaction catalysed by zeolite encapsulated complexes of these hydrazone type of ligands. Details of these studies are presented in this thesis.

CONTENTS

PART I

Part B

NEW COMPLEXES OF Fe(III), Co(II), Ni(II) AND Cu(II) WITH ACETOACETANILIDE-2-HYDROXYPHENYLHYDRAZONE

Part C

Fe(III), Co(II), Ni(II) AND Cu(II) COMPLEXES OF ACETOACETANILIDE-3,5-DIHYDRO-2,4-DIONEPYRIMIDYL-HYDRAZONE(AUACACA)

PART II

Chapter I

GENERAL INTRODUCTION

Coordination chemistry is undoubtedly the most active research area in inorganic chemistry. Several thousands of coordination complexes have been synthesized and investigated during the past few decades. Ever since the importance of coordination phenomenon in biological processes was realized, lot of metal containing macromolecules have been synthesized and studied to understand the mechanism of complex biological reactions. This has resulted in the emergence of an important branch of inorganic chemistry viz. bioinorganic chemistry. Similarly the importance of coordination of substrate molecules on metal ions in catalysis was understood and a lot of research work is being carried out on this aspect. Since structure and reactivity are interdependent, studies on molecular structure of transition metal complexes are of paramount importance. Excellent modern theories on metal ligand bonding are available. These theories aid in interpreting the experimental data obtained using sophisticated instrumental techniques available to the research workers.

I.1.2 Hydrazones

Hydrazones are characterized by the presence of the triatomic grouping C=N-N-. They can be considered as Schiff bases derived from acid hydrazides. The most

important property of hydrazones is their high physiological activity [1-6]. Extensive studies have revealed that the lone pair on trigonally hybridized nitrogen atom of the azomethine group is responsible [7-11] for the chemical and biological activity. It has been reported that metal complexes of hydrazones have diverse applications. They find use as plasticizers, polymerization inhibitors and antioxidants. They are used as fungicides and pesticides in biological and biochemical context. The hydrazones and their complexes described in the present thesis are obtained by the coupling reaction of a diazonium salt with the reactive methylene group. Therefore a brief description of a few similar coupling reactions, the structures of the products obtained and the possible donor modes of such compounds are presented in this chapter.

A lot of complexes derived from hydrazones such as thiosemicarbazones have been reported [12-15]; compounds of this type have a great biological activity as antitumoral and antiviral agents.

Aromatic diazo compound was discovered as early as 1858 [16]. Kekule and Hidegh discovered the coupling reaction of diazonium salts [17]. Diazonium ion attacks the atom of the coupling molecule which has the greatest electron density. Therefore diazonium salts couple readily with aromatic hydroxyl compounds, aromatic amines, phenols, naphthol ethers etc. yielding highly coloured azo compounds known as dyes[18,19]. Even though coupling usually takes place with aromatic compounds, there are several aliphatic compounds capable of coupling with aryl diazonium ion. These aliphatic compounds are methane carrying or have more

ionisable or resonating substituents bestowing on the carbon atom an electron density enough for substitution by aryl diazonium ion.

The first report of the coupling of a diazonium salt with an activated aliphatic carbon atom was by Victor Meyer [20]. Benzene diazonium sulphate was found to react with the sodium salt of nitroethane to give a coloured product. The product was assigned an azo structure (I).

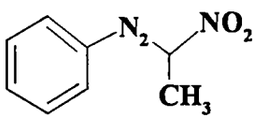

(I)

The product of such coupling reactions are capable of existing in azo or hydrazone forms. Therefore most of the early work on this topic was to determine whether the products were of azo or hydrazone structure. Even though it was difficult to establish the structure with certainty it was assumed that the hydrazone form is the stable form when coupling occurs at a methyl or methylene carbon. UV and IR absorption spectral data have been reported to support this assumption [21]. In a few compounds where the coupling occurs in a methyl carbon without the elimination of a group, the only possible structure is the azo structure.

Various research groups have worked to establish the mechanism of these coupling reactions [22-25]. The methylene group in β-diketones reacts readily with diazonium salts. The product has been formulated as the mono hydrazone (II) of a triketone. The coupling of diazonium salts with β-ketoanilides give dyes with different shades depending upon the nature of the anilides and the diazonium salts.

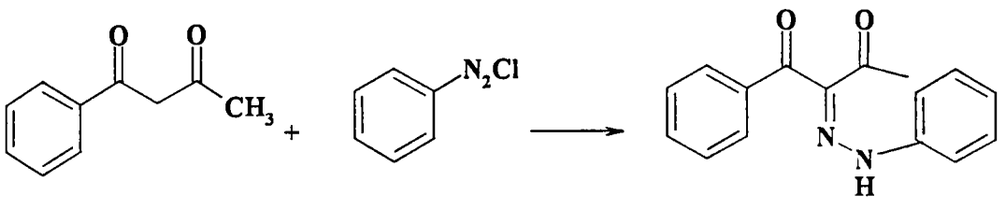

(II)

Benzoyl acetone has been converted into the monophenylhydrazone in 90% yield[26]. A variety of β-diketones has been employed in the same general reactions. Cyclic β-diketones such as cyclohexane-1,3-dione[27], methone[28-30] and indan-1,3-dione[31,32] react as readily as the acyclic analogues.

It has been reported that 2-arylhydrazones of 1,2,3-tricarbonyl compounds prepared by coupling diazonium salts with β-diketones or β-diketoesters[33] exist exclusively in an intramolecularly hydrogen bonded tautomeric forms (III) or (IV) rather than in any of the other tautomeric forms. The NMR spectra of these compounds are characterized by a very low field signal diagnostic of an intramolecularly hydrogen bonded proton [34-38].

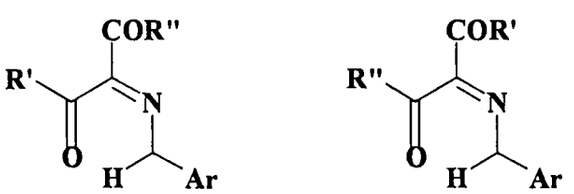

(III) (IV)

The IR studies also support the hydrogen bonded forms. The spectrum shows the presence of free C=O as well as hydrogen bonded C=O [34-36, 39]. In the case of the

coupling products from unsymmetrical β-diketone such as benzoylacetone, two tautomeric forms (V) and (VI) are possible.

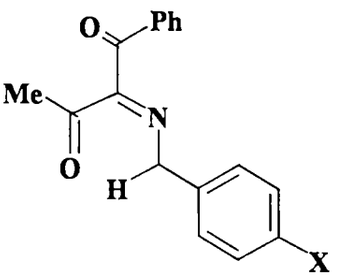

(V)

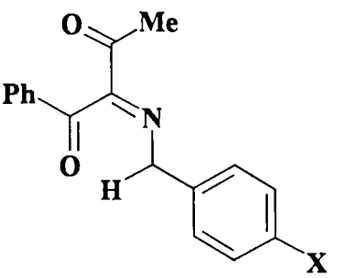

(VI)

Structure (V) is the preferred one. Electron releasing substituents in the acyl group of the aryl hydrazone residue increase the proportion of (V). Electron releasing power in the aryl hydrazone residue increases the deshielding of hydrazone proton resulting in a more unsymmetrical hydrogen bonded structure [40]. On the other hand increasing the electron withdrawing nature of the alkyl group attached to C=O involved in H-bonding would make the oxygen of the adjacent C=O groups less electron rich which will result in a weaker H bond. NMR data have been in support of this [40,41].

Mass spectra have been of help in distinguishing the azo and hydrazone forms of organic compounds. The azo and hydrazone forms contain the chain C-N-N-C-. However the mode of fragmentation in mass spectra has been found to depend on the nature of bonds between the atoms [42]. It has been reported that the cleavage in the azo tautomer occurs on both sides of –N=N- moiety, while in the case of hydrazone form the bond breaks at -N-N= [43-45]. Therefore the mass spectra of the azo tautomer is characterized by the presence of $P-N_2$ (P- Parent) peak due to the elimination of

N_2 along with parent ion and the hydrazone tautomer shows the presence of a peak due to PNH^+ ion. The azo-hydrazo tautomerism of three industrially important dyes 1-phenylazo-4-naphthol, 1-phenylazo-2-naphthol and 2-phenylazo-1-naphthol have been investigated earlier by using quantum mechanical methods [46].

I.1.2 Metal complexes of azodyes and hydrazones

The dyeing process involve coordination phenomenon with metal ions [47-59]. On changing the metal ions the colour changes and this clearly shows the formation of coordination compounds during dyeing processes [47-50, 54].

Copper complexes of 2-hydroxy-5methylazobenzene, *o*-hydroxyazobenzene, 2-hydroxy 5,5^1-dimethylazobenzene, benzeneazo-β-naphthol and ***m***-tolylazo-β-naphthol have been analyzed and it was found that these dyes satisfy the coordination number of copper [60]. Copper complexes of *o*-dihydroxyazo and azomethine dyes have also been prepared [61]. Report on the complexes of Cr, Fe, Ni and Zn complexes of mono and di *o*-substituted dyes is available [62]. Cu(II) and Ni(II) complexes of 1-phenyl 2,3-dimethyl 4(2-hydroxynaphthylazo) 5-pyrazolone have been synthesized and their magnetic and thermal behaviour studied [63]. Ni(II) complexes of resorcinolazoantipyrine have been prepared and characterized [64]. In all these azo dye complexes only one of the nitrogens of the azo group is involved in coordination.

The products obtained by coupling diazonium salts with active methylene group are versatile polydentate ligands. Early studies on the donor behaviour of this type of ligands were with Cu(II). The ligand 3,3^1-(4,4^1-biphenylenebisazo), bis-2,4-pentanedione and 3-(phenylazo)-2,4-pentanedione form chelates with Cu(II).

Studies have shown that the former ligand exists mainly in azo form while the latter in an equilibrium mixture of azo and hydrazone forms in solution. Interestingly, these ligands retain their azo form in Cu(II) chelates [65]. On the other hand 3-(phenylazo)-1-phenyl-1,3-butanedione and 2-(phenylazo)-1,3-diphenyl-1,2-propanedione were assigned a hydrazone structure(VII) on the basis of their spectral behaviour.

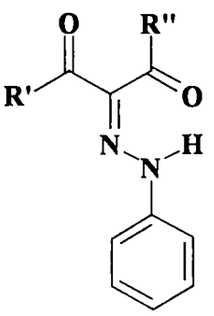

(VII)

These ligands retain their hydrazone form in their chelates with Cu(II), Ni(II) and Pd(II) as shown in VIII [66].

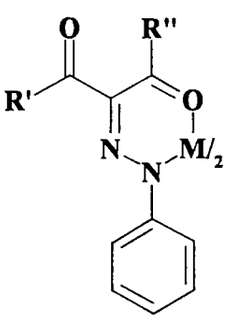

VIII

Complexes of divalent transition metal ions and tetravalent lanthanide ions with carboxyphenylhydrazone-β-diketone or β-ketoester as ligands have been investigated[67,68]. β-Diketone complexes are extensively studied. Similarly hydrazone complexes of metals are also well known. Ligands having combinations of these two chelating functions are interesting. Considerable work has been done for developing such polydentate macrocyclic hydrazone ligands and their complexes [69]. A few such ligands were prepared by coupling the diazonium salt of 2-aminoacetophenone with pentane-2,4-dione,1-phenyl-1,3-propanedione, 1,1,1-trifluoropentane-2,4-dione and dimedone. Bis[pentane-2,4-dionebenzoyl-hydrozonato(2-)] vanadium(IV) and bis[4-phenylbutane-2,4-dione benzoyl-hydrozonato(2-)] vanadium(IV) have been prepared and their EPR spectra recorded. The trigonal prismatic complexes have axial symmetry as evidenced by EPR [70]. Polydentate macrocyclic hydrazone chelates have been prepared by reacting arene diazonium and tetrazonium ions with 1,3-diketones and metal 1,3-diketonates [69]. In the complexes, the ligand exists in the intramolecularly hydrogen bonded dihydrazone state. Formylferrocene-5-phenyloxazole-2-carbonylhydrazone complexes of bivalent transition metal ions have been reported [70]. Hassanali has reported the complexes of isatin isonicotinylhydrazone with several transition metal ions [71]. Metal 1,3-diketonates readily undergo electrophilic substitutions. 2,4-Pentanedionates of metals Al(III), Cu(II), Cr(III) and Pd(II) undergo substitution by phenyldiazonium ions [69]. Cu(II) chelates exists in the hydrazone form (IX) while in Cr(III), Pd(II) complexes, ligand exists in the azo form (X).

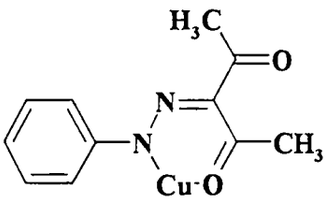

(IX)

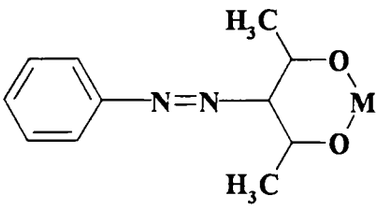

(X)

Metal complexes of 1,2-dihydro-1-phenyl-2,3-dimethyl-4-(2',4'-pentanedione-3'-hydrazono)pyrazol-5-one have been prepared and investigated in detail. The ligand is reported to exist in the hydrazone form in all the complexes [72]. Complexes 1,2-dihydro-1-phenyl-2,3-dimethyl-4-[N-phenylacetylacetamido-hydrazono]-pyrazol-5-one and 1,2-dihydro-1-phenyl-2,3-dimethyl-4-[ethyl-3'-oxobutanoate-2'-hydrazono]-pyrazol-5-one obtained by coupling the diazonium salt of 4-aminoantipyrene with acetoacetanilide and ethylacetoacetate respectively have been synthesized and investigated [73].

Complexes of Ni(II), Cu(II), Zn(II) and Cd(II) containing hydrazones derive from 6-amino-5-formyl-1,3-dimethyluracil and nicotinic acid/isonicotinic acid hydrazides are reported [74]. The complexes are monomeric and four co-ordinated and the hydrazone ligands act as tridentate ligands. Neither carbonyl oxygen atoms from the uracil ring nor the endocyclic nitrogen atom from pyridine are involved in the co-ordination to the metal.

A hydrazone complex in higher oxidation state was also reported [75]. The reaction of excess 2-hydroxy-1-naphthaldehyde with a solution obtained from the manganese acetate with malonyl dihydrazone in ethanol in 1:1 molar ratio under

reflux led to the precipitation of a manganese (IV) hydrazone complex. Here air acts as an oxidizing agent. When this reaction was carried out in an atmosphere of dinitrogen, Mn(II) complex was obtained.

A series of homo- and heterobinuclear copper(II), manganese(II) and VO^{2+} complexes with asymmetric 2,6-diformyl-*4*-R-phenol bis (hydrazones) have been reported. The values of the exchange parameters of these compounds have been determined. The experimental results have been compared with the quantum chemical calculations of the model fragments of binuclear metal chelates.[76]

I.1.3 Scope of the present work

The present work was undertaken with a view to synthesise some new zeolite encapsulated transition metal complexes. This ended up in the syntheses of some new metal hydrazone type of ligands obtained by diazotizing amino compounds and coupling at active methylene sites. Since the complexes are hitherto unknown, a detailed characterization of these was attempted using spectral and magnetic data. The complexes were then encapsulated in zeolite cavities and the encapsulated species were characterized. A comparative study of the catalytic activity of the metal complexes and their encapsulated analogues was also undertaken.

In the first part of this thesis, syntheses of Fe, Co, Ni and Cu complexes using three hydrazone types of ligands are given. Details regarding the characterization of these complexes with a view to establishing the molecular structures are presented in this part.

In the second part of the thesis the encapsulation of these complexes in zeolite cavities and the characterization of the encapsulated metal species are described. A comparative study of the catalytic activities of the simple and encapsulated complexes for cyclohexanol oxidation was also carried out.

References

1. F.A.French, E.J.Blanz, *J. Med. Chem.*, 9 (1966) 585.
2. Idem, *Cancer Res.*, 26 (1966) 1638.
3. Idem, *Ibid*, 28 (1968) 2419.
4. K.C.Agrawal, B.A.Booth, A.C.Sartorelli, *J. Med. Chem.*, 11 (1968) 700.
5. M.Mohan, N.S.Gupta, M.P.Gupta, A.Kumar, M.Kumar, N.K.Jha, *Inorg. Chim. Acta.*, 152 (1988) 25.
6. M.Mohan, A.Kumar, M.Kumar, N.K.Jha, *Ibid*, 136 (1987) 65.
7. T.S.Ma , T.M.Tien, *Antibiotics and Chemotherapy*, 3 (1953) 491.
8. Q.Abbert, *Nature*, 9 (1961) 370.
9. J.M.Price, *Federation Proc.*, 20 (1961) 223.
10. L.Sacconi, *J. Am. Chem. Soc.*, 74 (1952) 4503
11. A.Korolkovas, J.H.Burckhalter, *Essentials of Medicinal Chemistry*, Interscience Pub. N.Y (1976).
12. D.Kovala-Demertzi, A.Domopoulon, M.Demertzis, C.Raptopoulon, A.Terzis, *Polyhedron*, 13 (1994) 1917.
13. D.X.West, M.A.Lockwood, A.Castineiras, *Transit. Met. Chem.*, 22 (1997) 447.
14. D.X.West, G.H.Gebremedhin, R.J.Butcher, J.P.Jasinski, *Transit. Met. Chem.*, 20 (1995) 84.
15. D.Kovala-Demertzi, A.Domopoulon, D.Kovala-Demertzi, M.A.Demertzis, G.Valle, A.Papageorgion, *J. Inorg. Biochem.*, 68 (1997) 147.
16. P.Griess, *Ann.*, 106 (1858) 123.

17. Kekule, Hidegh, *Ann.*, 3 (1870) 233.

18. H.Zollinger, *Azo and Diazo Chemistry*, Wiley, NewYork (1981).

19. K.H.Saunders, R.L.M.Allen, *The Aromatic Diazo Compounds*, Arnold, Australia (1985).

20. Meyer Ambuhl, *Ber.*, 8 (1875) 751.

21. Wiley, Jarboe, *J. Am. Chem. Soc.*, 77 (1955) 403.

22. Dimroth, *Ber.*, 40 (1907) 2404.

23. Dimroth, Hartman, *Ber.*, 41 (1908) 4012.

24. Dimroth, Liechtlin, Friedemann, *Ber.*, 50 (1917) 1534.

25. Auwers, *Ann.*, 378 (1910) 243.

26. Chattaway, Lye, *J. Chem. Soc.* (1933) 480.

27. Vorlander, *Ann.*, 294 (1897) 253.

28. Lifschitz, *Ber.*, 47 (1914) 1401.

29. Iyer, Chakravarti, *J. Indian. Ins. Sci.*, 17A, 41 (1934) [C.A., 28, 4390 (1934)]

30. Iyer, *J. Indian. Inst. Sci.*, 21A, Pt. 6, 65 (1938) [C.A., 33, 148 (1939)]

31. Wislicenus, Reitzenstein, *Ann.*, 277 (1893) 362.

32. Das, Ghosh, *J. Am. Chem. Soc.*, 43 (1921) 1739.

33. S.M.Parmerter, *Org. Reactions*, 10 (1959) 1.

34. J.Elguero, R.Jacquier, G.Tarrago, *Bull. Soc. Chim. Fr.* (1966) 2781.

35. H.C.Yao, *J. Org. Chem.*, 29 (1964) 2959.

36. C.Reichardt, W.Grahn, *Tetrahedron Letters* (1971) 3745.

37. Idem, *Chem.Ber.*, 103 (1970) 1065.

38. A.K.Bose, I.Kugajevsky, *Tetrahedron*, 23 (1967) 1489.

39. E.M.Tanner, *Spectrochim. Acta*, 20 (1959).

40. D.C.Nonhebel, *Tetrahedron*, 24 (1968) 1869.

41. J.L.Burdett, M.T.Rogers, *J. Am. Chem. Soc.*, 81 (1959) 4682.

42. H.Budzikiewiz, C.Djerassi, D.H.Williams, *Mass Spectrometry of Organic Compounds*, Holden-Day Inc. (1967).

43. K.Kobayashi, K.Kurihara, K.Hirose, *Bull. Chem. Soc. Japan*, 45 (1972) 3551.

44. Idem, *Ibid*, 45 (1972) 1700.

45. T.E.Beukelman, *The Analytical Chemistry of Synthetic Dyes* (Ed:K.Venkitaraman) John Wiley, NewYork (1977).

46. L.Antonov, S.Kawanchi, M.Satoh, J.Komyama, *Dyes and Pigments*, 38 (1-3) (1998) 157.

47. K.Venkitaraman, *Chemistry of Synthetic Dyes*, Academic Press, NewYork (1952).

48. Arkhipor, Kharitonova, *J. Appl. Chem. USSR*, 24 (1951) 733.

49. Idem, *J. Soc. Dyers Colourists*, 67 (1951) 471.

50. Gaunt, *Ibid*, 65 (1949) 429.

51. Strakhov, *J. Appl. Chem. USSR*, 24 (1951) 142.

52. Idem, *J. Soc. Dyers Colourists*, 64 (1951) 292.

53. C.D.Gustavson, *J. Soc. Leather Traders Chem.*, 36 (1952)182.

54. Shuttleworth, *J. Amer. Leather Chemists Assoc.*, 47 (1952) 387.

55. Bell, Whewell, *J. Soc. Dyers Colourists*, 68 (1952) 299.

56. Schoberl, *Ibid*, 33 (1952) 4.

57. Baumann, *Am. Dyestuff Reptr.*, 41 (1952) 453.

58. Turnbull, *Am. Dyestuff Reptr.*, 75 (1952) 82.

59. G.T.Morgan, J.D.Mainsmith, *J. Soc. Dyers Colourists.*, 121 (1922) 2866.

60. H.D.K.Drew, J.K.Landquist, *J. Chem. Soc.* (1938) 292.

61. C.F.Callis, N.C.Nielsen, J.C.Bailer (Jr), J. Am. Chem. Soc.,74 (1952) 3461

62. H.D.K.Drew, R.E.Fairbairn, *J. Chem. Soc.* (1939) 823.

63. M.R.G.Nair, C.P.Prabhakaran, *J. Inorg. Nucl. Chem.*, 43 (1981) 3390.

64. M.R.G.Nair, *Ph.D Thesis*, Dept. of Chem., Kerala University (1985).

65. A.M.Talati, R.N.Kapadia, *Ind. J. Chem.*, 12 (1974) 767

66. N.Tankarajan, K.Krishnankutty, *Ind. J. Chem.*, 23A (1984) 401.

67. Basheir.A.El-Shetary, Farouk I.Zidan, Mohammed.S.Abdel-Moez, *Afinidad*, 14 (1988) 417.

68. A.G.Evans, J.C.Evans, B.A.El-Shetary, C.C.Rowlands, P.H.Morgan, *J. Coord. Chem.*, 9 (1979) 19.

69. K.Krishnankutty, Johns Michael, *J. Coord. Chem.*, 22 (1991) 327.

70. Liang, Vongmin, Liu, Choo-Min, *Trans. Met. Chem.*, 23 (1998) 97.

71. M.A.Hassanali, *Ind. J. Chem.*, 36A (1997) 241.

72. Reena Ravindran, *Ph.D Thesis*, Dept. of Chemistry, Kerala University (1995).

73. M.Girijakumaran, *Ph.D Thesis*, Dept. of Chemistry, Kerala University (1999).

74. F.H.Urena, N.A.I.Cabeza, M.N.M.Carretero, A.L.P.Chamorro, *Acta. Chim. Slov.*, 47 (2000) 481.

75. R.A.Lal, A.Kumar, J.Chakraborty, *Ind. J. Chem.*, 40 A (2001) 422.

76. V.V.Lukov, S.I.Levchenkov, S.V.Posokhova, I.N.Shcherbakov, V.A.Kogan, *Russian J. Coordination Chemistry*, 28, 3 (2002)

Chapter II

MATERIALS AND METHODS

The details of the reagents used and the methods of purification employed are given in this chapter. Detailed account of the preparation of the ligands and their metal complexes are given in this chapter. The techniques employed for their characterization are also described in this chapter.

I.2.1 Reagents

Metal salts employed in the present investigation were: $FeCl_3$ (Qualigens), $CoCl_2.6H_2O$ (Merck GR), $NiCl_2.6H_2O$ (NICE LR) and $CuCl_2.2H_2O$ (Merck GR).

LR grade acetone, benzene, ethanol and methanol were purified by standard methods [1]. Spectroscopic grade methanol were used for spectral and conductance measurements. All the other solvents were used as such.

o-Aminophenol (CDH LR), acetoacetanilide (s.d.fine LR), acetylacetone (Merck GR) and 5-aminouracil (Aldrich) were used for the preparation of the ligands.

All the other reagents used in the present study were CDH AR or Merck GR grade chemicals.

I.2.2 Characterization techniques

I.2.2.1 Chemical Analyses

Iron, cobalt, nickel and copper were estimated by standard methods. For volumetric and gravimetric estimations, the complexes were decomposed with conc. sulphuric acid. The resultant solution was made up with water and was used for the estimation of metals.

Copper was estimated gravimetrically as cuprousthiocyanate, nickel as nickeldimethylglyoximate and cobalt as cobaltpyridinethiocyanate. Iron was estimated as their oxide, Fe_2O_3 [2].

1.2.2.2 Elemental Analyses

Carbon, hydrogen and nitrogen in the metal complexes were determined using Heraeus Carlo Erba 1108 elemental analyzer at RSIC, CDRI, Lucknow.

1.2.2.3 IR Spectra

The IR spectra of the ligands and of the complexes were recorded in KBR pellet in the range 400-4000 cm^{-1} on a Perkin Elmer 881 IR Spectrophotometer at RSIC, CDRI, Lucknow.

1.2.2.4 Conductivity measurements.

In the present study, methanol was used for conductance measurements. The conductance of the complexes of approximately 10^{-3} M solution was measured at room temperature using Century CC 601 Digital Conductivity Meter.

1.2.2.5 Magnetic measurements

The magnetic susceptibility measurements were done at room temperature on a simple Gouy type balance, using $Co[Hg(SCN)_4]$ as calibrant [3]. The effective magnetic moment was calculated using the equation

$$\mu_{eff} = 2.84\ (X'_mT)^{1/2}\ BM \qquad (Eq.\ II.1)$$

where,

T = absolute temperature

X'_m = molar susceptibility corrected for diamagnetism of all atoms present in the complex .

1.2.2.6 EPR Spectra

The glass spectra of the Cu complexes were recorded at liquid nitrogen temperature using a Varian E-109 X/Q band Spectrophotometer taking tetracyanoethylene (TCNE, g=2.0027) as a standard at RSIC, IIT, Bombay. μ_{eff} values were also determined from the EPR parameter by substituting g_{II} and $g_{\perp}$ in the Eq. II.2.

$$\mu_{eff}^2 = g_{II}^2 + g_{\perp}^2 + 3KT/\lambda o\ (g-2) \qquad (Eq.\ II.2)$$

where λo is the spin of orbit coupling constant for the free metal ion.

The density of the unpaired electrons at the central metal atom was computed [4] using Eq. II .3.

$$\alpha^2_{Cu} = (A_{II}/P) + (g_{II}-2) + 3/7\ (g_{\perp}-2) + 0.04 \qquad (Eq.\ II.3)$$

where $1-\alpha^2$ measures the covalency associated with the bonding of metal ion to the ligand and P = 0.036.

1.2.2.7 $^1H_1$ NMR Spectra

The $^1H_1$ NMR of the ligands in $CDCl_3$ was recorded at Sophisticated Instrumentation Facility (SIF), Indian Institute of Science, Bangalore on an amx 400 instument.

1.2.2.8 Thermogravimetric analysis

Thermogravimetric curves of the samples were recorded on a Mettler Toledo STAR^e Thermal Analysis System. In all the measurements, sample approximately 3mg, heating rate 10°C min^{-1} and an atmosphere of nitrogen (flow rate 60ml min^{-1} were used).

1.2.2.9 Electro Spray Mass Spectra (ESMS)

The electrospray mass spectra were recorded on a Micromass Quattro II triple quadrupole mass spectrometer. The samples dissolved in suitable solvents such as chloroform/methanol/acetronitrile/water were introduced into the ESI source through a syringe pump at the rate of 5μl per min. The ESI capillary was set at 3.5 KV and the cone voltage was 40V. The spectra were collected in 6s and the print outs are averaged spectra of 6-8 scans.

1.2.3 Preparation method and characterization

The hydrazones used in the present study were prepared by diazotising a primary amine and coupling with compounds containing active methylene group. Primary amines used were *o*-aminophenol and 5-aminouracil. Acetylacetone and acetoacetanilide are the compounds containing active methylene group. The ligands thus synthesized are acetylacetone-2-hydroxyphenylhydrazone (APAcAc),

acetoacetanilide-2-hydroxyphenylhydrazone (APAcAcA) and acetoacetanilide-3,5-dihydro-2,4-dione pyrimidylhydrazone (AUAcAcA) respectively. They have the following structures:

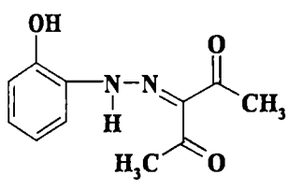

APAcAc

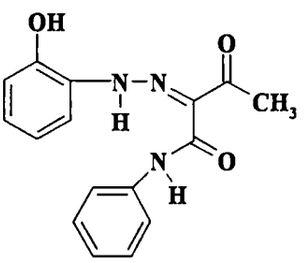

APAcAcA

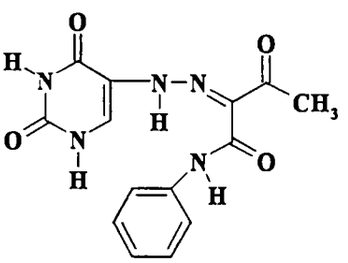

AUAcAcA

The purity of the compounds was tested by TLC. They were characterized on the basis of analytical and spectral data. The functional groups in the ligand were identified with the help of FTIR spectra. $^1H_1$ NMR spectra are in conformity with the above structures. The electron spray mass spectra (ESMS) were taken to show the fragmentation pattern of the ligand. The mass spectra clearly suggest the existence of the ligands in the hydrazone form.

1.2.3.1 Preparation of the ligand APAcAc

This ligand was prepared by the coupling of acetyl acetone with the diazonium salt obtained from *o*-aminophenol. About 0.05 mol of *o*-aminophenol was dissolved with stirring by slow addition of 1:1 HCl. This solution was brought to 5°C by cooling in an ice bath, stirred for 2-3 hours. It should be noted that the diazotisation mixture should never contain more than 20% of free HCl. An aqueous solution of $NaNO_2$ (0.06 mol) was added to the above drop by drop in about 3-4

hours. Temperature should be maintained at 5°C by keeping in ice bath. After that acetylacetone dissolved in 10% NaOH was added to it. The product obtained was filtered, washed with water, dried and stored for further use. The yield was 60%.

1.2.3.2 Characterization of APAcAc

The ligand was characterized on the basis of analytical and spectral data (Table II.1).

Table II.1
Analytical data and physical characteristics of APAcAc.

Compound	Colour	Carbon %	Hydrogen %	Nitrogen %
APAcAc	Orange	59.20(obs)	5.01 (obs)	12.20(obs)
		59.92(cal)	5.45 (cal)	12.71(cal)

The ligand does not melt until 204°C.

The IR spectral bands of the ligand and their probable assignments are given in the Table II.2.

The IR spectrum of the ligand shows a broad band around 3420 cm^{-1} assignable to stretching of -OH and -NH groups. The band due to H-bonded -OH of the enol form of the acetylacetone moiety is also merged with this broad band. The bands in the region 2900-3100 cm^{-1} can be assigned to -CH stretching vibration of alkyl and aryl groups. The band at 1626 cm^{-1} is due to free C=O group. The $\nu_{C=O}$ (H-bonded) is observed at 1600 cm^{-1} and $\nu_{C=N}$ of the azomethine group is observed at 1513 cm^{-1} as a very strong band. The band observed at 930 cm^{-1} is characteristic of

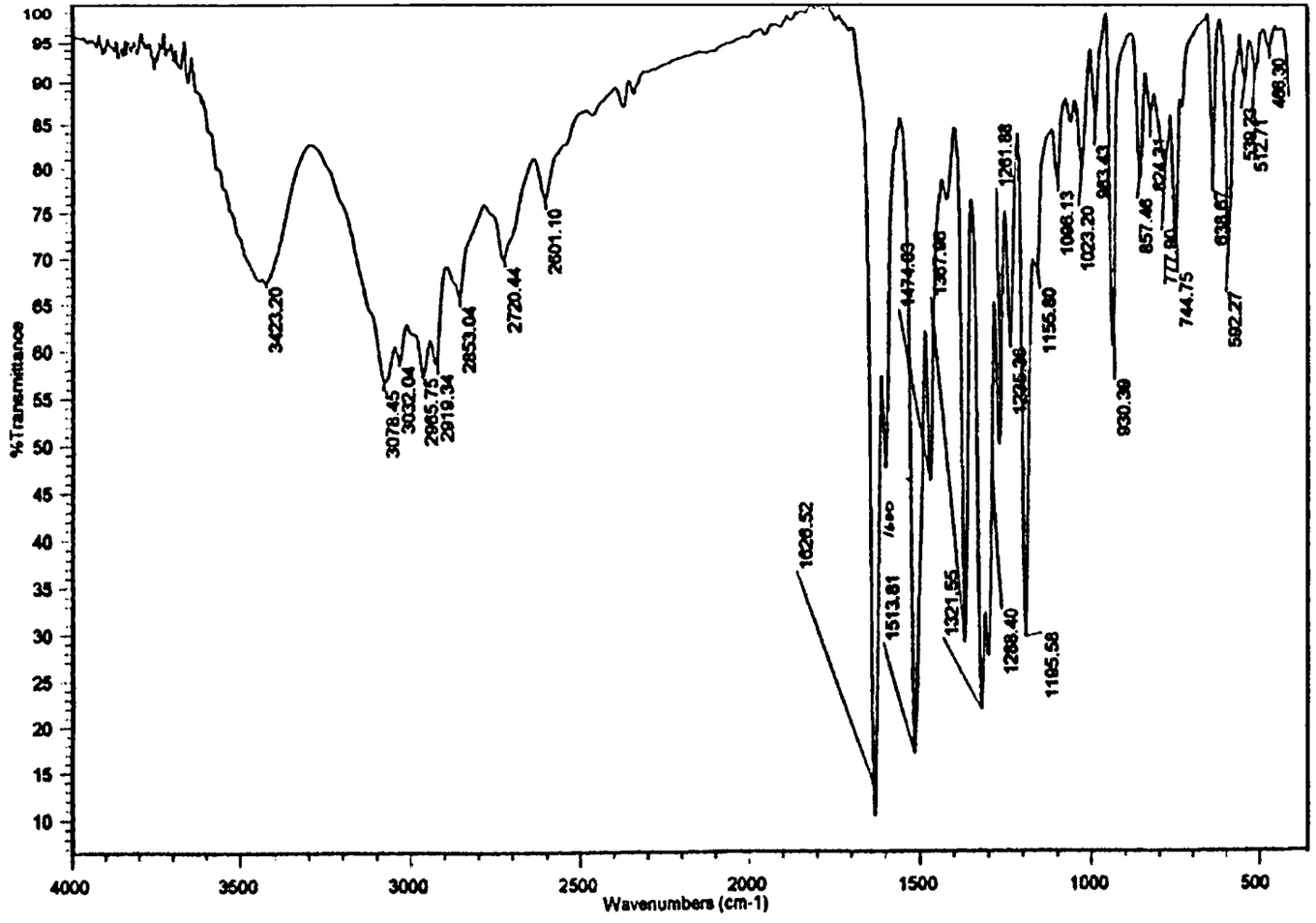

Figure I.2.1 IR Spectrum of ApAcAc

$\nu_{N\text{-}N}$ [5,6]. The IR spectral bands are in agreement with the proposed structure. The spectrum is presented in Fig. I.2.1

Table II.2.
IR Spectral bands of APAcAc and their assignments

Bands	Assignments
3420 m	ν_{OH}
3078 m	ν_{NH}
3032 m	
2965 m	-CH of CH_2
2919 m	
2853 w	
1626 vs	Hydrogen bonded $\nu_{C=O}$
1600 m	$\nu_{C=N}$
1513 vs	
1474 m	
1367 s	
1321 s	
1288 s	
1261 m	
1235 w	
1195 s	δ_{CH} (in plane) of phenyl ring
930 m	$\nu_{N\text{-}N}$
778 w	Π_{CH} of monosubstituted benzene
744 w	
638 w	C=O (in plane) bending
592 m	

The $^1H_1$ NMR spectral data of the ligand in $CDCl_3$ are given in the Table II.3.

The spectrum shows a methyl signal at 2.6 δ. The signal due to $-CH_2$ of the enol form is observed at 3.49 δ. The signals for H-bonded OH of the enol form and NH are expected above 10 δ. These were not observed as this region was not scanned. The spectrum is in conformity with the proposed structure.

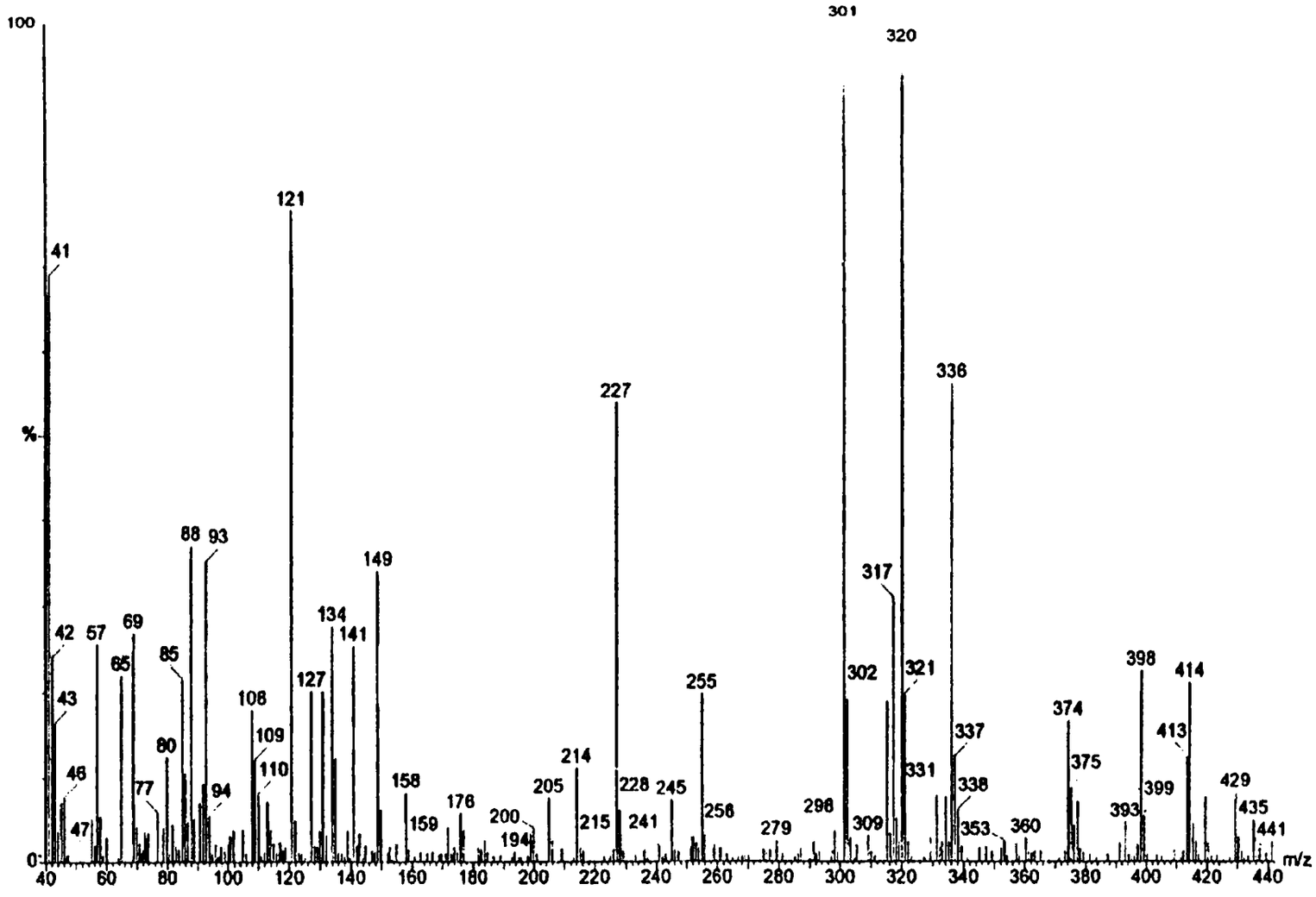

Figure 1.2.2 Mass Spectrum of APAcAc

Table II.3.
$^1H_1$ NMR data of the ligand APAcAc

$^1H_1$ NMR Chemical Shift (ppm)	Groups
2.60 (3 H)	CH_3 - C=O
3.49 (2 H)	$-CH_2$
5.12 (1 H)	Ar-OH
7.00 (4 H)	Aryl protons

The electron spray mass spectrum of APAcAc was examined to see the fragmentation pattern of the ligand. The mass spectrum shows a fragment at an m/z value of 441. This suggests that the ligand exists in a dimeric form probably through H-bonding. The presence of fragments at m/z values 121 and 320 shows that the fragmentation has taken place at –C=N-. The mass spectrum clearly suggests existence of ligand in the hydrazone form. The mass spectrum is presented in Fig. I.2.2

1.2.3.3 Preparation of APAcAcA

The method adopted for the preparation of the ligand is similar to that of APAcAc. The diazonium salt obtained from *o*-aminophenol is coupled with acetoacetanilide. The yield was around 60%. Both the ligands were found to be soluble in methanol, acetone, benzene, dimethylformamide, glacial acetic acid, DMSO, diethylether, ethanol etc. and insoluble in hexane.

1.2.3.4 Characterisation of APAcAcA

The ligand was characterized on the basis of analytical and spectral data (Table II.4).

Table II.4.
Analytical data and physical characteristics of APAcAcA.

Compound	Colour	Carbon %	Hydrogen %	Nitrogen %
APAcAcA	Brown	64.35(obs)	5.10 (obs)	14.09 (obs)
		64.64 (cal)	5.05 (cal)	14.14 (cal)

From the melting point determination it was found that the ligand starts charring from 205°C and decomposes between 215 and 217°C. The analytical data given in the table shows that the ligand has the molecular formulae expected from the chemical reaction. The ligand is likely to be a potential multidentate ligand.

The functional groups in the ligands were identified with the help of IR spectral data. The IR spectral bands and their probable assignments are given in the Table II.5. IR spectrum for the ligand APAcAcA is presented in Fig. I.2.3.

The ligand is likely to have two OH groups on one of the phenyl ring and the other due to the enolisation of acetoacetanilide. Also an NH group from the aminophenol part is expected. These groups normally absorb above 3300 cm^{-1} in the IR spectrum. A strong band with a maximum at 3423 cm^{-1} can be attributed to OH and NH groups. A broad band of medium intensity 3230 cm^{-1} can be assigned to H-bonded OH stretch. The $\nu_{C=O}$ which is involved in H-bonding is observed at 1593 cm^{-1}. The structure in the figure shows two CN groups. One C=O group is probably

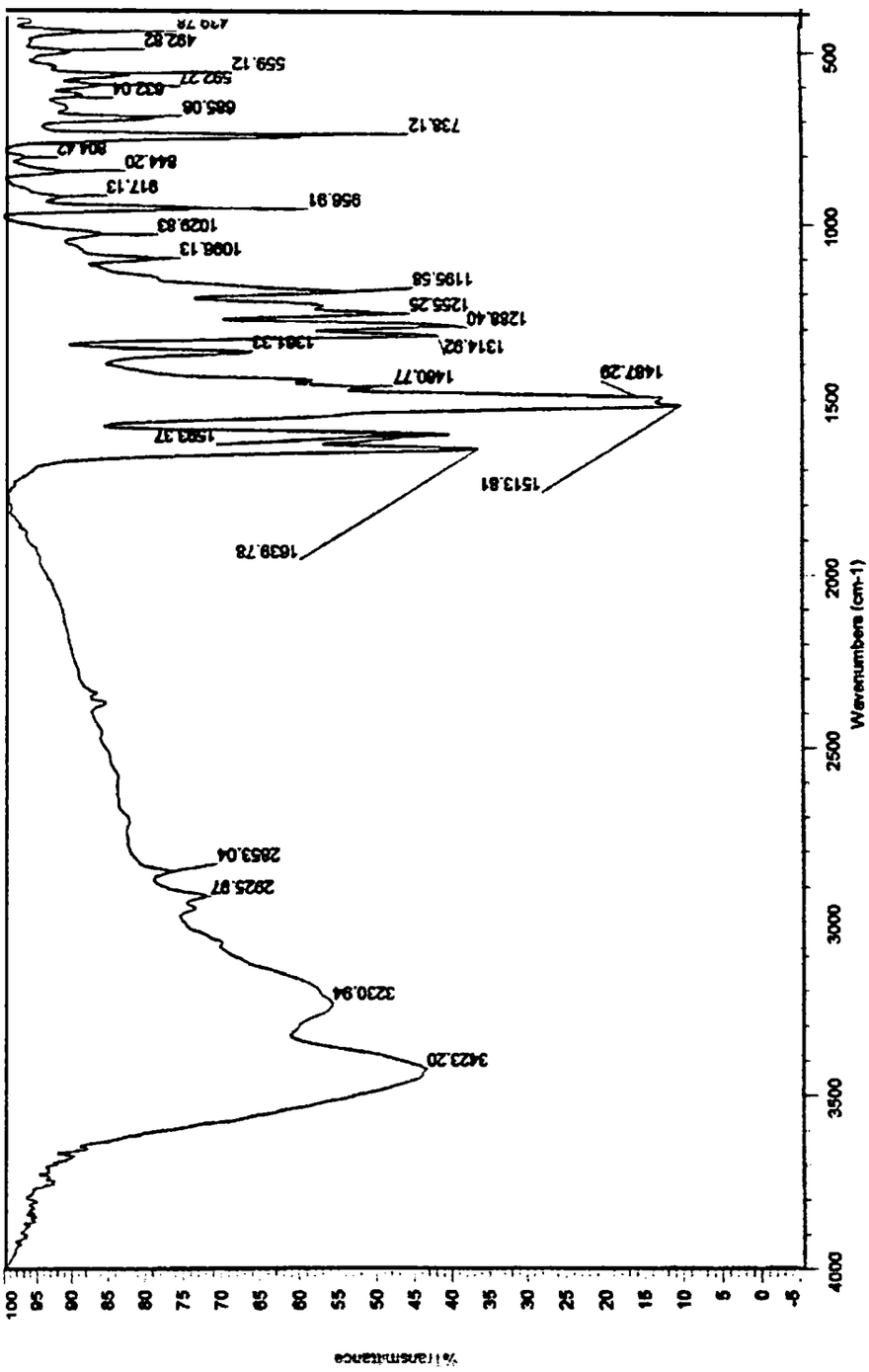

Figure 1.2.3 IR Spectrum of ApAcAcA

intermolecularly H-bonded and hence it give rise to a band at 1513 cm^{-1}. Other group vibrations expected for substituted phenyl ring and methyl groups are observed and they have been assigned.

Table II.5.
The IR spectral bands and the probable assignments of APAcAcA

Bands (cm^{-1})	Assignments
3423 s	ν_{OH} +ν_{NH}
3230 m	ν_{OH} of hydrogen bonded
2925 m	ν asymmetric C-H
2853 m	ν symmetric C-H
1634 s	$\nu_{C=O}$
1593 s	$\nu_{C=N}$
1513 vs	$\nu_{C=N}$ hydrogen bonded
1487 vs	
1461 m	
1361 m	C-H deformation
1314 s	
1288 s	N-phenyl stretch
1255 m	δ C-H (in plane) of
1195 m	phenyl ring
1096 w	ν asymmetric C -C

The $^1H_1$ NMR spectral data are presented in the Table II.6. Signal at 11.46 δ indicates a H-bonded OH group. Aromatic protons show signals around 7.20 δ which accounts for 9 protons. Signals due to Ar-NH and NH-C=O are merged with these signals and comes around 7.20 δ. NH-C=O shows a singlet at 2.17 δ.

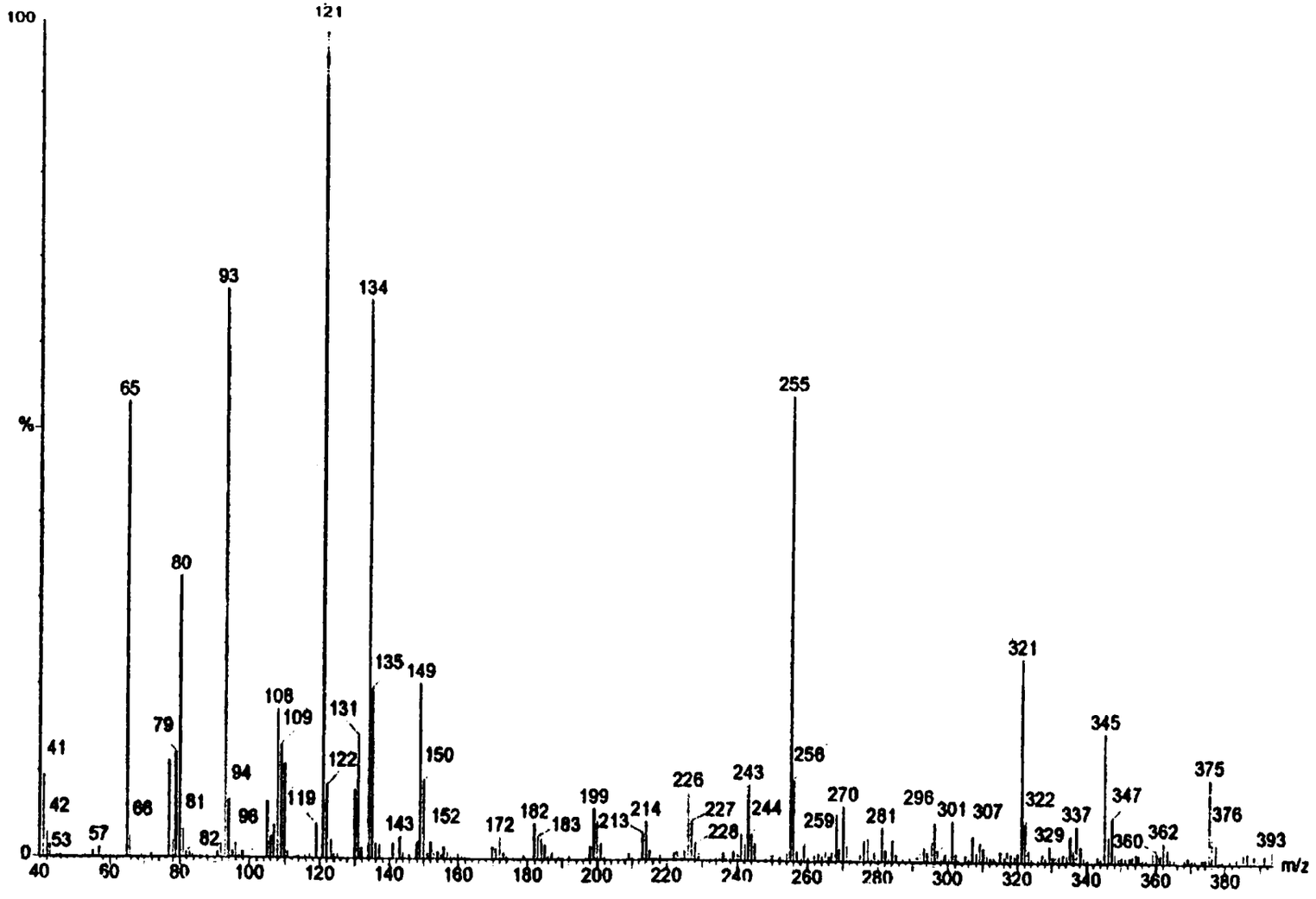

Figure I.2.4 Mass Spectrum of ApAcAcA

Table II.6
$^1H_1$ NMR Spectral data of APAcAcA

Groups	$^1H_1$ NMR Chemical Shifts (ppm)
CH_3-C= O	2.17 δ
Ar-NH C=O | NH	Around 7.20 δ
Aryl protons	Around 7.20 δ
Hydrogen bonded OH	11.46 δ

In APAcAcA the m/z value at 296 corresponds to the molecular ion. In this ligand also the most stable fragment is formed at m/z value 121 (–NH-N=C-) which supports the hydrazone form of the ligand. The mass spectrum is presented in Fig. I.2.4.

1.2.3.5 Preparation of AUAcAcA

This ligand is prepared as described earlier. The ligand was found to be partially soluble in methanol, acetone, glacial acetic acid, DMSO, dichloromethane, hexane, $CHCl_3$, diethylether etc. It is found to be soluble in NH_4OH and DMF.

1.2.3.6 Characterization ofAUAcAcA

The ligand was characterized on the basis of analytical and spectral data (Table II.7).

Table II.7.
Analytical data and Physical characteristics of AUAcAcA.

Compound	Colour	Carbon %	Hydrogen %	Nitrogen %
AUAcAcA	Yellow	52.21 (obs)	4.12.(obs)	23.84 (obs)
		53.16 (cal)	4.43 (cal)	22.22 (cal)

The ligand doesn't melt until 210°C. The analytical data given in the table shows that the ligand has the molecular formulae expected from the chemical reaction. The ligand is likely to be a potential multidentate ligand.

The functional groups in the ligands were identified with the help of IR spectral data. The IR spectral bands and their probable assignments are given in the Table II.8.

The IR spectrum of the ligand (Fig. I.2.5) is very complicated as it contains four NH groups and four C=O groups in addition to the methyl and phenyl groups. The bands in the region 3200-3410 cm^{-1} can be assigned to NH groups. The very strong band at 1713 cm^{-1} can be assigned to free C=O group in acetoacetanilide moiety. The band at 1650 cm^{-1} is due to intermolecularly H-bonded C=O group. The band 1600 cm^{-1} can be assigned to C=O groups in the ring. The $\nu_{C=N}$ vibration of the hydrazone form of the ligand is observed at 1633 cm^{-1}.

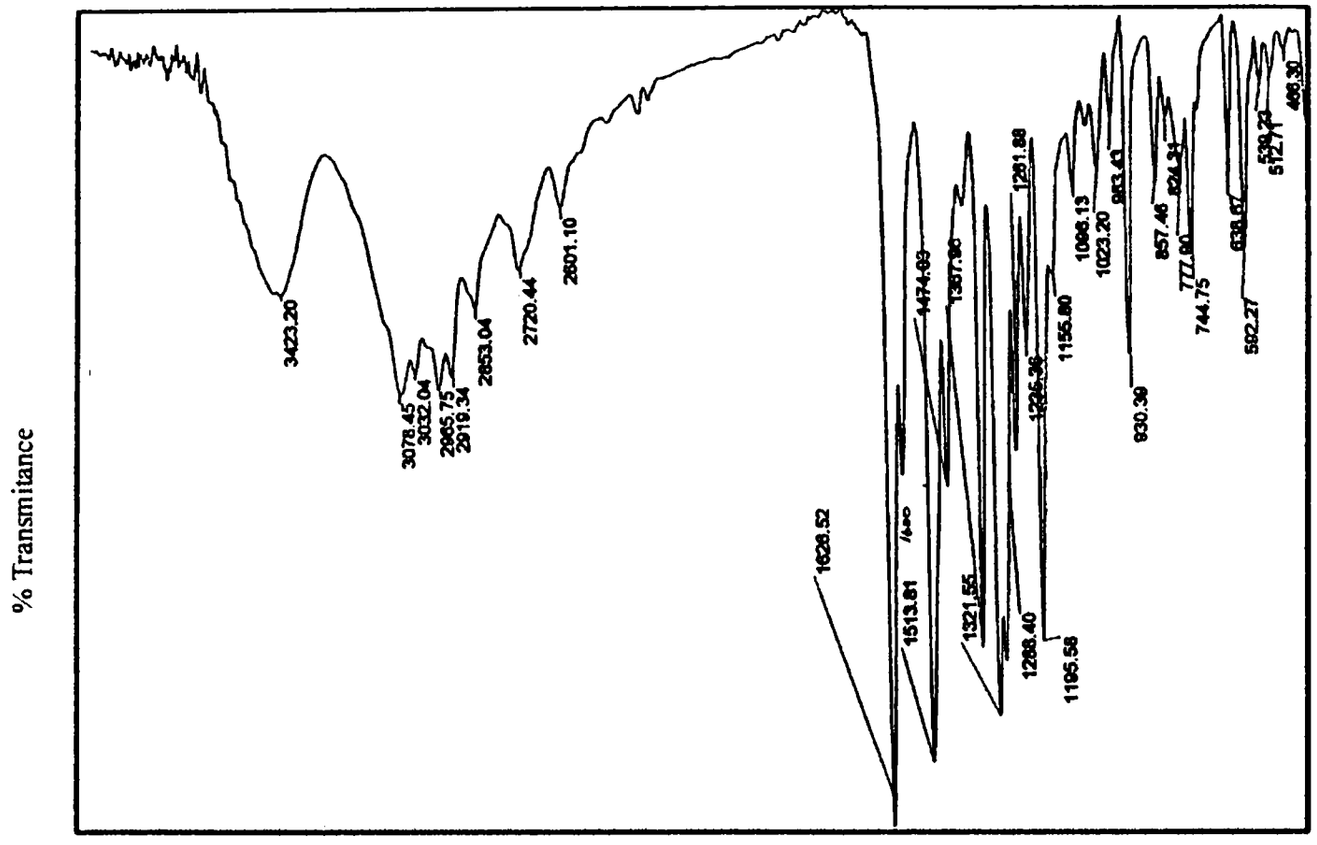

Wave numbers cm-1

Figure1.2.5 IR Spectrum of AUAcAcA

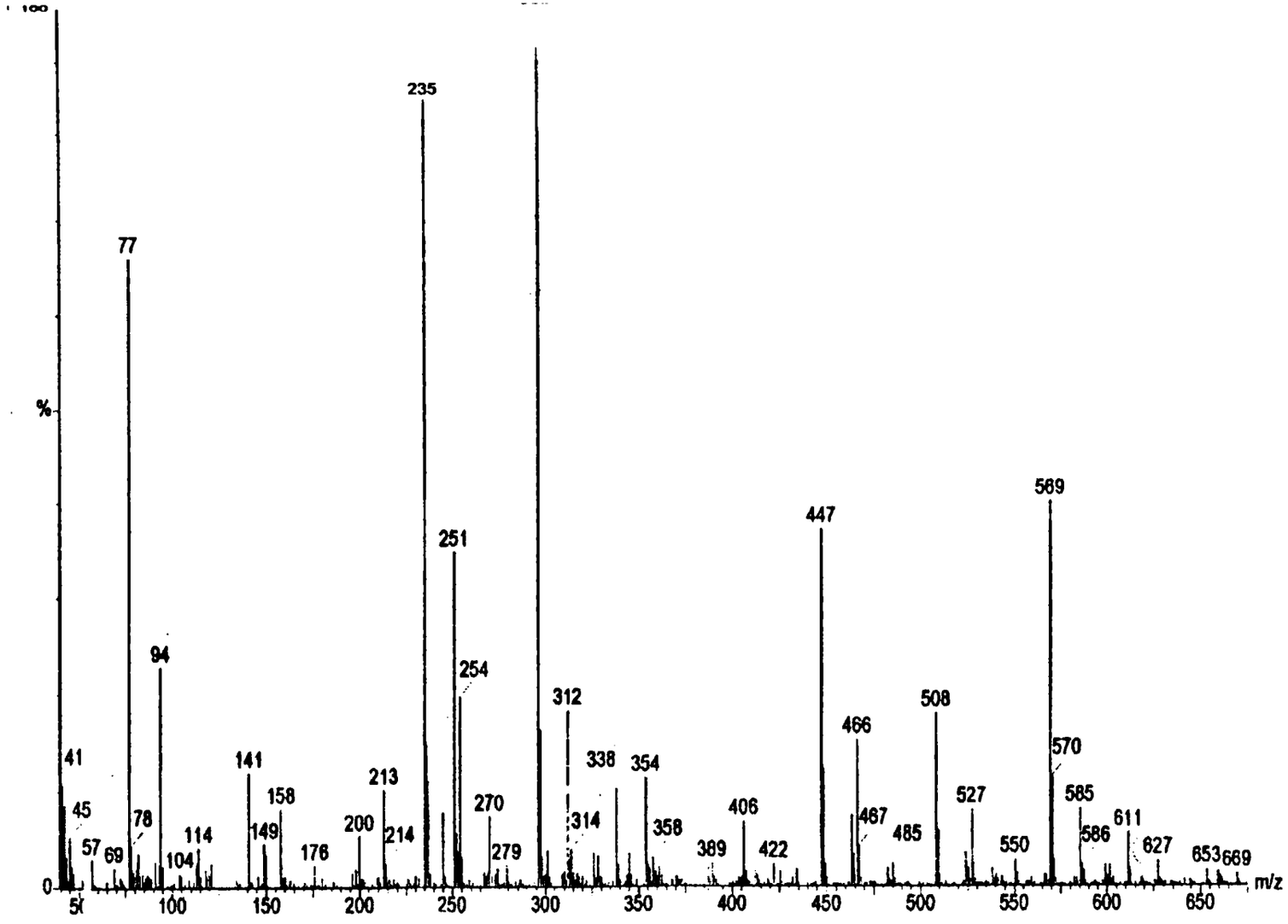

Figure I.2.6 Mass Spectrum of AUAcAcA

Table II.8.
The IR Spectral bands and the probable assignments of AUAcAcA

Bands (cm^{-1})	Assignments
3410m	
3850m	ν_{N-H} group
3270s	
3058m	
2959m	ν_{C-H} group
2926m	
2846w	
1713vs	$\nu_{C=O}$ (free)
1650s	$\nu_{C=O}$ (H-bonded)
1633s	$\nu_{C=O}$ ring
1600s	$\nu_{C=N}$
1540s	
1487m	
1447m	
1388m	
1348m	
1295m	
1255m	
1155m	
1030w	

In the electron spray mass spectra of AUAcAcA (Fig. I.2.6), the peak at m/z, 314 corresponds to the molecular ion of the ligand. There is a peak at 176 which shows that the cleavage takes place at (–NH-N=C-) which supports the hydrazone structure proposed for the ligand.

References

1. A.Weissberger, D.S.Proskauer, J.A.Riddick, E.Troops, *Organic Solvents*, Interscience Publishers, NewYork (1956) 2.
2. A.I.Vogel, *A Text Book of Qualitative Chemical Analysis*, 5th edition, Longman Scientific and Technical, UK (1989).
3. B.N.Figgis, R.S.Nyholm, *J. Chem. Soc.*, (1958).
4. D.Kivelson, R.Neiman, *J. Chem. Phys.*, 35 (1961)149.
5. S.N.Shetti, A.S.Murty, G.L.Tembe, *Transit. Met. Chem.*, 18 (1993) 467.
6. D.X.West, R.M.Makeever, J.P.Scovill, D.L.Klayman, *Polyhedron*, 3 (1984) 947.

CHAPTER III

Part A

STUDIES ON SOME NEW COMPLEXES OF Fe(III), Co(II), Ni(II) AND Cu(II) WITH ACETYLACETONE-2 HYDROXYPHENYLHYDRAZONE (APACAC)

Hydrazones have the triatomic grouping C-N=N, and can be considered as Schiff bases derived from acid hydrazides or a coupled product of a diazonium salt with a reactive methylene group of a β-carbonyl compound. Diazo coupling reactions have been recognized as an electrophilic substitution reaction. Diazonium salts reacts with aromatic hydroxy compounds, aromatic amines, hydrocarbons, phenols and naphthyl ethers to give dyes (coloured azo compounds). However, there are several aliphatic compounds capable of coupling with aryl diazonium ion. Whether azo/hydrazo structure is possible can be obtained from the various spectral data.

The hydrazones used in the present study were prepared by diazotising a primary amine and coupling with compounds containing active methylene group. Acetylacetone and *o*-aminophenol were used to synthesize acetylacetone-2-hydroxyphenylhydrazone (APAcAc). The structure is given in Fig. I.3a.1.

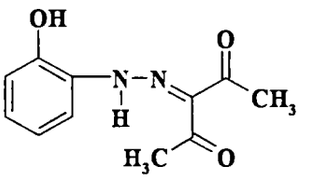

Figure I. 3a. 1 APAcAc

I.3a.1 Experimental

Preparative details and spectral characterization of the ligand are described in part I, chapter II.

Fe(III), Co(II), Ni(II) and Cu(II) complexes of the ligand were prepared and characterized. The results are presented in this chapter.

I.3a.1.1 General method for the preparation of the complexes

About 0.01 mol of the metal chloride was dissolved in methanol. To this a methanolic solution of the ligand (0.03 mol) was added when an instantaneous colour change was observed in all the cases. The solution was refluxed for 3 h for the completion of the reaction. Solid complexes separated on slow evaporation of this solution were filtered washed first with benzene and then with ether to remove excess ligand if any and dried over P_4O_{10} under vacuum.

I.3a.2 Results and discussion.

I.3a.2.1 Chemical analyses

Fe, Co, Ni, and Cu were estimated by standard methods (chapter II). The analytical data along with the empirical formulae are given in Table III.1.

Table III.1.
Analytical data and Physical characteristics of (APAcAc) complexes

Complex	Colour	Metal %	Anion %	C %	H %	N %
$Fe(APAcAc)_3$	Green	7.74 (7.24)	-	55.76 (55.48)	4.48 (4.62)	11.82 (11.76)
Co(APAcAc)Cl	Brown	18.13 (18.72)	10.88 (11.30)	41.95 (42.08)	2.98 (3.51)	9.32 (8.92)
$Ni_2(APAcAc)_3Cl$	Brown	14.20 (14.48)	3.98 (4.37)	49.60 (48.84)	4.07 (4.52)	10.86 (10.36)
Cu(APAcAc)Cl	Brown	19.82 (19.96)	11.38 (11.14)	40.90 (41.47)	3.03 (3.45)	8.42 (8.79)

I.3a.2.2 Electrical conductance and electrolytic nature

The molar conductance values of approximately 10^{-3} M solutions of the complexes in methanol were determined. The values are presented in Table III.2. The expected molar conductance values for 1:1 electrolyte in methanol [1] is approximately 100 $ohm^{-1}cm^2mol^{-1}$. The low conductance values observed for the present complexes suggest non-electrolytic behavior for them.

I.3a.2.3 Magnetic behaviour.

The effective magnetic moment values of the complexes calculated from the corrected magnetic susceptibilities are given in Table III.2.

High spin Fe(III) complexes have the ground state $^6A_1$, and therefore magnetic moment values very close to the spin only value for five unpaired electrons (5.92BM) are expected. The low spin complexes with $^2T_{2g}$ ground state have considerable orbital contribution and a value close to 2.3BM is usually observed. The magnetic moment values lower than those expected found in many Fe(III) can be due to antiferromagnetic interaction between iron atoms [2], high spin-low spin equilibria [3-5] or due to the presence

of quartet ground state for the free ion [6]. The magnetic moment value of the present Fe(III) complex show the absence of any of the factors responsible for the lowering of the magnetic moment.

The magnetic moment values are of great significance in a structural context in the case of Co(II) complexes [7]. Magnetic moments of tetrahedral, octahedral and square planar complexes differ significantly and therefore structural type can be easily identified using magnetic data. In octahedral complexes, the ground state ($^4T_{1g}$) is orbitally degenerate and this causes large orbital contribution to the magnetic moment. Experimentally observed magnetic moment values lie in the range 4.7-5.2 BM. For the tetrahedral Co(II) complexes, the ground state is $^4A_2$. Higher energy $^4T_1$ and $^4T_2$ states mix with the ground state under the influence of spin orbit coupling and the experimentally observed values are in the range 4.4-4.7 BM.

Square planar and square pyramidal complexes of Co(II) are rare. These configurations give rise to magnetic moment values in the range 2.2-2.6 BM [8,9]. The magnetic moment value of the present Co(II) complex is 3.91 BM which is suggestive of a tetrahedral geometry for the complex.

The magnetic moment values of Ni(II) complexes are of great help in ascertaining the geometry. The spin only value for octahedral Ni(II) with two unpaired electrons is 2.83BM. However, octahedral Ni(II) complexes, the magnetic moment value observed is between 2.8-3.3 BM due to spin orbit coupling and higher state mixing with the ground state $^3A_{2g}$. In tetrahedral Ni(II), the ground state is orbital triplet with a large orbital contribution and hence the value observed is in the range 3.5-4.2 BM. The square planar

Ni(II) complexes are diamagnetic since a spin singlet is the ground state. The present Ni(II) complex $Ni_2(APAcAc)_3Cl$ shows a magnetic moment value of 2.78 which is nearer to the value expected for octahedral Ni(II).

In the case of Cu(II) complexes magnetic measurements are not of much use in ascertaining the geometry. Cu(II) with one unpaired electron shows a magnetic moment value of 1.72 under proper magnetic dilution. This value can be increased as a result of spin orbit coupling [10] (λ= 830cm^{-1}). The magnetic moment of Cu(II) complexes vary from 1.8 to 2.2 BM [11]. It has been reported that for octahedral complexes, the magnetic moments are in the range 1.9-2.0 BM at room temperature [11]. For Cu(II) in tetrahedral environment, a moment of 2.2 BM at room temperature has been predicted but value can be considerably lower if the low symmetry ligand fields produced are large compared to spin-orbit coupling [12]. Many Cu(II) complexes show magnetic moments well below spin only value due to antiferromagnetic interaction. In the present APAcAc complex of Cu(II), the magnetic moment observed is 1.65 BM. This is slightly lower than the spin only value but rule out the existence of any appreciable Cu-Cu interaction.

Table III.2.
Magnetic and Conductance data of APAcAc complexes

Complex	Magnetic moment μ_{eff} (BM)	Conductance* Λ_M**	Nature of the electrolyte
$Fe(APAcAc)_3$	5.98	10	Non-electrolyte
Co(APAcAc)Cl	3.91	23	"
$Ni_2(APAcAc)_3Cl$	2.78	28	"
Cu(APAcAc)Cl	1.65	21	"

*10^{-3} M solution (methanol) **ohm^{-1}cm^2 mol^{-1}

I.3a.2.4 IR spectra and bonding

The IR spectral bands of the ligand APAcAc and its complexes along with their probable assignments are given in Table III.3. The spectra are presented in Fig. I.3a.2. The assignments of the spectral bands are made by comparing the spectral features of *o*-aminophenol and acetyl acetone. The spectra of the complexes are more or less similar to that of the ligand with minor shifts of some of the bands. The ligand has two carbonyl groups of the acetylacetone moiety, a phenolic -OH and an azomethine group. The ligand shows a broad band at 3420 cm^{-1} assignable to -OH stretch. In the spectra of the complexes, this band is absent. This clearly shows that the hydrogen of the -OH group is replaced by the metal. The ν_{NH} vibration of the ligand is retained in the complexes. Thus, the ligand is monoanionic and is bonded through oxygen after deprotonation. The vibration at 1626 cm^{-1} present in the ligand is assigned to free C=O group. This band occurs in the spectra of all the complexes without any appreciable change. So this group is not involved in bonding. The band at 1600 cm^{-1} present in the ligand is attributed to intramolecularly H-bonded C=O. This band does not show any change in the spectrum of the complexes indicating that the H-bonded structure is retained in the complexes. The ν_{CN} at 1513 cm^{-1}gets shifted to around 1500 cm^{-1} in the spectra of the complexes showing the participation of azomethine group in complex formation. The band at 930 in the ligand is displaced to higher wavenumber. Such shifts are very characteristic of several hydrazone ligand coordinated through the azomethine nitrogen atom [13,14]. Thus, the ligand acts as a monoanionic bidentate coordinating through phenolic oxygen and azomethine nitrogen in all the complexes.

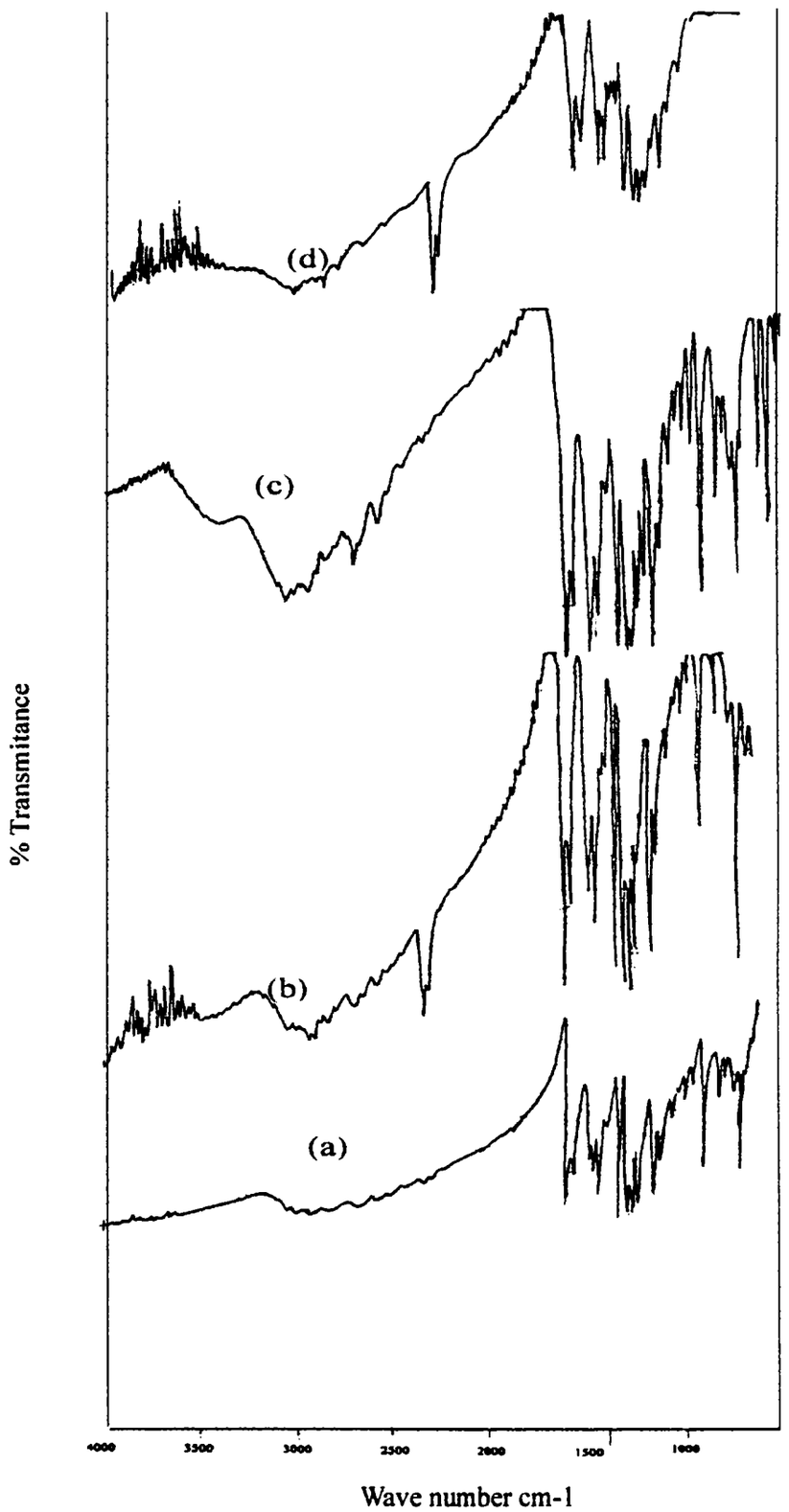

Figure I.3a.2 IR Spectra of (a) Fe (APAcAc)3 (b) Co(APAcAc)Cl
(c)Ni2(APAcAc)3Cl (d)Cu(APAcAc)Cl

Table III.3
The IR spectral bands of APAcAc and its complexes with probable assignments.

APAcAc	$Fe(APAcAc)_3$	Co(APAcAc)Cl	$Ni_2(APAcAc)_3Cl$	Cu(APAcAc)Cl	Assignments
3420m	-	-	-	-	ν_{OH}
3078m	3063m	3063m	3076m	3076m	ν_{NH}
3032m	-	-	-	-	ν_{CH}
2965m	2955m	2955m	2962m	2921m	ν_{CH}
2919m	-	2847m	-	2854m	
1626vs	1627s	1630m	1640s	1634s	$\nu_{C=O}$(free)
1600m	1593s	1600s	1589m	1595s	$\nu_{C=O}$ (H-bonded)
1513vs	1510s	1505s	1519s	1505s	ν_{CN}
1474m	1472m	1472m	1479s	1472m	
1367s	1371s	1371s	1378m	1378m	
1321s	1317s	1324s	1330s	1324s	
1288s	1297s	1290s	1303m	1290s	
1261m	1270m	1270s	1276m	1270m	
1195s	1196s	1196s	1202m	1202m	δ_{CH}(of phenyl ring)
930m	937m	932m	946w	-	ν_{N-N}
744w	758	750w	764	-	π_{CH}(of monosubstituted benzene)
638w	-	638w	-	642	

m-medium; vs-very strong; s-strong; w-weak

I.3a.2.5 Electronic spectra and Structure

The band maxima along with probable assignments are given in the Table III.4 and the spectra are presented in Fig. I.3a.3. The spectrum of the Fe(III) complex shows two bands, one at 380nm (26320 cm^{-1}) and the other at 480nm (20830 cm^{-1}). The former can be assigned to n-л* transition of the ligand, since this band is present in the spectrum of the ligand also. The latter band is due to charge transfer transition. In high spin Fe(III) complexes, the ground state $^6A_1$ is derived from ^6S ground term of the free ion. Since no other sextet is possible, all the transition are spin and Laporte forbidden [15]. It is very difficult to have any spectra-structure correlation in the case of Fe(III) as all the weak forbidden transitions are often masked by charge transfer bands. A spin forbidden band $^6A_1 \rightarrow {}^4T_1$ expected [16,17] in the region 450-600 nm is masked by the charge transfer band at 480nm.

In the spectrum of Co(II) complex, in addition to the n→л* and charge transfer bands at 360 (27770 cm^{-1}) and 470 nm (21270 cm^{-1}) respectively, a band is observed at 690 nm (14490 cm^{-1}) assignable to d-d transition. The electronic spectra of Co(II) in various geometrical structures are now well understood [18]. The three transitions expected for octahedral Co(II) are $^4T_{1g}(F) \rightarrow {}^4T_{2g}(F)$; $^4T_{1g}(F) \rightarrow {}^4A_{2g}(F)$ and $^4T_{1g}(F) \rightarrow {}^4T_{1g}(P)$. These occur in the range 9000-8000, 18000-16000 and 21000-20500 cm^{-1} respectively. Three spin allowed transitions are $^4A_2(F) \rightarrow {}^4T_1(P)$; $^4A_2(F) \rightarrow {}^4T_1(F)$ and $^4A_2(F) \rightarrow {}^4T_2(F)$. Of these, the transition $^4A_2(F) \rightarrow {}^4T_2(F)$ is very weak and is rarely observed. In the present case, the band observed at 14490 cm^{-1} can be assigned to $^4A_2(F) \rightarrow {}^4T_1(P)$ of tetrahedral Co(II). Transition $^4A_2(F) \rightarrow {}^4T_2(F)$ is orbitally forbidden and is not generally observed. The $^4A_2(F) \rightarrow {}^4T_1(F)$ is not observed in the present case as the near IR region in

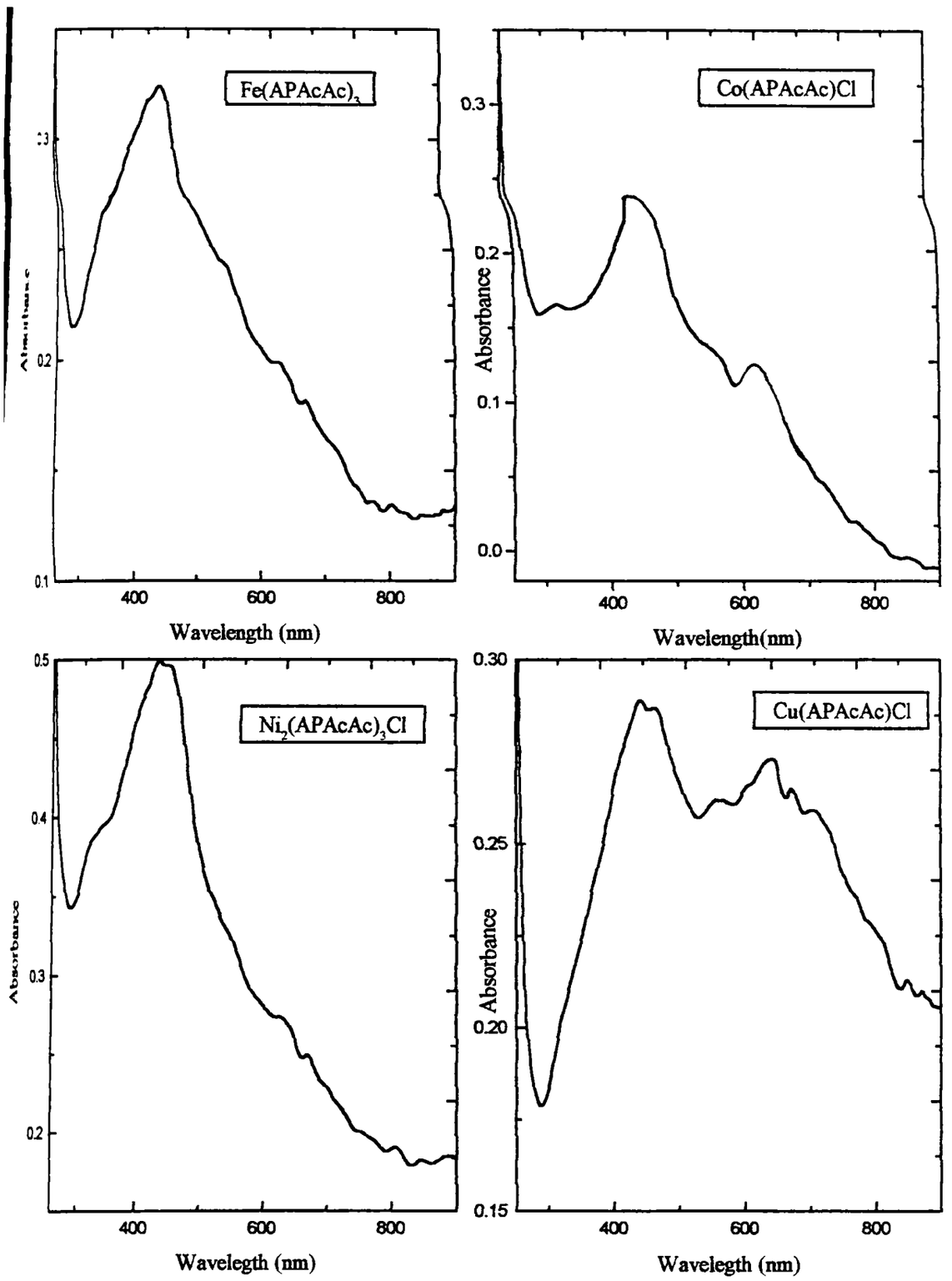

Figure I.3a.3 Electronic Spectra of APAcAc complexes

which this band occurs was not scanned during this study.

The spectrum of the present Ni(II) complex also shows the ligand band at 350 nm (28570 cm^{-1}) and a charge transfer band at 460 nm (21740 cm^{-1}). In addition to these bands a d-d band is observed at 550nm (18180 cm^{-1}). The electronic transitions expected for octahedral Ni(II) are $^3A_{2g}\rightarrow{}^3T_{2g}(F)$; $^3A_{2g}\rightarrow{}^3T_{1g}(F)$ and $^3A_{2g}\rightarrow{}^3T_{1g}(P)$ [19]. These transitions occur at approximately 1000 nm, 600 nm and 400 nm respectively. For tetrahedral Ni(II) though three transitions are expected, only the following two are generally observed.

$^3T_1(F)\rightarrow{}^3T_2(F)$; (at 660nm)

$^3T_1(F)\rightarrow{}^3T_1(P)$; (at 1250nm)

The third transition $^3T_1(F)\rightarrow{}^3A_2$ being a two electron transition is relatively improbable. In the present case, the band observed at 18180 cm^{-1} can be assigned to $^3A_{2g}\rightarrow{}^3T_{1g}(F)$ transition of octahedral Ni(II). The transition $^3A_{2g}\rightarrow{}^3T_{1g}(P)$ is probably masked by the charge transfer band. The magnetic data also support such a structure. The present Cu(II) complex shows the ligand band at 340 nm (29410 cm^{-1}) and charge transfer band at 450 nm (22220 cm^{-1}). This complex also shows two bands one at 620 nm (16130 cm^{-1}) and the other at 680 nm (14705 cm^{-1}). Copper(II) complexes are susceptible to Jahn-Teller distortion and regular octahedral complexes are not formed. A weakly or strongly tetragonally distorted octahedral complexes, the latter approaching square planar structures, are usually found. The symmetry is lowered from O_h to D_{4h} and the splitting diagram for D_{4h} symmetry suggests three transitions viz. $^2B_{1g}\rightarrow{}^2A_{1g}$; $^2B_{1g}\rightarrow{}^2B_{2g}(F)$ and $^3B_{1g}\rightarrow{}^2E_g$. However, only one broad or split band around 650 nm is usually observed. The bands observed at 620 and 680 nm in the present complex can be

attributed to the split components of $^2E_g \rightarrow {}^2T_{2g}$ of octahedral Cu(II) due to tetragonal distortion [20].

Table III.4.
Electronic Spectral data of APAcAc complexes

Complex	λ_{max} nm	ν_{max} cm^{-1}	Assignments
$Fe(APAcAc)_3$	380	26320	$\Pi \rightarrow \Pi^*$
	480	20830	Charge Transfer
Co(APAcAc)Cl	360	27770	$\Pi \rightarrow \Pi^*$
	470	21270	Charge Transfer
	690	14490	$^4A_2(F) \rightarrow {}^4T_1(P)$
$Ni_2(APAcAc)_3Cl$	350	28570	$\Pi \rightarrow \Pi^*$
	460	21740	Charge Transfer
	550	18180	$^3A_{2g} \rightarrow {}^3T_{1g}$
Cu(APAcAc)Cl	340	29410	$\Pi \rightarrow \Pi^*$
	450	22220	Charge Transfer
	620	16130	$^2E_g \rightarrow {}^2T_g$
	680	14700	

I.3a.2.6 EPR Spectra

The EPR study of the bonding in Cu(II) complex of β-ketoenolates and Schiff bases were reported earlier. EPR spectrum of Cu(APAcAc)Cl is given in Fig. III.3 and the spectral data are presented in Table I.3a.4. From the measured value of A_{II} and using the approximate formula established by Kivelson and Neiman [21], $\alpha^2_{Cu} = (A_{II}/P) + (g_{II}-2) + 3/7\ (g-2) + 0.04$ with P~ 0.036 cm^{-1}, the α values can be calculated. The bonding parameter α is a measure of the covalency of the in-plane σ bonding. A value of $\alpha^2=1$ indicates complete ionic character while $\alpha^2= 0.5$ denotes essentially 100% covalent bonding assuming negligibly small values of the overlap integral. The greatest amount of covalent character in the σ bonding is exhibited by the bidentate Schiff base chelates ($\alpha^2= 0.72$ to 0.79) while the complexes of β-ketoenolates and tetradentate Schiff bases

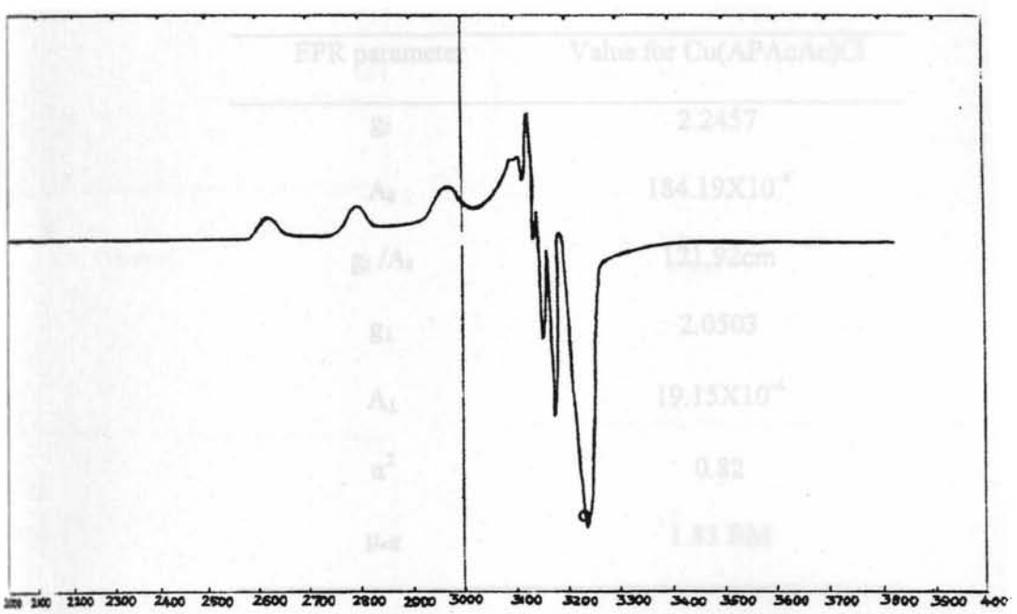

Figure I.3a.4 E.P.R Spectrum of Cu (APAcAc)Cl

are equally less covalent (α^2= 0.81 to 0.85). β-ketoamides possess the greatest ionic character in the σ bonding. The electronegativity of the nitrogen in the amide group may be responsible for the ionicity [22].

Table III.5
EPR data of Cu(APAcAc)Cl

EPR parameter	Value for Cu(APAcAc)Cl
$g_{\|\|}$	2.2457
$A_{\|\|}$	$184.19X10^{-4}$
$g_{\|\|}/A_{\|\|}$	121.92cm
$g_{\perp}$	2.0503
$A_{\perp}$	$19.15X10^{-4}$
α^2	0.82
μ_{eff}	1.83 BM

I.3a.2.7 Thermal Analysis

The term thermal analysis incorporates those techniques in which some physical parameters of the system is determined and recorded as a function of temperature. Various techniques of thermal analyses are available. Among these techniques, thermogravimetry is widely used for finding the stability of compounds. Thermogravimetry is a technique in which a substance in a desired environment is heated or cooled at a controlled rate and the weight or mass of the substance is recorded as a function of temperature. Thermogravimetric analysis provides a quantitative measurement of any weight change associated with a transition. The change in mass is as a result of the rupture and or formation of chemical bonds at higher temperatures and

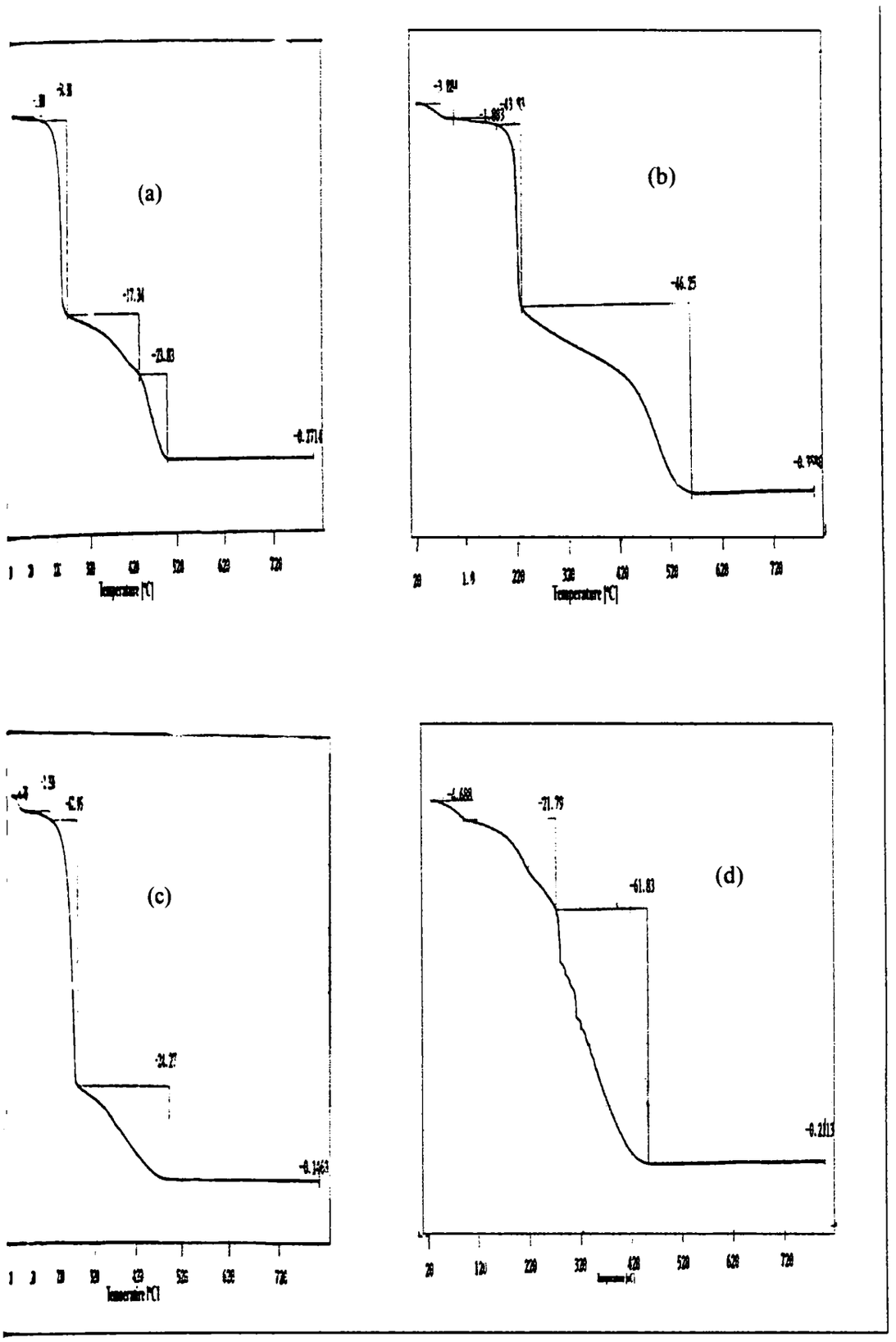

Figure 1.3a.5 T.G. Curves of (a) Fe(APAcAc)3 (b) Co (APAcAc)Cl
(c) Ni2 (APAcAc)3Cl (d) Cu (APAcAc)Cl

evolution of volatile products. From TG curves it is possible to explain the thermodynamics and kinetics of various reactions[23,24]. Mainly two methods are employed in TG- isothermal or static method and non isothermal or dynamic method. From the non isothermal TG used in the present study, phenomenological aspects are discussed. It is possible to find out the thermal stability of the substance, initiating temperature (T_i), the final temperature (T_f) and the temperature of maximum loss (T_s), the physicochemical reactions which occur over definite temperature ranges, the intermediate substance formed and the final products of the reaction.

I.3a.2.8 TG studies of APAcAc complexes

The thermal decomposition behaviour of the APAcAc complexes was studied by TG. The TG curves are given in Fig. I.3a.5 and the data are given in Table III.6.

Table III.6
TG data of Fe(III), Co(II), Ni(II) and Cu(II) complexes of APAcAc.

Complex	Stability (°C)	Decomposition Range
$Fe(APAcAc)_3$	170	171-256 256-440 440-500
Co(APAcAc)Cl	184	184-231 231-560
$Ni_2(APAcAc)_3Cl$	194	194-273 273-493
Cu(APAcAc)Cl	170	170-274 274-453

The Fe(III) complex is stable upto 170°C and continues upto 256°C. The next stage starts immediately after the first. This stage is from 256-440°C. The final stage is from 440-500 °C. It has not been possible to identify the fragments eliminated at different stages.

The Co(II) complex decomposes in two major stages. The complex is stable upto 184 °C. The first stage of decomposition starts at 184 °C and continues upto 231°C. The final stage is from 231-560 °C. In the case of this complex also the mass loss does not correspond to any specific fragment. The Ni(II) complex also decomposes in two stages. These stages are from 194-273 °C and 273-493 °C.

The Cu(II) complex is stable only upto 170°C and decomposes in two major stages. The first one starts at 170 °C and continues upto 274 °C. The second stage is from 274-453 °C and beyond 453 °C there is no significant weight loss upto 800 °C. All the complexes are stable upto 170°C. The stability of the complexes is in the following order: Fe < Co < Ni > Cu.

Part B

NEW COMPLEXES OF Fe(III), Co(II), Ni(II) AND Cu(II) WITH ACETOACETANILIDE-2-HYDROXYPHENYLHYDRAZONE

Complexes of acetylacetone-2-hydroxyphenylhydrazone were described in the previous section. In this section some new complexes of Fe(III), Co(II), Ni(II) and Cu(II) with another hydrazone type of ligand acetoacetanilide-2-hydroxyphenylhydrazone (APAcAcA) obtained by diazotizing *o*-aminophenol and coupling with acetoacetanilide are described. The structure of APAcAcA is given in the Fig. III.5.

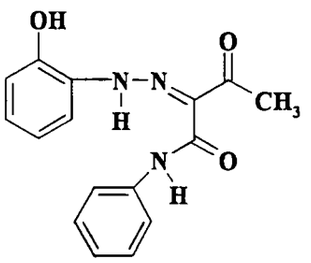

Figure I.3b.1 APAcAcA

The ligand was characterized on the basis of analytical and spectral data. The preparation and characterization of the complexes Fe(III), Co(II), Ni(II) and Cu(II) are presented in this section.

I.3b.1 Experimental

Preparative details and characterization of the ligand using spectral techniques are given in chapter II.

I.3b.1.1 General method of preparation of the complexes

The method employed for the preparation of APAcAcA complexes is similar to that employed for the APAcAc complexes. Methanolic solution of the metal chloride (0.01 mol) was mixed with a methanolic solution of the ligand (0.03 mol). A coloured solution obtained was refluxed for 3h for the completion of the reaction. Complexes separated on slow evaporation of this solution were filtered, washed successively with benzene and ether and dried over P_4O_{10} under vacuum.

I.3b.2 Results and discussion

I.3.2.2 Chemical analyses

Metals in the complexes were estimated as described in chapter II. The analytical data along with physical characteristics and empirical formulae are given in Table III.7.

Table III.7
Analytical and Physical characteristics of (APAcAcA) complexes

Complex	Colour	Metal %	C %	H %	N %
$Fe(APAcAcA)_3$	Yellow	5.91 (5.80)	61.02 (61.61)	4.48 (4.49)	13.34 (13.10)
$Co(APAcAcA)_2$	Green	9.05 (8.98)	58.99 (58.90)	4.30 (3.92)	12.90 (11.88)
$Ni(APAcAcA)_2$	Yellow	9.02 (9.12)	59.01 (59.62)	4.30 (4.20)	12.91 (12.88)
$Cu(APAcAcA)_2$	Brown	9.68 (9.48)	58.58 (57.30)	4.30 (4.19)	12.81 (12.58)

The analytical data shows that the ligand acts as monoanionic in all the complexes.

I.3b.2.2 Electrical Conductance

The electrolytic nature of the complexes was ascertained by carrying out conductance measurements of the complexes in methanol (10^{-3}M). The data given in Table III.8 show the complexes to be non electrolytes.

Table III.8
Magnetic and Conductance data of APAcAcA complexes

Complex	μ_{eff} (BM)	Conductance* Λ_{M}**	Nature of the electrolyte
$Fe(APAcAcA)_3$	6.01	8	Non-electrolyte
$Co(APAcAcA)_2$	3.42	12	"
$Ni(APAcAcA)_2$	3.51	15	"
$Cu(APAcAcA)_2$	1.78	20	"

*10^{-3} M solution (methanol) **$ohm^{-1}cm^2\ mol^{-1}$

I.3b.2.3 IR spectra and bonding

The spectral bands of the ligand and the complexes along with the probable assignments of the band are given in Table III.9 and spectra are presented in Fig. I.3b.2.

The ligand shows a strong broad band in the region 3200-3450 cm^{-1} due to phenolic -OH and two -NH groups. This band is retained in the spectra of the complexes without much change in position and structure. However, the analytical data requires that the ligand is monoanionic and therefore one of the hydrogens of these groups gets deprotonated and bonded to the metal. This hydrogen is likely to be one of the NH groups. A band at 1634 cm^{-1} in the ligand spectrum can be assigned to free C=O while

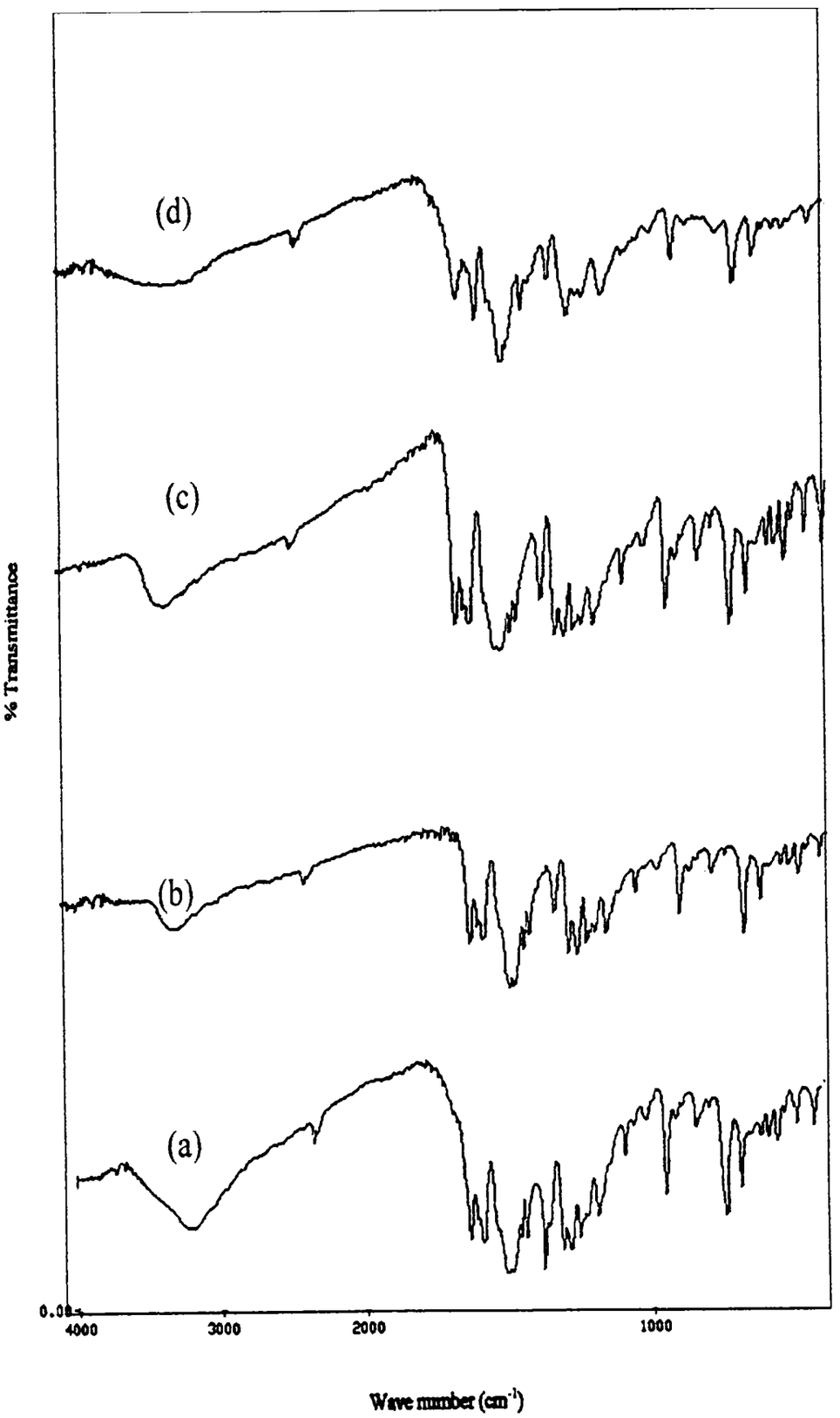

Figure I.3b.2 IR Spectra of (a) Fe(APAcACA)3 (b) Co(APAcAcA)2
(b)Ni (APAcAcA)2 (d) Cu(APAcAcA)2

Table III.9
IR spectral bands and probable assignments of APAcAcA and its complexes

APAcAcA	$Fe(APAcAcA)_3$	$Co(APAcAcA)_2$	$Ni(APAcAcA)_2$	$Cu(APAcAcA)_2$	Assignments
3423sb	3400mb	3410mb	3420mb	3400b	$\nu_{OH}+\nu_{NH}$
3230m	3228m	3196m	3184m	3232m	ν_{OH}(H-bonded)
2925m	2900m	2910m	2950m	2915m	ν_{asy}CH
2853m	2815m	-	-	-	ν_{asy}CH
1634s	1620s	1615s	1610s	1610s	$\nu_{C=O}$(free)
1593s	1594s	1594s	1594s	1596s	$\nu_{C=O}$(H-bonded)
1513vs	1515s	1508vs	1510vs	1516s	ν_{CN}
1487vs	-	1496s	1495s	-	-
1461m	1465m	1465m	1464m	1446m	ν_{NH}
1361m	1384m	1364s	1364m	1358m	δ_{CH}
1314s	1317s	1316s	1316s	-	-
1288s	1289s	1288m	1287s	1295s	N-phenyl stretch
1255m	1258m	1257m	1257s	1245s	Phenyl ring
1195m	1193s	1193m	1192m	1182m	-
1096w	1099w	1098m	1098w	1090w	Benzene ring breathing
1029w	1023w	1024w	1024w	-	-
956s	965	968	966	967	ν_{N-N}
844w	848w	848w	848w	901w	π_{CH}
804w	803w	-	802w	806w	$\nu_{C=O}$

m-medium; vs-very strong; s-strong; w-weak

the band at 1593cm^{-1} to strongly hydrogen bonded C=O. The band at 1513 cm^{-1} is attributable to ν_{C-N}. In the complexes $\nu_{C=O}$ (free) gets shifted to lower energy showing the participation of this group in complex formation. The ν_{CN} at 1513 cm^{-1} does not undergo any shift on complex formation suggesting the non participation of azomethine nitrogen in coordination. The ν_{N-N} at 956 cm^{-1} was shifted to higher wavenumbers in the complexes which is characteristic of hydrazones. Thus APAcAcA acts as a monoanionic bidentate ligand coordinating through free C=O and nitrogen of the NH group forming stable six membered ring.

I.3b.2.4 Magnetic properties

The room temperature magnetic susceptibilities were determined by Gouy method. The magnetic moments calculated from the corrected magnetic susceptibilities are given in Table III.8. The value exhibited by the Fe(III) complex (6.01 BM) is the value expected for five unpaired electrons. Even though this magnetic moment value does not suggest a particular stereochemistry the value clearly shows the absence of any antiferromagnetic interaction. The magnetic moment value exhibited by the Co(II) complex (3.42 BM) is suggestive of tetrahedral geometry for the complex.

The Ni(II) complex shows a magnetic moment value of 3.51 BM. Octahedral or tetrahedral Ni(II) complexes will have two unpaired electrons and the spin only value expected for two unpaired electrons is 2.83 BM. Octahedral Ni(II) complexes having non degenerate ground state ($^3A_{2g}$) shows magnetic moments nearer to spin only value. Tetrahedral Ni(II) complexes on the other hand shows a magnetic moment value much

higher than spin only value, since the ground state, $^3T_1$ has large orbital contribution. The value observed in the present case is in the range expected for tetrahedral Ni(II).

The magnetic moment value observed for the present Cu(II) complex is 1.78 BM which is very nearly equal to the spin only value for one unpaired electron. The magnetic moment value shows the presence of magnetically dilute Cu(II) in the complex without any Cu-Cu interaction.

I.3b.2.5 Electronic Spectra

The electronic spectral bands observed for the complexes are given in Table III.10 along with the probable assignments and the spectra are presented in Fig. I.3b.3.

Table III.10
Electronic Spectral data of APAcAcA complexes

Complex	λ_{max} nm	ν_{max} cm^{-1}	Assignments
Fe(APAcAcA)3	325	30770	Charge transfer
	450	22220	
$Co(APAcAcA)_2$	330	30300	Л→ Л*
	440	22730	Charge transfer
	725	13790	$^4A_2 \rightarrow {}^4T_1(P)$
$Ni(APAcAcA)_2$	350	28570	Л→ Л*
	460	21740	Charge transfer
	725	13790	$^3T_1(F) \rightarrow {}^3T_1(P)$
$Cu(APAcAcA)_2$	350	28570	Л→ Л*
	430	23250	Charge transfer
	700	14280	Overlapped split components of $^2E_g \rightarrow {}^2T_{2g}$

The electronic spectrum of the Fe(III) complex shows two bands, one at 325nm (30770 cm^{-1}) and the other at 450 nm (22220 cm^{-1}). The former can be assigned to intra

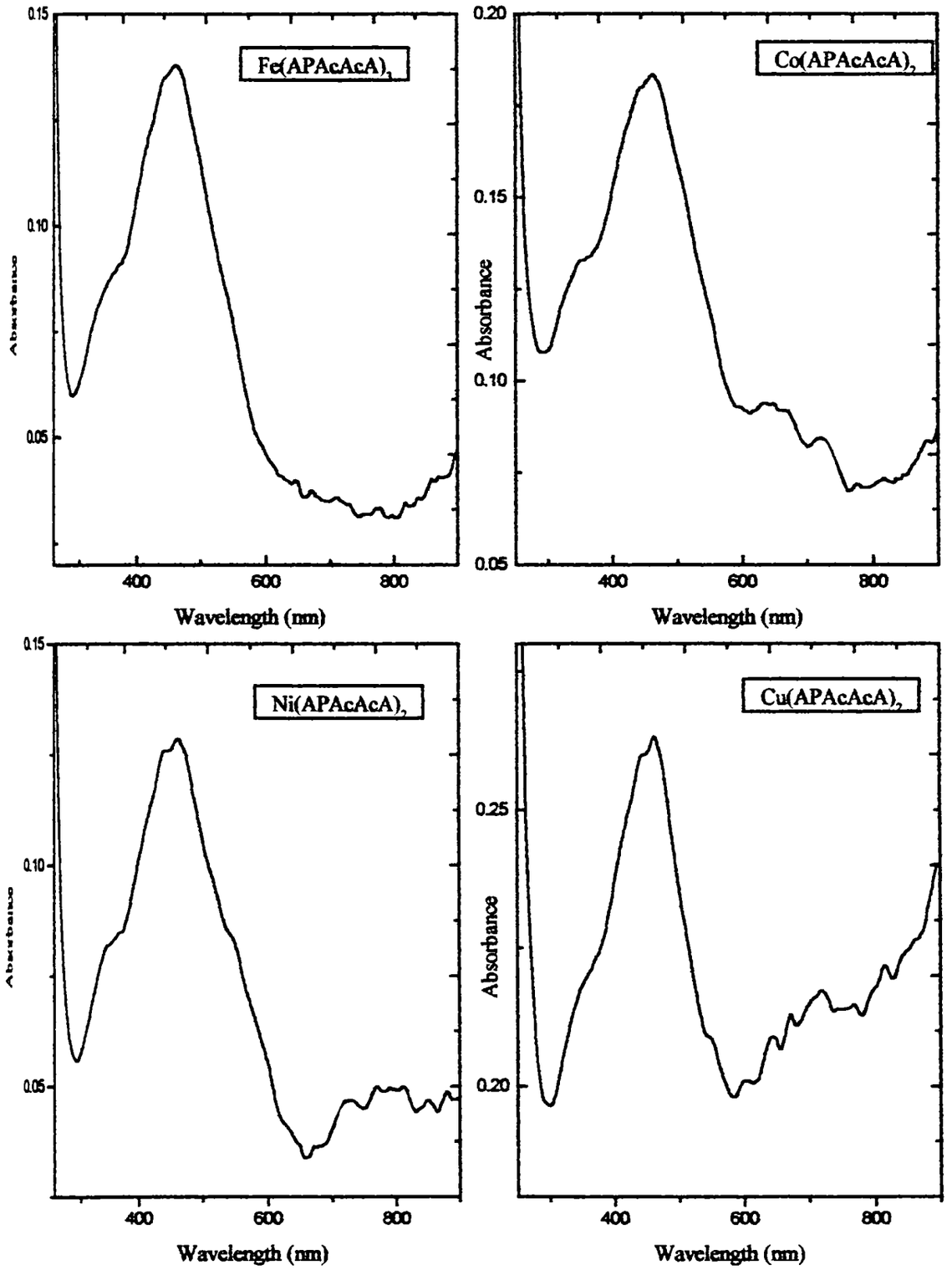

Figure I.3b.3 Electronic Spectra of APAcAcA complexes

ligand transition and the latter to charge transfer transitions. No d-d band could be detected as all the d-d transition for Fe(III) complexes are both spin and Laporte forbidden.

The Co(II) complex shows three bands. The band at 330nm (30300 cm^{-1})is due to electronic transition in the ligand. The band at 440nm (22720 cm^{-1}) can be assigned to charge transfer. The d-d band observed at 740nm (13500 cm^{-1}) is characteristic of tetrahedral Co(II) and can be assigned to the transition $^4A_2 \rightarrow {}^4T_1(P)$. The other two d-d transition expected for tetrahedral Co(II) are in the near IR region and could not be located for the present complex as this region was not investigated. The geometry assigned for the present complex on the basis of electronic spectrum is in conformity with the magnetic data also.

The Ni(II) complex also shows two bands assignable to intra ligand transition (350nm) and a charge transfer band (460nm) in addition to the d-d band at 725 nm (13790 cm^{-1}). The d-d transition can be assigned to $^3T_1(F) \rightarrow {}^3T_1(P)$ of tetrahedral Ni(II).

The Cu(II) complex shows the ligand band at 350nm and a charge transfer band at 430 nm. The d-d band is observed at 700nm (14280 cm^{-1}) as a broad one. This may be due to the overlapped split components of $^2E_g \rightarrow {}^2T_{2g}$ O_h due to lowering of symmetry to D_{4h}. The spectrum suggests that the complex has tetragonally distorted octahedral structure.

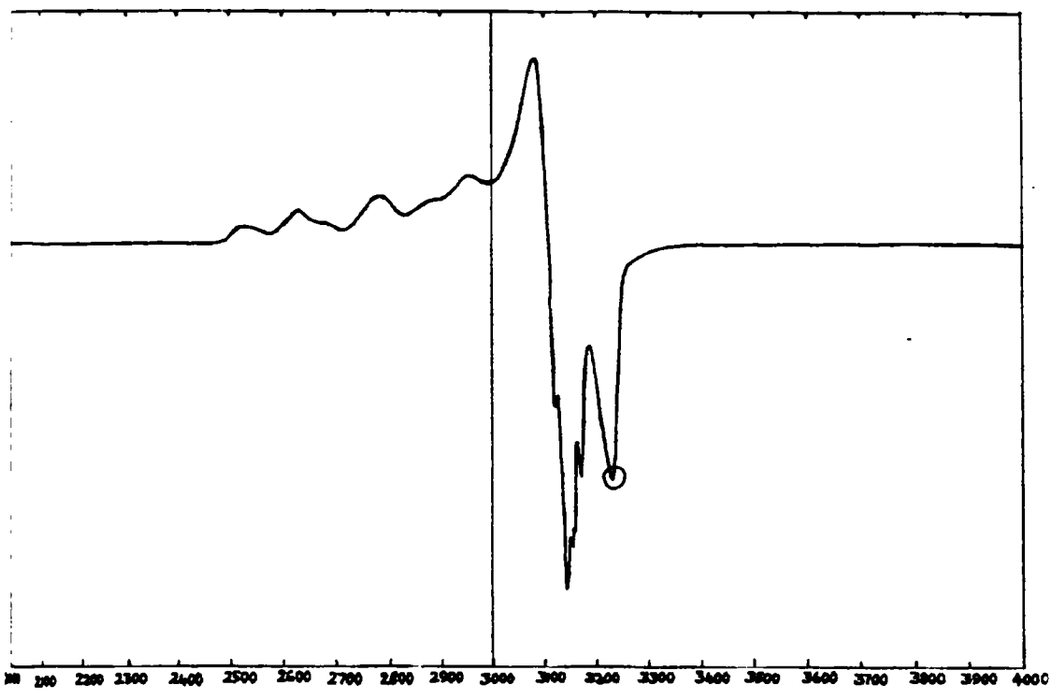

Figure I.3b.4 E.PR Spectrum of Cu(APAcAcA)2

I.3b.2.6 EPR spectrum.

The EPR data of $Cu(APAcAcA)_2$ Table III.11 and the spectrum is presented in Fig. I.3b.4. The spectra of copper complexes are characterized by axial g and hyperfine tensors $g_{\parallel}$ and $g_{\perp}$ and $A_{\parallel}$ and $A_{\perp}$. The g values for the copper complexes with $g_{\parallel} > g_{\perp}$ indicates that the unpaired electron of copper occupies the $3d_{x^2-y^2}$ orbital. The molecular orbital coefficient, smaller than unity indicates the covalent nature of bonding between the metal and ligand orbitals.

Table III.11
EPR data of $Cu(APAcAcA)_2$

EPR parameter	Value for $Cu(APAcAcA)_2$
$g_{\parallel}$	2.3915
$A_{\parallel}$	$173.34X10^{-4}$
$g_{\parallel}/A_{\parallel}$	137.97cm
$g_{\perp}$	2.047
$A_{\perp}$	$19.12X10^{-4}$
α^2	0.93
μ_{eff}	1.87 BM

I.3b.2.7 TG Studies

The TG curves of the APAcAcA complexes are given in Table III.12 and the curves are in Fig. I.3b.5

The complexes are stable above 200°C. The Fe(III) complex is stable upto 238°C. It shows a major decomposition stage which starts from 238 and is complete at

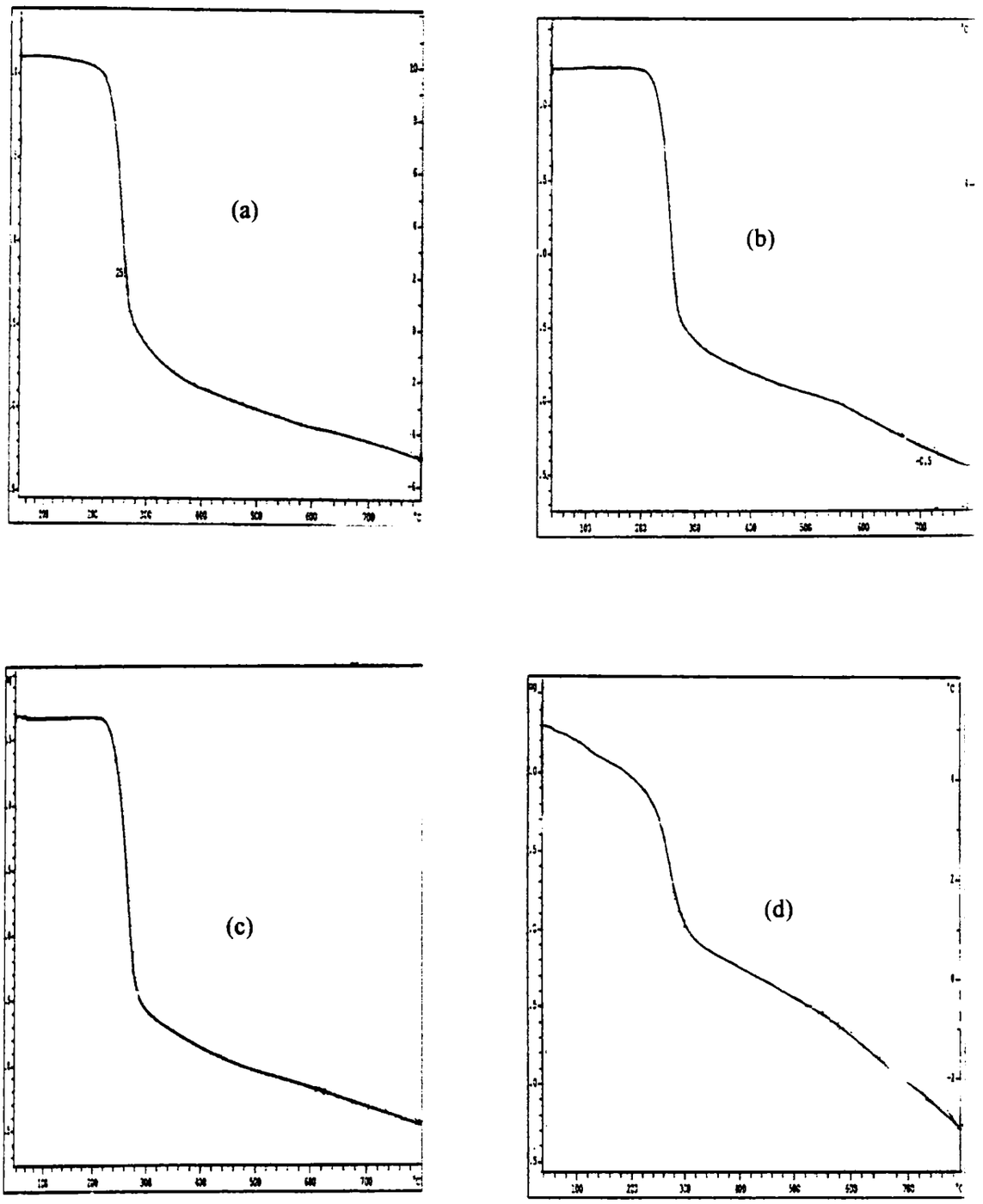

Figure I.3c.5 T.G. Curve of (a) Fe(ApAcAcA)3 (b) Co(APAcAcA)2
(c) Ni (APAcAcA)2 (d) Cu (APAcAcA)2

280 °C. After this stage there is a continuous weight loss upto 800°C probably due to the oxidation of carbon particles.

Table III.12
TG data of APAcAcA complexes

Complex	Stability (°C)	Decomposition range
$Fe(APAcAcA)_3$	238	238-256
$Co(APAcAcA)_2$	220	220-280
$Ni(APAcAcA)_2$	220	220-300
$Cu(APAcAcA)_2$	210	210-300

The Co(II) complex is stable upto 200°C. The major decomposition temperature is between 200°C and 280°C. Ni(II) complex is stable at 220°C and the major decomposition occur in between 220°C to 300°C. further that temperature there is a continuous weight loss until 800°C.

The Cu(II) complex has only a single decomposition stage. The compound is stable at 210°C and the major decomposition starts at 220°C and is completed at 300°C. As in the case of other complexes of APAcAcA, there is a continuous mass loss after the major decomposition upto 800°C.

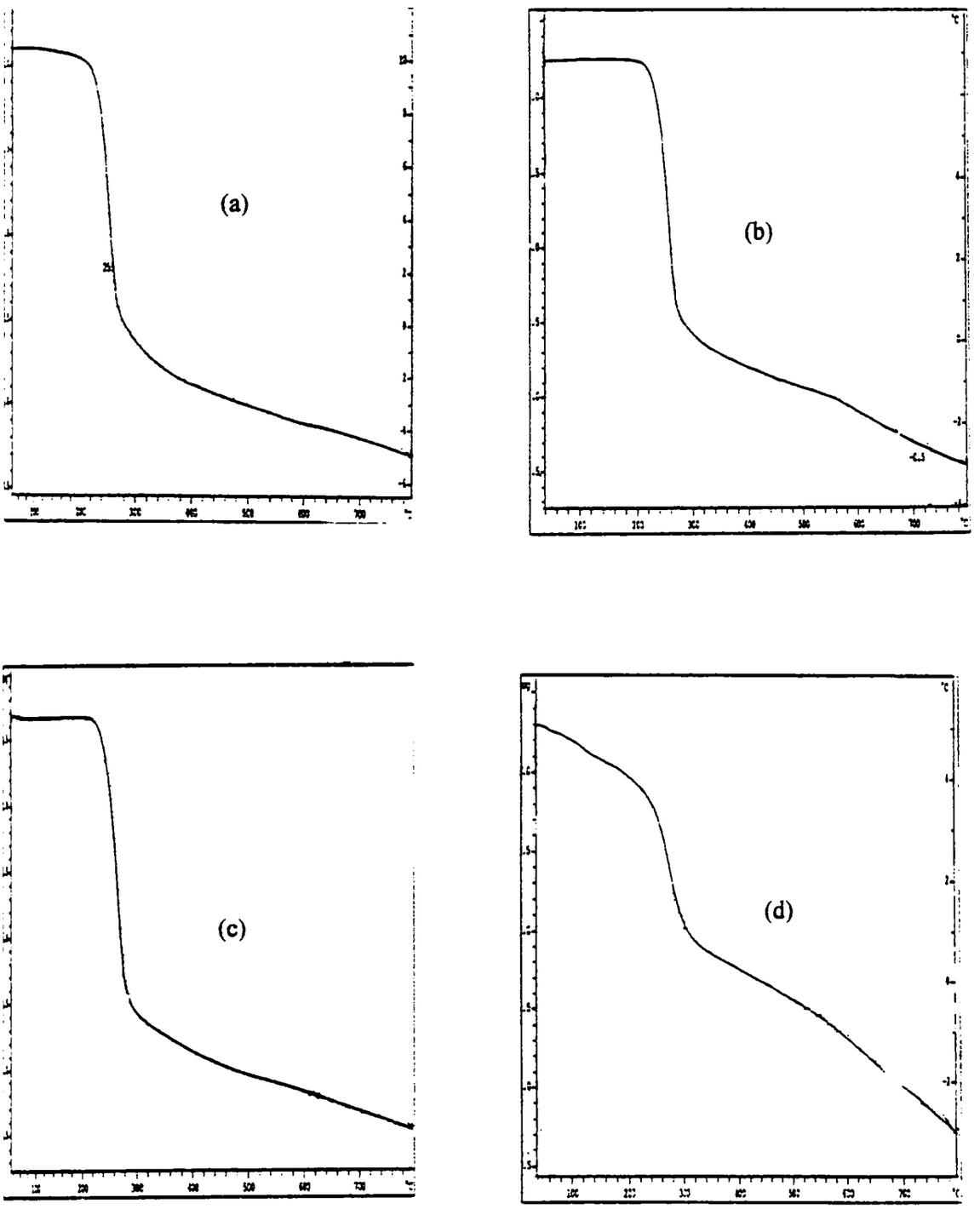

Figure I.3c.5 T.G. Curve of (a) Fe(ApAcAcA)3 (b) Co(APAcAcA)2
(c) Ni (APAcAcA)2 (d) Cu (APAcAcA)2

Part C

Fe(III), Co(II), Ni(II) AND Cu(II) COMPLEXES OF ACETOACETANILIDE-3,5-DIHYDRO-2,4-DIONEPYRIMIDYL-HYDRAZONE(AUACACA)

Complexes of Schiff bases derived from 5-aminouracil have been reported[25]. Complexes of hydrazone with uracil derivatives have got potential pharmacologic applications due to the fact that the azomethine bond may be hydrolyzed in the acid pH of cancer cells, liberating the uracil derivative, which may act as an efficient alkylating or antimetabolite drug [25]. In this section, the complexes of a hydrazone type of ligand obtained by the diazotization of 5-aminouracil and coupling with acetoacetanilide are described. The ligand has the following structure (Fig. III.12).

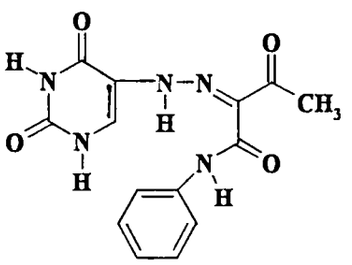

Figure I.3c.1 AUAcAcA

The ligand was complexed with Fe(III), Co(II), Ni(II) and Cu(II) and the solid complexes isolated were characterized using spectral and magnetic techniques. The results are presented below.

I.3c.1 Experimental

Details regarding the preparation and spectral characterization of the ligand are given in chapter II.

1.3c.1.1 Preparation of the complexes

About 0.03 mol of the ligand was dissolved in 1:1 ammonia solution. Excess of ammonia was boiled off by heating on a water bath. It was then filtered and to this solution, metal salt solution (0.01 mol) was added. The precipitate thus formed was filtered, washed and dried over P_4O_{10} under vacuum.

1.3c.2 Results and discussion

1.3c.2.1 Elemental Analyses

Metal content in the complexes was estimated as described earlier (chapter II).Carbon, hydrogen and nitrogen were determined by microanalytical methods. The analytical data and physical characteristics are given in Table III.13.

Table III.13
Analytical and Physical characteristics of (AUAcAcA) complexes

Complex	Colour	Metal %	Anion %	C%	H%	N%
Fe(AUAcAcA)ClOH	Green	13.12 (13.21)	8.30 (8.38)	40.38 (39.75)	2.77 (2.60)	15.99 (16.56)
Co(AUAcAcA)Cl	Brown	16.55 (17.09)	13.85 (14.38)	41.92 (41.01)	2.97 (2.69)	8.67 (8.72)
Ni(AUAcAcA)Cl	Green	17.01 (17.10)	14.22 (14.33)	41.56 (41.03)	2.77 (2.69)	8.31 (8.66)
Cu(AUAcAcA)Cl	Green	16.75 (16.98)	15.13 (15.42)	40.82 (40.75)	2.81 (2.67)	8.53 (8.60)

The analytical data show that the complexes have the empirical formulae Fe(AUAcAcA)ClOH, Co(AUAcAcA)Cl, Ni(AUAcAcA)Cl and Cu(AUAcAcA)Cl. The data suggests that the ligand function as monoanionic in all the complexes.

I.3c.2.2 Electrical conductance

The electrical conductances of the complexes in methanol (10^{-3} M) are given in Table III.14. The molar conductance values of all the complexes are much less than that expected for 1:1 electrolytes.

Table III.14
Magnetic and Conductance data of AUAcAcA complexes

Complex	Magnetic moment μ_{eff} (BM)	Conductance* Λ_{M}**	Nature of the electrolyte
Fe(AUAcAcA)Cl OH	5.65	31	Non-electrolyte
Co(AUAcAcA)Cl	4.91	20	"
Ni(AUAcAcA)Cl	3.10	17	"
Cu(AUAcAcA)Cl	1.59	10	"

*10^{-3}M solution (methanol) **$ohm^{-1}cm^2\ mol^{-1}$

I.3c.2.3 IR spectra and bonding

The IR spectrum of the ligand in the region 3200-3500 cm^{-1} is complicated due to the presence of several NH and OH groups. The spectrum shows three bands in the region 3270-3410 cm^{-1}. These can be attributed to NH stretching vibration. The band at 1713 cm^{-1} is assigned to free C=O of the acetoacetanilide moiety. The band at 1600 cm^{-1} can be assigned to C=N and a band at 1650 cm^{-1} to hydrogen bonded C=O. The $\nu_{C=O}$ of the ring is observed at 1633 cm^{-1}. In the spectra of the complexes the free C=O frequency is shifted to about 1670 cm^{-1}. Therefore, this C=O is one of the coordination

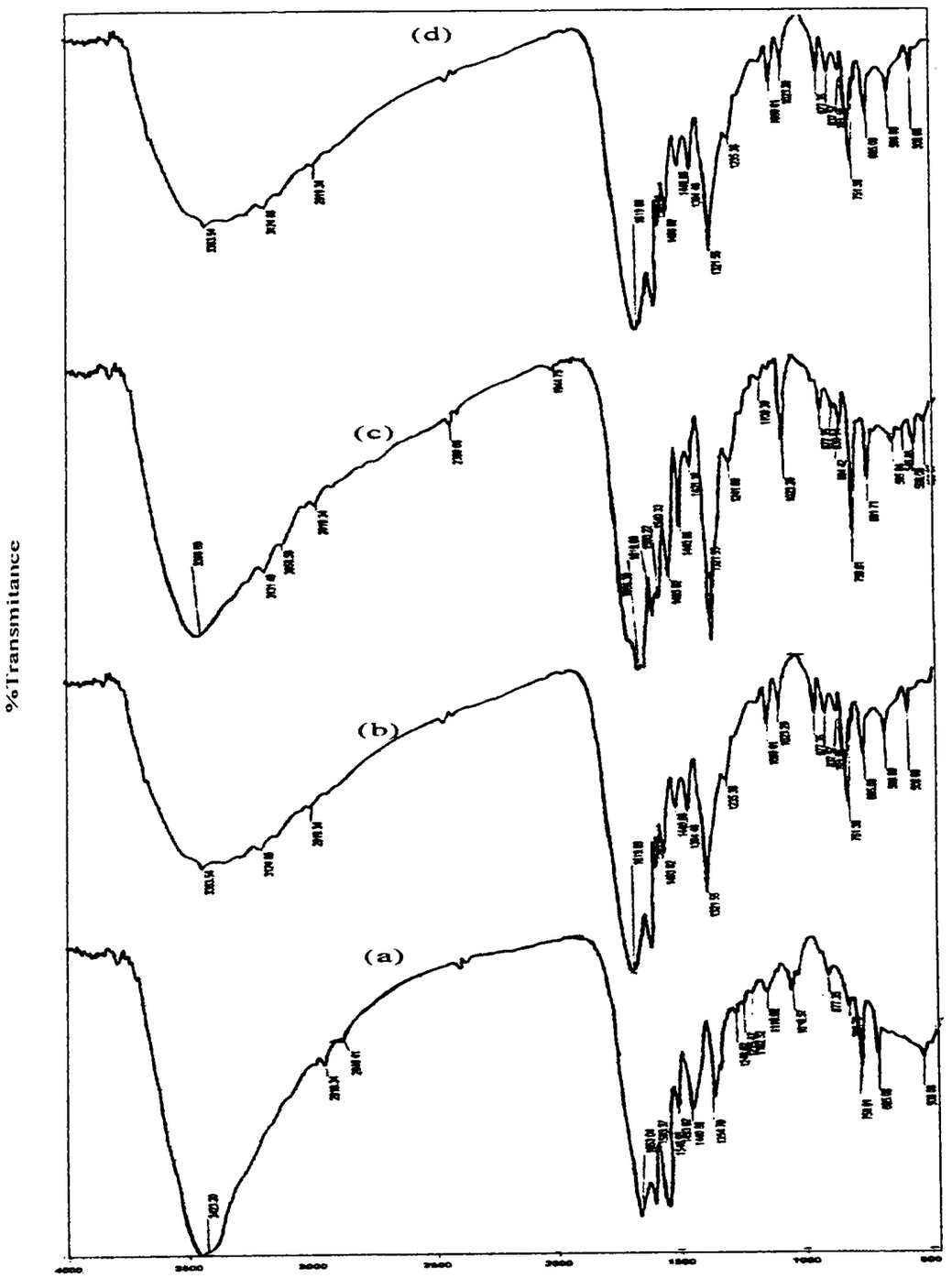

Figure I.3c.2 IR Spectra of (a) Fe (AUAcAcA)ClOH (b) Co(AUAcAcA)Cl
(c) Ni(AUAcAcAcA)Cl (d) Cu(AUAcAcA)Cl

sites. The ν_{CN} at 1600 cm^{-1} is shifted to 1546 cm^{-1} in the complexes. The spectra of the complexes show a broad band at 3425 cm^{-1} having shoulders on the lower energy side of this band. The structure of the bands in this region shows a definite change on complexation. It is likely that hydrogen of one of the NH groups other than those on the ring is deprotonated and bonded to the metal. Thus AUAcAcA acts as a monovalent tridentate ligand in the complexes. The ring $\nu_{C=O}$ remains without any change in the spectra of the complexes. The -OH stretching frequency of the -OH group present in the Fe(III) complex could not be precisely located as the band is probably merged with the -NH stretching frequencies. The band at 1008 cm^{-1} is shifted to higher wavenumbers in the spectrum of the complexes. The IR spectral bands and their probable assignments are given in the Table III.15 and the spectra are presented in Fig. I.3c.2

I.3c.2.4 Magnetism

The effective magnetic moment values are given in Table III.14. The Fe(III) complex shows a magnetic moment value of 5.65 BM which is lower than the spin only value for five unpaired electrons. The magnetic moment value clearly indicates the presence of metal-metal interaction in the complex. The complex may have an octahedral structure due to the interaction between two molecular species of the complex.

The magnetic moment observed for the Co(II) complex is 4.91 BM. This value is much higher than the spin only value expected for high spin Co(II). The value is nearer to the value expected for the octahedral Co(II). The electronic spectral values also support this configuration. The magnetic moment observed for the Ni(II) complex is 3.10 BM. This value is expected for a distorted tetrahedral complex [26].

The magnetic moment shown by the present Cu(II) complex clearly shows the presence of copper-copper interaction.

Table III.15
IR Spectral bands of AUAcAcA and their complexes.

AUAcAcA	Fe(AUAcAcA)ClOH	Co(AUAcAcA)Cl	Ni(AUAcAcA)Cl	Cu(AUAcAcA)Cl	Assignments
3350m	3409sb	3409sb	3396sb	3363sb	ν_{NH}
2926m	2919m	2925m	2920m	2919m	
1713vs	1670s sh	1680s	1690s	1670s sh	$\nu_{C=O}$(free)
1650s	1653s	1660s	1666s	1620s	$\nu_{C=O}$(H-bonded)
1633s	1546s	1553s	1560s	1546s	$\nu_{C=N}$
1600s	1593s	1606s	1619s	1600s	$\nu_{C=O}$(ring)
1540s	1546s	1553s	1540s	1546s	δ_{NH}
1487m	1493m	1487s	1493m	1494m	δ_{NH}
1447m	1440m	1447m	1440s	1440m	$\nu_{C=C}$
1348m	1355m	1328m	1321m	1322m	δ_{NH}
1295m	1248m	1241m	1242m	1235m	
1155w	1116w	1128w	1109w	1070w	ν_{sym}C-C
1008	1016	1009	1023	1023	ν_{N-N}
751w	758m	758w	758m	751w	
678w	685w	698w	691w	685m	π_{CH}
519w	506m	499w	506w	506w	

Sb-strong broad; m-medium; s sh-shoulder; s-strong; w-weak

I.3c.2.5 Electronic spectra and structure

The electronic spectral bands of the present complex along with their probable assignments are given in the Table III.16 and the spectra are presented in Fig. III.14.

Table III.16
Electronic Spectral data of AUAcAcA complexes

Complex	λ_{max} nm	ν_{max} cm^{-1}	Assignments
Fe(AUAcAcA)Cl(OH)	330	30300	$\Pi \rightarrow \Pi^*$
	430	23250	Charge tranfer
Co(AUAcAcA)Cl	340	29410	$\Pi \rightarrow \Pi^*$
	425	23530	Charge transfer
	530	18870	$^4T_{1g}(F) \rightarrow {}^4T_{1g}(P)$
Ni(AUAcAcA)Cl	330	30300	$\Pi \rightarrow \Pi^*$
	420	23800	Charge transfer
	650	15380	$^3T_1(F) \rightarrow {}^3T_1(P)$
Cu(AUAcAcA)Cl	320	31250	$\Pi \rightarrow \Pi^*$
	430	23250	Charge transfer
	700	14280	$^2E_g \rightarrow {}^2T_{2g}$

The electronic spectra of all the complexes show a intra ligand band around 330nm and a charge transfer band around 430nm. In addition to these Co(II), Ni(II) and Cu(II) complexes show bands in the visible region assignable to d-d transition. The spectrum of the present Co(II) complex is characteristic of octahedral Co(II). The magnetic data is also of support of octahedral geometry for this complex. The spectrum of the Ni(II) complex shows a d-d band at 650 nm (15380 cm^{-1}). This band is assignable to $^3T_1(F) \rightarrow {}^3T_1(P)$ of octahedral Ni(II). The Cu(II) complex shows a broad band with a band maximum at 700nm (14280 cm^{-1}). This can be assigned to the overlapped split components of $^2E_g \rightarrow {}^2T_{2g}$ due to tetragonal distortion.

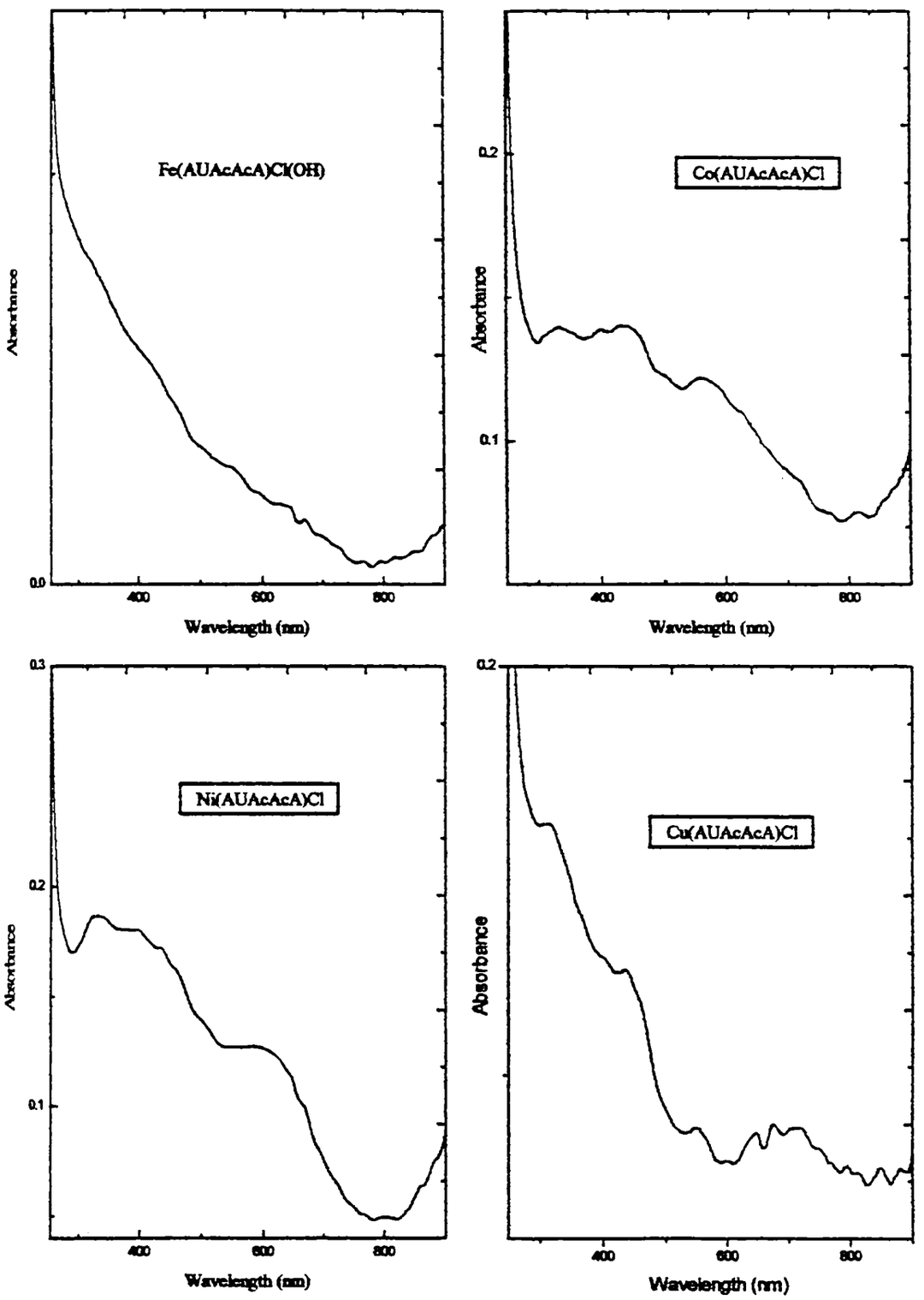

Figure III. 14 Electronic Spectra of AUAcAcA complexes

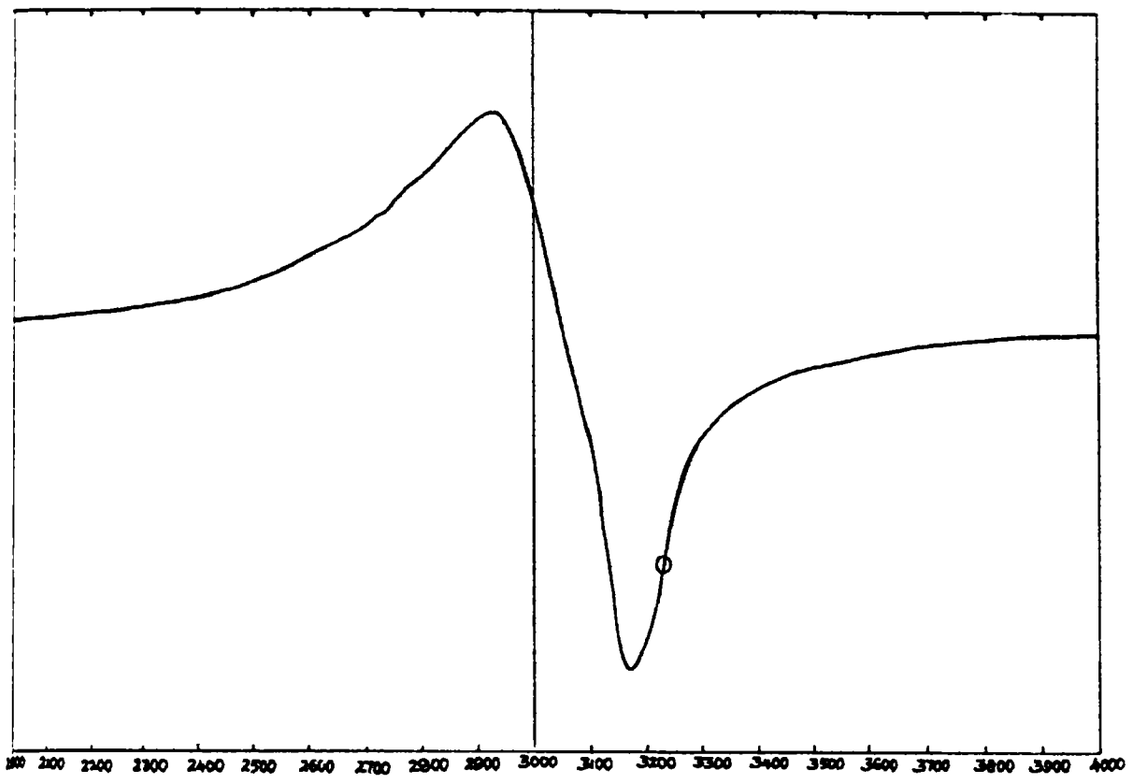

Figure I.3c.5 EPR Spectrum of Cu(AUAcAcA)Cl

I.3c.2.6 EPR Spectral studies

The EPR data for the copper(II) complex is presented in Table III.17 and the spectra is presented in Fig I.3c.4

Table III.17
The EPR data of Cu(AUAcAcA)Cl

EPR parameter	Values for Cu(AUAcAcA)Cl
$g_{\|\|}$	2.4532
$A_{\|\|}$	$144.98X10^{-4}$
$g_{\|\|}/A_{\|\|}$	169.21cm
$g_{\perp}$	2.117
$A_{\perp}$	$29.65X10^{-4}$
α^2	0.946
μ_{eff}	1.94

I.3c.2.7 TG Studies

The TG curves of AUAcAcA complexes are given in Fig. III.16 and the thermal data is given in Table III.18.

Fe(III) complex decomposes in two stages, the first major decomposition starts at 105°C and continues upto 332°C. The second stage is from 332 to 522°C. After this temperature there is no weight loss upto 1000°C. The Co(II) complex is stable upto 174°C and then decomposes in two stages. The first stage is from 174 to 342°C and the second stage is from 342 to 469°C. The decomposition is complete at this temperature and there is no weight loss from this temperature upto 1000°C.

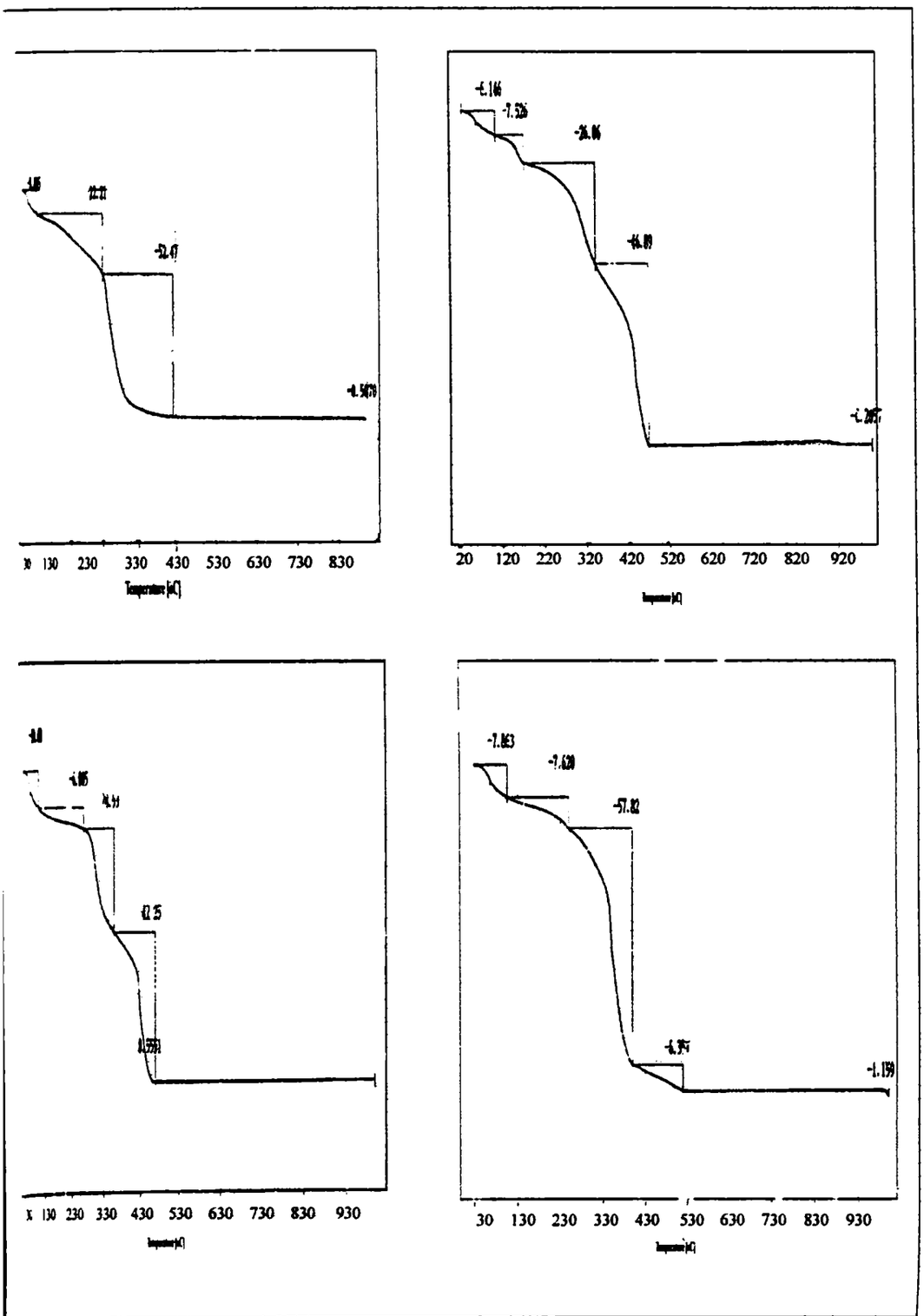

Figure I.3b.3 T.G Curves of (a) Fe(AUAcAcA)Cl OH (b) Co(AUAcAcA) Cl
(c) Ni(AUAcAcA) Cl (d) Cu(AUAcAcA)Cl

Table III.18
TG data of AUAcAcA complexes

Complex	Stability (°C)	Major decomposition stages
Fe(AUAcAcA)Cl(OH)	105	105-332 332-522
Co(AUAcAcA)Cl	174	174-342 342-469
Ni(AUAcAcA)Cl	271	271-360 360-470
Cu(AUAcAcA)Cl	250	250-399

For the Ni(II) complex is stable upto 271°C. Major step of decomposition starts at 271°C and is completed at 360°C. The next decomposition starts from 360°C upto 470°C and there is no weight loss further this temperature. Cu(II) complex is stable upto 105°C and there is only one major decomposition temperature which starts at 250°C and continues upto 399°C.

Thus complexes are all stable above 100oC. Very small weight loss is seen in the case of all the complexes from room temperature onwards this small weight loss is due to the loss of moisture adsorbed on the complexes. The IR spectrum of the complexes at that of the first major decomposition stage is similar to that of the complexes indicating that the decomposition of the ligands has not begun at this stage. The TG data indicate the stability order of the complexes as follows: Ni > Cu > Co > Fe.

References

1. J.A.Walmsley, S.V.Tyree, *Inorg. Chem.*, 2 (1963) 312.
2. J.Lewis, F.E.Mabba, Richards, *J. Chem. Soc. A.*, 1064 (1967).
3. A.H.White, R.Roper, E.Kokot, H.Watermann, R.L.Martin, *Aust.*, 17 (1964) 295.
4. M.F.Tweedle, L.J.Wilson, *J. Am. Chem. Soc.* 98 (1976) 4524.
5. E.K.Barefield, D.H.Busch, S.M.Nelson, *Quart. Rev.*, 22 (1963) 457.
6. R.L.Martin, A.H.White, *Inorg. Chem.*, 6 (1967) 712.
7. R.L.Cartin, *Transition Metal Chemistry*, R.L.Cartin(Eds.) Mercel Dekker Inc. NewYork (1965).
8. B.Chiswell, S.E.Livingstone, *J. Chem. Soc.*, 97 (1960)
9. B.N.Figgis, J.Lewis, *Progress in Inorganic Chemistry*, F.A.Cotton (Ed.) Interscience, NewYork., 6 (1964) 37.
10. A.V.Ablov, N.V.Gerbeleu, B.T.Oloi, *Russ. J. Inorg. Chem.*, 15 (1970) 1405.
11. A.B.P.Lever, *Coord. Chem. Rev.*, 3 (1958) 19.
12. B.N.Figgis, *Nature*, 182 (1958) 1568.
13. S.N.Shetti, A.S.Murthy, G.L.Tembe, *Transit. Met. Chem.*, 18 (1993) 467.
14. D.X.West, R.M.Makeever, J.P.Scovill, D.L.Klayman, *Polyhedron*, 3 (1984) 947.
15. C.J.Ballhausen, *Introduction to Ligand Field Theory*, Mc Graw-Hill, NewYork (1962).
16. L.M.Reitt, W.A.Baker, Erickson, *J. Am. Chem. Soc.*, 90 (1968) 4794.
17. M.Brance, P.Checconi, B.Pispisa, *J. Chem. Soc. Dalton Trans.* (1976) 481.
18. D.M.L.Goodgame, M.Goodgame, F.A.Cotton., *J. Am. Chem. Soc.* 83 (1961) 4161.

19. W.Manch, W.C.Fernalius, *J.Chem. Educ.*, 38 (1961) 192.

20. L.F.Larkworthy, K.C.Patel, *J. Inorg. Nucl. Chem.*, 32 (1970) 1263.

21. D.Kivelson, R.Neiman, *J. Chem. Phys.*, 35 (1961) 149.

22. V.C.Swett, E.P.Dudek, *J. Phys. Chem.*, 72 (4) (1968) 1244.

23. J.H.Flynn, *Thermal analysis*, Proceedings 2nd International Conference, Worcester, Academic Press, New York (1968) 2.

24. J.Sestak, V.Satava, W.W.Wendlandt, *Thermochim. Acta.*, 7 (1973) 33.

25. F.H.Urena, N.A.I.Cabeza, M.N.M.Carretero, A.L.P-Chamorro, *Acta. Chim. Slov.*, 47 (2000) 481.

26. F.A.Cotton, G.Wilkinson, *Advanced Inorganic Chemistry*, 5th edition, Wiley, New York (1988) 747.

Part II

Chapter I

INTRODUCTION

The economic advancement of any country is dependent on its industrial development. For the comfortable living in a modern society there is need for the production of new materials which will cater the needs of a variety of industries. It is in this context, the importance of chemical industries becomes obvious. Materials have to be produced in large quantities and at reasonable speed and at economically viable routes. The relevance for the search for suitable catalysts is to provide selectivity and high yield and at the same time to decrease the energy requirement. Development of suitable catalyst systems has helped in controlling the chemical reactions to minimize pollution level[1,2]. Industrial catalysts can be broadly classified into two types: homogeneous and heterogeneous, and both of these have been extensively used in industries. Heterogeneous catalysts, mainly metals and metal oxides, are used for the production of highly useful chemicals in large quantities [3-7]. Homogeneous catalysts operate at milder temperature and pressure conditions and exhibit high selectivity. Metal complexes and organometallic compounds are excellent homogeneous catalysts which find application in the preparation of valuable chemicals in very pure state. However, homogeneous catalysts have several disadvantages over heterogeneous catalysts. The major difficulty

encountered in the case of homogeneous catalysts is separation of the products and reactants.

II.1.1 Heterogenization of homogeneous catalysts

For the industrial application of a homogeneous catalyst it is important to get good strategies for the catalyst-product separation and catalyst recycling. The reaction system should be multiphasic for these purposes. Several types of heterogeneous catalytic reactions are developed using heterogenized homogeneous catalysts. The heterogeneous catalysts include supported metal complexes, zeolite-encapsulated complexes, colloidal nanoparticles and intercalated metal complexes.

One important method of heterogenization is by anchoring the organometallic complexes on the support through a bond between the metal and an atom on the surface of the support. Many such catalysts have been prepared by anchoring carbonyl clusters on supports [3-5, 8]. Due to the structural changes taking place on bonding of the metal atom of the cluster to the support, the reactivity of these catalysts will be different from the reactivity of the parent clusters. Even though these types of catalysts have the advantages of both heterogeneous and homogeneous systems they are unstable and often disintegrate under drastic reaction conditions.

Another method of heterogenization is to anchor the homogeneous metal complex to the solids – usually metal oxides or organic polymers by binding one or more ligands. The advantage is that the metal sites are away from the atoms co-ordinated to the metal. There are two ways in which this can be achieved. In one method, the solid surface is functionalized and the complex is fixed by ligand exchange [9]. In the other method, the

complex containing functionalized ligand is reacted with the solid surface to form supported complex [10]. These supported complexes retain the activity of the metal complex. However, the metal complexes get leached in liquid phase reactions. Sometimes there is a possibility of this catalyst getting aggregated to form binuclear species.

In yet another method of heterogenization, the complexes are supported on liquid phase. The reactions can be catalyzed in biphasic medium where the separation of the catalyst from the reactants and products become easy. Therefore, metal complex catalysts supported on liquid phase have been extensively used [11-15]. The success of the use of this type of catalyst depends on factors such as solubility of the reactants in catalyst phase metal leaching etc.

II.1.2 Zeolite encapsulated metal complexes

Zeolites are well suited for the preparation of encapsulated complexes by virtue of the large supercages. Zeolites which are aluminosilicates consists of a network of SiO_4 and AlO_4 tetrahedra joined through shared oxygen bridges. The large cavities resulting through such networking is called α-cages and the small ones are known as β-cages. Eventhough the basic building blocks of the zeolite is a sodalite unit, a cubooctahedran, the difference in the arrangement of these units give three different varieties of zeolites A, X and Y. These differ in SiO_2/Al_2O_3 mole ratio and cage dimensions. In synthetic zeolites, the net negative charge on the lattice is balanced by protons which can be exchanged with desired transition metal ions. In X and Y zeolites, the α-cage diameter is 13 Å and therefore complexes having 10-13 Å diameter can be synthesized inside the α-

cage. Since the openings to the cages are small complexes get trapped inside. Reactant molecules can enter the cavity, undergo reaction at the active metal site and emerge as products. The encapsulated complexes have several advantages over the homogeneous metal complex catalysts. They can withstand higher temperature. Their activity is sometimes more than the parent complex, and the sieving and orienting properties of the zeolite network make them highly selective. Above all these, separation of catalysts from the reactants and products is easy. Thus the encapsulated metal complex catalysts combine the features of both the guest molecule and the host lattice.

Early works on the encapsulated metal complexes have been on monodentate based complexes. Excellent reviews on this topic are available [16,17]. More recently work on polydentate ligand complexes has been reported. These include the encapsulated complexes of ethylenediamine, tetraethylene pentamine, DMG, phenanthroline, bi and terpyridine and some Schiff base complexes [18-21].

Zeolites themselves have considerable catalytic properties and have been used to catalyse a large number of reactions [22-24]. An important application of zeolite catalyst is in cracking reactions [25].

II.1.3 Catalysis by zeolite encapsulated metal complexes.

Metallo-phthalocyanins encaged in zeolites have been proposed as enzyme mimics [26]. Zeolite encapsulated iron phthalocynanine (FePc) catalysts have been used in hydrocarbon oxidations. The resistance of the zeolite-encaged complexes against oxidative destruction was found to far exceed than that of free iron phthalocyanins [27, 28]. Herron studied the oxidation of cyclohexane/cyclododecane (CHx)/(CDo) mixture with

iodosobenzene on FePc encaged in zeolite Y. Over free FePc, the bulkier reactant CDo is oxidized three times faster than the smaller one (CHx). By contrast, if the complex is encapsulated in zeolite NaY, cyclohexane is preferentially oxidized. This can be attributed to reactant shape selectivity [29]. Again over the free iron phthalocyanine the oxidation of n-octane occurs with equal selectivities in 2, 3 and 4 positions (oxidation in 1-position is not observed). Encapsulation of the complex in zeolite Y results in the preferred oxidation towards the end of the alkane chain which is an example of regioselectivity[29,30]. Stereoselectivity was reported in the epoxidation of stilbene. Whereas the trans form is preferentially epoxidised over Mn(salen)Y, FePcY and Fe(*t*-butyl) PcY, *cis*-stilbene is more easily oxidized in homogeneous catalysis[31,32]. Zeolite encapsulated iron phthalocyanine was also proved to be an active and stable catalysts in the oxidation of hydroquinone and in the triple catalytic oxidation of 1-decene and cyclohexene. Product distribution, selectivity and yield were similar to those obtained with free iron phthalocynanine. The oxidation of hydroquinone occurs in the zeolite domain, but the other reactions take place more probably in the bulk liquid [33].

[$Cu(His)_2$] systems in zeolite Y , the first example of immobilized transition metal ion aminoacid complexes in zeolites, is formed by a simple ion exchange method and it resulted in the formation of a typical coordination geometry frequently encountered in biological Cu proteins. The presence of a free coordination site opens the way for an oxidation catalyst at relatively low temperature in the presence of peroxides especially olefin epoxidations and alcohol oxidations[34]. One of the most extensively studied systems has been zeolite encapsulated (salen) manganese(III) complexes, which have served as efficient epoxidation catalysts in both the homogeneous and heterogeneous phases [35-37].

EPR spectroscopy has been used to provide an unequivocal evidence for the encapsulation of copper and manganese Schiff base salen and saloph (saloph=N,N'-bis(salicylidene)-1,2-phenylenediamine) complexes inside the super cages of zeolite Y. EPR spectroscopic studies suggests that the distortion in molecular geometry arising out of encapsulation and the consequent depletion of electron density metal site are the probable causes for enhanced catalytic activity of the zeolite encapsulated copper and manganese complexes [38]. Mn(III) and Mn(IV) Schiff base complexes in zeolite Y have been synthesized by established synthetic procedures. EPR measurements indicated that aerial oxidation has transformed some of the Mn(II) cations to Mn(III). Electrochemical techniques were used to specifically probe the fraction of electroactive species present in the outermost layers of the zeolite particles and revealed that Mn(III) is the prominent species. These complexes are the most accessible and active in heterogeneous catalytic reactions in the liquid phase, and so the voltammetric measurements provide important information concerning the specific evolution of the reversible Mn(III)/Mn(II) redox couple near the surface of the zeolite particles. Also, Mn(II) is EPR active whereas Mn(III) is EPR inactive. Thus for a given total amount of manganese, the oxidation of Mn(II) to Mn(III), either complexed or un complexed can be conveniently followed by monitering the decrease in the area of Mn(II) EPR signal [39].

Encapsulated Cu(II) and Co(II) complexes act as good oxidation catalysts. The complex [Cu(salen)], encapsulated in the supercages of zeoliteY was shown to be a catalyst for the selective oxidation of cyclohexanol to cyclohexanone in the presence of hydrogen peroxide under milder condition (80°C) [40]. Co(salophen)-zeolite catalyst prepared using template synthesis method was proved to be active in the ruthenium-

catalysed oxidation of benzyl alcohol. It was found that the choice of the solvent was not so critical as in the case of free complex and the oxidation rate is higher than the free complex [41]. Bedioui et al. have synthesized metal Schiff base complexes inside the supercages of zeolite and studied the electron transfer mechanism and their electrocatalytic applications [42-46].

The catalytic behaviour of the entrapped bulky transition metal complexes has been investigated in the stereoselective epoxidation of (-)-α-pinene. In most cases conversion of 100% could be achieved [47]. The optically pure compounds have got a steadily increasing demand in the pharmaceutical and agrochemical field. The use of chiral catalysts is thus important in synthetic organic chemistry. Very recently various reports claiming the occlusion of chiral catalyst in the pore structure of faujasite type zeolites Y and EMT have been published [48-52].

The photophysical and photochemical properties of $[Ru(bpy)_3]^{2-}$ in the supercages of zeolite Y have been studied in detail [53-60]. Electrochemical studies of the zeolite Y encapsulated $[Ru(bpy)_3]^{2+}$and $[Fe(bpy)_3]^{2+}$ complex coated electrodes and their electron transfer processes at the coated electrode were studied. The result of the zeolite encapsulated metal complex coated electrodes support the extrazeolite electron-transfer mechanism. They are also found to be photoactive [61].

Spin cross over phenomena was observed in zeolite encapsulated complexes. The complex cation, Co(II)tris(bipyridyl) encapsulated in the zeolite Y supercage exhibits thermally driven interconversion between a low-spin and a high spin state- a phenomenon not observed for this either in solution or in the solid state[62].

The zeolite encapsulated complexes have been used in a variety of industrially important reactions. Trinuclear, μ_3-oxo mixed metal acetate complexes encapsulated in zeolite Y, exhibit high catalytic activity in the selective aerial oxidation of para xylene to terephthalic acid [63]. Zeolite encapsulated binuclear complex of 3-formylsalicylicacid (fsal) is a novel solid catalyst system for the partial oxidation of organic compounds. Encapsulated Cu(II) complex is catalytically very efficient as compared to Co(II) and Ni(II) complexes for the partial oxidation of benzyl alcohol and ethylbenzene and is stable to be recycled without much deterioration [64].

Reaction of a nitrene donor with an alkene to yield an aziridine has been much less studied. The first metal catalysed nitrogen atom transfer process observed involved the reaction of benzene sulphonyl azide with cyclohexene [65]. Mansuy and co-workers showed that styrene could react with a nitrene precursor (N-(p-tolylsulfonyl)imino)phenylio-dinane, PhI=NTs to form the aziridine in 80% yield with Mn(III)-derived porphyrin catalysts [66, 67]. Evans et al. showed that Cu^{2+} cations in solution can act as an efficient catalyst for the aziridination of alkenes using the same nitrene donor [68]. Assymmetric heterogeneous aziridination of alkenes is possible using Cu exchanged zeolite modified with a chiral bis(oxazoline) ligand [69, 70]. Transition metal exchanged zeolite Y (Cr, Mn, Fe, Co, Ni, Cu, Zn) are compared as catalysts for the aziridination of styrene using PhI=NTs as the nitrene precursor. It was found that Cu exchanged zeolite Y is the best aziridination catalyst, but it is found that other metal exchanged zeolites are also catalytically active [71].

References

1. G.Kim, *Ind. Eng. Chem. Prod. Res. Dev.*, 21 (1982) 267.
2. W.B.Williamson, J.C.Summers, J.F.Skowron, "*Catalyst technologies for Future Automotive Emission systems*", SAE Transactions Paper 880103, 97 (1988) 341.
3. J.Haber, *Pure & Appl. Chem.*,66 (8) (1994)1597.
4. H.Heinemann, *Stud. Surf. Sci. Catal.*, 101 (1997) 69.
5. P.G.Menon, *Chem. Rev.*, 94 (1994) 1021.
6. M.V.Twigg (Ed),"*Catalyst Handbook*", Wolfle Publishing, London (1989).
7. J.R.Jennings, (Ed),"*Catalytic Ammonia Synthesis-Fundamentals and Practice*", Plenium Press, New York (1991).
8. D.Antolovik, E.R.Davidson, *J. Am. Chem. Soc.*, 109 (1987) 5828.
9. F.A.Cotton, G.Wilkinson, *Advanced Inorganic Chemistry*, 5th edition, Wiley Interscience, New York (1988) 1224.
10. J.Smidt, W.Hafner, R.Jira, J.Sedlmeier, R.Sieber, R.Ruttinger, H.Kojer, *Angew. Chem.*, 71 (1959) 176.
11. G.W.Parshall, *Homogeneous catalysis*, Wiley Interscience, New York (1980).
12. J.F.Roth, J.H.Graddock, A.Hershman, F.E.Poullk, *Chem. Tech.*, 1 (1971) 600.
13. R.L.Pruett, *Ann. N.Y. Academy Sci.*, 295 (1977) 239.
14. W.C.Scidel, C.A.Tolman, *Ann. N.Y. Academy Sci.*,415 (1983) 201.
15. W.S.Knowles, *Acc. Chem. Res.*, 16 (1983) 106.
16. J.H.Lunsford, *Catal. Rev. Sci. Eng.*, 12 (1975) 137.
17. G.A.Ozin, C.Gil, *Chem. Rev.*, 89 (1989)1749.
18. J.H.Lunsford, *Rev. Inorg. Chem.*,9(1987)1.

19. B.V.Romanovsky, *Macromol. Symp*, 80 (1994)157.

20. R.Parton, D.de.Vos, P.A.Jacobs, *Zeolite Microporous Solids, Synthesis, Structure and Reactivity*, E.G.Derouane, F.Lemos, C.Naccache, F.R.Ribeiro (Eds), Kluwer Academic Publishers, Dordrecht, The Netherlands (1992) 555.

21. J.Weitkamp, *Proceeds from the Ninth International Zeolite Conference*, R.Von.Ballmoss, J.B.Higgins, M.M.J.Treacy (Eds) Butterworth-Heinemann, Boston, 1 (1993) 13.

22. S.M.Csicsery, *Zeolites*, 4 (1984) 202.

23. E.M.Flanigen, *Pure & Appl. Chem.*, 52 (1980) 2191.

24. C.Naccache, Y.B.Taarit, *Pure & Appl. Chem.*, 52 (1980) 2175.

25. D.W.Breck, *J. Chem. Edu.*, 41 (1964) 678.

26. G.Meyer, D.W.Wohl, G.Schulz-Ekloff, *Zeolites*, 4 (1984) 30.

27. N.Herron, G.D.Stucky, C.A.Tolman, *J. Chem. Soc. Chem. Commun.*, (1986) 1521.

28. R.F.Parton, L.Uytterhoeven, P.A.Jacobs, *Stud. Surf. Sci. Catal.*, 59 (1991) 395.

29. N.Herron, *J. Coord. Chem.*, 19 (1988) 25.

30. R.F.Parton, D.R.C.Huybrechts, Ph.Buskens. P.A.Jacobs, *Catalysis and Adsorption by Zeolites*, G.Ohlmann, H.Pfeifer, R.Fricke (Eds.), *Stud. Surf. Sci. Catal.*, Elsevier, Amsterdam Vol.65 (1991) pp 47.

31. C.Bowers, P.K.Dutta, *J. Catal.*, 122 (1990) 271.

32. M.Ichikawa, T.Kimura, A.Fukuoka, *Chemistry of Microporous crystals*, T.Inui, S.Namba, T.Tatsumi (Eds.) Stud. Surf. Sci. Catal., Elsevier, Amsterdam, Vol.60 (1991) pp 335.

33. A.Zsigmond, F.Notheisz, M.Bartok, J.E.Backvall., *Heterogeneous Catalysis and Fine Chemicals III*, M.Guisnet, J.Barbier, J.Barrault, C.Bouchoule, D.Duprez, G.Perot, C.Montassier (Eds.) *Stud. Surf. Sci. Catal.*, Elsevier, Amsterdam, Vol.78 (1993) pp. 417.

34. B.M.Weckhuysen, A.A.Verberckmoes, I.P.Vannijvel, J.A.Pelgrims, P.L.Buskens, P.A.Jacobs, R.A.Schoonheydt, *Angew. Chem. Int. Ed.*, 34 (1995) 2652.

35. E.N.Jacobsen, W.Zhang, *J. Org. Chem.*, 56 (1991) 2296.

36. S.P.Varkey, C.Ratnasamy, P.Ratnasamy, *J. Mol. Catal.*, 135 (1998) 295.

37. P.Piaggio, P.McMorn, C.Langham, D.Bethull, P.C.Bulmanpage, F.E.Hancock, G.J.Hutchings, *New J. Chem.*, (1998)1167.

38. T.H.Bennur, D.Srinivas, P.Ratnasamy, *Microporous and Mesoporous Materials*, 48 (2001) 111.

39. A.Domenech, P.Formentin, H.Garcia, M.J.Sabater, *J. Inorg. Chem.*, (2000) 1339.

40. C.Ratnasamy, A.Murugkar, S.Padhye, *Ind. J. Chem.*, 35A (1996) 1.

41. A.Zsigmond, F.Notheisz, Z.Frater, J.E.Backvall, *Heterogeneous Catalysis and Fine Chemicals IV*, H.V.Blaser et al (Eds.) (1997) 453.

42. K.Masfer, B.Carre, F.Bedioni, J.Devynck, *J. Mater. Chem.*, 3 (1993) 873.

43. F.Bedioni, E.De.Boysson, J.Devynck, K.J.Balkus Jr, *J. Electroanal. Chem.*, 315 (1991) 313.

44. F.Bedioni, E.De.Boysson, J.Devynck, K.J.Balkus Jr., *J. Chem. Soc. Faraday Trans.*, 87 (1991) 3831.

45. Gaillon, N.Sajot, F.Bedioni, J.Devynck, K.J.Balkus Jr., *J. Electroanal. Chem.*, 345 (1993) 157.

46. F.Bedioni, L.R.E.Briot, J.Devynck, S.L.Bell, K.J.Balkus Jr., *J. Electroanal. Chem.*, 373 (1994) 19.

47. C. Schuster, E.Mollmann, A.Tompos, W.F.Holderich, *Catal. Lett.*, 74 (2001) 1.

48. M.E.Leonowiez, J.A.Lawton, M.K.Rubin, *Science*, 264 (1994) 1910.

49. S.L.Lawton, M.E.Leonowiez, R.D.Partridge, P.Chu, M.K.Rubin, *Microporous and Mesoporous Materials*, 23 (1998) 109.

50. I.Guray, J.Warzywoda, N.Bac, A.Sacco Jr., *Microporous and Mesoporous Materials*, 31 (1999) 241.

51. G.G.Juttu, R.F.Lobo, *Microporous and Mesoporous Materials*, 40 (2000) 9.

52. S.L.Lawton, A.S.Fung, G.J.Kennedy, L.B.Alemany, C.D.Chang, G.H.Hatzikos, D.N.Lissy, M.K.Rubin, H.K.C.Timken, S.Steuernagel, D.E.Woessner, *J. Phys. Chem.*, 100 (1996) 3788.

53. K.Maruszewski, D.P.Strommen, K.Handrich, J.R.Kincaid, *Inorg. Chem.*, 30 (1991) 4579.

54. K.Maruszewski, D.P.Strommen, J.R.Kincaid, *J. Am. Chem. Soc.*, 115 (1993) 8345.

55. J.A.Incavo, P.K.Dutta., *J. Phys. Chem.*, 94 (!990) 3075.

56. Y.I.Kim, T.E.Mallouk, *J. Phys. Chem.*, 96 (1992) 2879.

57. J.S.Krueger, J.E.Mayer, T.E.Mallouk, *J. Am. Chem. Soc.*, 110 (1988) 8232.

58. L.Persand, A.J.Bard, A.Champion, M.A.Fox, T.E.Mallouk, S.C.Webber, J.M.White, *J. Am. Chem. Soc.*, 109 (1987) 7309.

59. W.Turbeville, D.S.Robins, P.K.Dutta, *J. Phys. Chem.*, 96 (1992) 5024.

60. P.K.Dutta, W.Turbeville, *J. Phys. Chem.*, 96 (1992) 9410.

61. V.Ganesan, R.Ramaraj, *Langmuir*, 14 (1998) 2497.

62. S.K.Tiwary, S.Vasudevan, *Chem. Phys. Lett.*, 277 (1997) 84.

63. S.A.Chavan, D.Srinivas, P. Ratnasamy, *Chem. Commun.* (2001) 1124.

64. K.O.Xavier, J.Chacko, K.K.M.Yusuff, *J. Mol. Catal. A: Chem.*, 178 (2002) 275.

65. H.Kwart, A.A.Khan, *J. Am. Chem. Soc.*, 89 (1967) 1951.

66. D.Mansuy, J.P.Mahy, A.Dureault, G.Bedi, P.Battioni, *J. Chem. Soc. Chem. Commun.*, (1984) 1161.

67. J.P.Mahy, G.Bedi, P.Battioni, D.Mansuy, *J. Chem. Soc. Perkin Trans. II* (1988) 1517.

68. D.A.Evans, M.M.Faut, M.T.Bilodeau, *J. Am. Chem. Soc.*, 116 (1994) 2742.

69. C.Langam, P.Piaggio, D.Bethell, D.F.Lee, P.McMorn, P.C.BulmanPage, D.J.Willock, C.Sly, F.E.Hancock, F.King, G.J.Hutchings, *Chem. Commun.* (1998) 1601.

70. C.Langham, S.Taylor, D.Bethell, P.McMorn, P.C.BulmanPage, D.J.Willock, C.Sly, F.E.Hancock, F.King, G.J.Hutchings, *J. Chem. Soc. Perkin Trans.II* (1999) 1043.

71. J.Gullick, S.Taylor, O.Kerton, P.McMourn, F.King, F.E.Hancock, D.Bethell, P.C.Bulman Page, G.J.Hutchings, *Catal. Lett.*, 75 (3-4) (2001) 151.

Chapter II

MATERIALS AND METHODS

II.2.1 Introduction

This chapter includes details regarding materials used for the synthesis of zeolite encapsulated metal complexes and techniques involving their synthesis and characterization.

II.2.2 Reagents used

The following metal salts were used:

$FeCl_3$ (Qualigens); $CoCl_2.6H_2O$ (Merck, GR); $NiCl_2.6H_2O$ (Nice, LR); $CuCl_2.2H_2O$ (Merck, GR)

The zeolite Y having silica to alumina ratio of 2.4 and surface area of 546 m^2/gm, used in the study was obtained from Sud-Chemie India Ltd, Binanipuram, Cochin.

tert-Butylhydroperoxide (70% w/v, Merck), cyclohexanol (Merck, LR) and chlorobenzene (Merck, LR) were used for the catalytic activity studies using encapsulated metal complexes. Gas cylinders oxygen, nitrogen and hydrogen (Sterling gases, Cochin) were also used for the catalytic studies.

LR grade acetone, methanol and acetonitrile were purified and used.

II.2.3 Ligands used for complexation in zeolite encapsulated metal Complexes

Ligands used in the synthesis of zeolite encapsulated Fe(III), Co(II), Ni(II) and Cu(II) complexes are acetylacetone-2-hydroxyphenylhydrazone (APAcAc), acetoacetanilide-2-hydroxyphenylhydrazone (APAcAcA) and acetoacetanilide-3,5-dihydro-2,4-dione pyrimidylhydrazone (AUAcAcA) respectively. The details regarding the synthesis of these ligands and their characterization are given in part I, chapter II of this thesis.

II.2.4 Synthesis of zeolite Y encapsulated metal complexes

The synthetic zeolite, HY was ion exchanged with 1M NaCl solution (500ml) under stirring for 24h at room temperature to convert any other ions if present to Na^+ ions. It was then filtered, washed until free of chloride ions, dried in an air oven and stored for further use.

In order to encapsulate the metal complexes in the zeolite cavity, at first we have to incorporate the metal complexes into the zeolite matrix. The monovalent sodium ions can be replaced with monovalent, bivalent or trivalent ions. The NaY zeolite (5g) was stirred with metal salt solution (0.007M, 500ml) at 70°C for 4h. The pH of the solution was adjusted to be below 4 since the structural frame work will collapse at higher pH. Also dealumination occurs at higher concentrations of the metal salt. It was then filtered and washed with deionised water until free of anions. The MY so obtained was dried in an air oven for 2h and finally dehydrated at 450°C for 4h.

The flexible ligand method was used for encapsulating metal complexes in zeoliteY [1]. In this approach, a flexible ligand must be able to diffuse freely through the zeolite pores but upon complexation with a previously exchanged metal ion, the complex become too large and rigid to escape the cage.

Metal exchanged zeolite MY (5g) and excess of ligand (ligand to metal ratio ~3) was mixed together in a mortar and taken in a glass ampoule. It was then sealed and heated at a temperature below the melting point of the ligand. We have to find the optimum temperature so as to effect the complexation reaction. The complex formed on the surface as well as the unreacted ligand was removed by soxhlet extraction with one or more solvents. Washing should be continued for another 24h after the extracting solvent becomes colourless to ensure the complete removal of the unwanted species. The uncomplexed metal ions in the zeolite and ionisable proton of the ligand, if present were removed by further stirring with NaCl solution (0.1M, 500ml) for 24h. It was then filtered, washed until free of chloride ions and finally dried in an air oven (100°C) for2h.

II.2.5 Physico-Chemical Measurements

II.2.5.1 Chemical Analysis to determine Si, Al, Na and transition metal ions in the zeolite samples

The procedure followed for the chemical analyses of encapsulated zeolite samples is given below.

The dried sample (~0.1g) was accurately weighed (w_1) into a beaker. The zeolite framework was destroyed by heating with conc. sulphuric acid (40ml, 98%). It was diluted and filtered through an ashless filter paper. The filtrate was collected in

a standard flask. The residue was incinerated in a platinum crucible for 1h at 1000°C and weighed (w_2). The residue was treated with hydrofluoric acid (10ml, 40%) and evaporated carefully to remove silicon as H_2SiF_6 [2]. It was then heated strongly at 1000°C, cooled and weighed (w_3). The percentage of silica was calculated using Eq. II.1.

$$\%SiO_2 = 100\ (w_3-w_2)\ /w_1 \qquad \text{(Eq. II.1)}$$

The residue in the crucible was fused with potassium persulphate, dissolved in water and was mixed with the filtrate in the standard flask. The Na, Al and the transition metal ions in the solution were determined from atomic absorption spectroscopy. The unit cell formulae of the zeolite was calculated from the Si/Al ratio [3].

II.2.5.2 Atomic absorption spectrophotometry (AAS)

Metal estimations using AAS were carried out using Perkin Elmer 3110, at Department of Chemical Oceanography, CUSAT, Cochin-16.

II.2.5.3 Elemental analyses

Microanalysis for carbon, hydrogen and nitrogen in the zeolite samples were done at RSIC, CDRI, Lucknow using Heraeus Carlo Erba 1108 elemental analyzer.

II.2.5.4 Surface Area Analyses

Surface area of the samples was measured by multipoint BET [4] method using a Micromeritics Gemini 2360 Surface area analyzer. Nitrogen gas was used as the adsorbate at liquid nitrogen temperature. It was determined using Eq. II.2.

$$\frac{1}{V(P-Po)} = \frac{1}{VmC} + \frac{(C-1)P}{VmCPo} \qquad \text{(Eq. II.2)}$$

V =Volume of the gas adsorbed at relative pressure P/ P_o

V_m=Volume of the gas in the monolayer

P_o = Saturation vapour pressure of the adsorbate at the experimental conditions.

C =a constant related to heat of adsorption and liquefaction of gas.

By plotting left side of the Eq. II.2 against P/ P_o, a straight line is obtained with a slope of (C-1)/ V_mC and an intercept $1/V_mC$. From these values, V_m and hence the number of moles of nitrogen absorbed, V_m can be calculated.

BET surface area is calculated using,

$$S_{BET} = X_m N A_m 10^{-20} \quad \text{(Eq. II.3)}$$

N = Avagadro's number

A_m = Cross- sectional area of the adsorbate molecule in Å

Pore volume of the sample at P/ P_o~0.9 is computed by converting the volume of nitrogen adsorbed at P/ P_o~0.9 to volume of liquid equivalent to it using Eq. II.4.

$$V_{tot} = V_{ads} D \quad \text{(Eq. II.4)}$$

where V_{tot} = total pore volume at P/ P_o~0.9

V_{ads} = volume of the gas adsorbed at relative pressure 0.9

D = density conversion factor.

II.2.5.5 X-ray diffraction spectroscopy

The parent zeolite and the zeolite encapsulated complexes were analyzed by Powder XRD for comparing their crystallinities. The X-ray diffractometer used in

the present investigation is Rigaka D Max C The procedural details are X-ray source, Ni filtered Cu Kα radiation (λ =1.5404) and a movable detector which scans the intensity of the diffracted radiation as a function of the angle 2θ between the incident and diffracted beams.

II.2.5.6 Scanning electron microscopy

The morphology of the samples was examined using JEOL-JSM-840A SEM at IISc, Bangalore. The SEM was taken to know whether there are any surface adsorbed species.

II.2.5.7 Magnetic measurements

The magnetic susceptibility measurements were carried out at room temperature on a simple Guoy type balance. The Gouy tube was standardized using $Co[Hg(SCN)_4]$as recommended by Figgis and Nyholm[5]. The effective magnetic moment was calculated using Eq. II.5

$$\mu_{eff} = 2.84\ (X'_mT)^{1/2}\ BM \qquad \text{(Eq. II.5)}$$

where T = absolute temperature

X'_m = molar susceptibility corrected for diamagnetism of all atoms present in the complex using Pascals constant and that of zeolite framework per unit metal.

II.2.5.8 Diffuse reflectance spectra

The diffuse reflectance spectra were recorded at room temperature in the range 250-850 nm with zeolite sample as reference using Ocean Optics, Inc. SD 2000, Fiber Optic Spectrometer with CCD detector. The spectra were computer processed and recorded. If it was plotted as percentage reflectance versus

wavelength, Kubelka-Munk[6,7] analysis has to be performed to get the spectra in the absorbance mode.

The Kubelka-Munk factor, F(R) is given by Eq. II. 6.

$$F(R) = (1-R)^2/2R = k/s \qquad \text{(Eq.II.6)}$$

where,

F(R) = Kubelka-Munk factor

R = the diffuse reflectance of the sample as compared to pure zeolite sample,

k = the molar absorption coefficient and

s = the scattering coefficient of the sample.

But in the present case the spectra were directly plotted in the absorbance mode.

II.2.5.9 Infrared spectra

Infrared spectra of the ligand and the encapsulated complexes in the region 4000-400 cm^{-1} were recorded by KBr technique using Perkin Elmer 881, IR Spectrophotometer at RSIC, CDRI, Lucknow.

II.2.5.10 EPR spectra

The X-band EPR spectrum of the powdered samples of encapsulated Cu complex was recorded at liquid nitrogen temperature using a Varian E-109 X/Q band spectrophotometer, taking tetracyanoethylene (TCNE, g = 2.0027) as a standard at RSIC, IIT, Bombay.

The μ_{eff} values were also determined from the EPR parameter by substituting g_{II} and g in the Eq. II.7

$$\mu_{eff} = g_{II}^2/4 + g_{\perp}^2/4 + 3KT/\lambda o\ (g-2) \qquad \text{(Eq. II.7)}$$

where λo is the spin of orbit coupling constant for the free metal ion.

The density of the unpaired electrons at the central metal atom was computed[8] using Eq. II.8.

$$\alpha^2_{Cu} = (A_{II}/P) + (g_{II}-2) + 3/7\ (g_{\perp}-2) + 0.04 \qquad \text{(Eq. II.8)}$$

where $1-\alpha^2$ measures the covalency associated with the bonding of metal ion to the ligand and P = 0.036.

II.2.5.11 Thermogravimetric analysis

Thermogravimetric (TG) curves of the samples were observed on a Mettler Toledo STAR^e Thermal analysis system. In all the measurements, sample mass ~ 3mg, heating rate 10°C min^{-1} and an atmosphere of N_2 (flow rate, 60ml min^{-1})were used.

II.2.5.12 Gas chromatographs

The catalytic activity studies were performed with a Chemito 8510 Gas Chromatograph equipped with a thermal conductivity detector. A carbowax column was used for separating various components in the reaction mixture.

References

1. N.Herron, *Inorg. Chem.*, 25 (1986) 4714.
2. A.I.Vogel, *A Text Book of Quantitative Inorganic Analysis*, Longmans-Green, London (1978).
3. C.Tollman, N.Herron, *Symposium in Hydroc. Oxidation*, 194th National meeting of the Am. Chem. Soc., New Orleans, LA, Aug 30-Sept 4 (1987).
4. C.N.Satterfield, *Heterogeneous Catalysis in Industrial Practice*, 2nd Edition, Mc.Graw-Hill, Singapore (1993).
5. B.N.Figgis, R.S.Nyholm, *J. Chem. Soc.* (1958) 4190.
6. H.G.Hecht, *Modern Aspects of Reflectance Spectroscopy*, W.W.Wendlandt (Ed.) Plenium Press, NewYork (1968).
7. S.K.Tiwary, S.Vasudevan, *Inorg. Chem.*,37 (1998) 5239.
8. D.Kivelson, R.Neiman, *J. Chem. Phys.*, 35 (1961) 149.

Chapter III

ZEOLITE ENCAPSULATED TRANSITION METAL COMPLEXES OF HYDRAZONES

II.3.1 Introduction

Zeolites are interesting class of microporous materials with tunable architecture and selectivity towards several catalytic reactions. These materials have attracted widespread attention in basic science as well as in technology field. Their unique physical and chemical characteristics offer opportunities for manipulation of active site micro environment. Some of the prominent physical characteristics of the zeolite are their ruggedness to temperature and pressure and their ability to recognize, discriminate and organize molecules. Because of these characteristics, zeolites are widely used in various industrial processes as catalysts for fluid catalytic cracking, hydrocracking, isomerization and polymerization reactions. These materials have more interesting applications as selective oxidation catalysts and as enzyme mimics, if metal complexes are encapsulated inside their cages. The encapsulation may increase the stability of the metal complex species avoiding degradation pathways and leading to higher turn over numbers. Further encapsulated complexes may have geometry different from that of the parent complex and may even have more vacant coordination sites. It was these considerations that prompted us to synthesize and characterize the zeolite Y encapsulated complexes of APAcAc, APAcAcA, and AUAcAcA and to study the catalytic activity of these encapsulated complexes.

II.3a.1 Experimental

Details regarding the synthesis and characterization of the ligands APAcAc, APAcAcA and AUAcAcA are given in part I, chapter II. These ligands were used for the preparation of zeolite encapsulated metal complexes. The general method of preparation of the zeolite encapsulated metal complexes is also described in part II, chapter II. The complexes were characterized using chemical analysis, SEM, XRD, surface area and pore volume, magnetic measurements, electronic, FTIR and EPR spectroscopy. Thermal behaviour was also studied using TG analysis.

II.3a.1.1 Synthesis of Fe(III), Co(II), Ni(II) and Cu(II) exchanged zeolites

Fe(III), Co(II), Ni(II) and Cu(II) exchanged zeolites were at first prepared by stirring NaY (5g) with $FeCl_3$ solution (0.001M, 500ml), $CoCl_2$ solution (0.007M, 500ml), $NiCl_2$ solution (0.007M, 500ml) and $CuCl_2$ solution (0.007M, 500ml) at 70°C for 4h. For Fe(III) a very low concentration of 0.001M solution was taken since dealumination take place at higher concentration. It was then filtered and washed with deionised water until free of anions. The MY thus obtained was dried in an air oven for 2h and finally dehydrated at 450°C for 4h.

II.3a.1.2 Analytical methods

The analytical methods and characterization techniques used are given in part II, chapter II.

II.3a.2 Results and Discussion

II.3a.2.1 Chemical analyses

The analytical data of the metal exchanged zeolite are shown in Table II.3a.1 Silica to alumina ratio was calculated using this data. Si/Al ratio of 2.43 corresponds to a unit cell formula $Na_{56}[(AlO_2)_{56}(SiO_2)_{138}]$ for NaY. The unit cell formula represents the composition of a unit cell in the metal exchanged zeolites[1].

Table II.3a.1
Analytical data of the metal exchanged zeolites

Sample	%Si	%Al	%Na	%Metal
NaY	25.64	10.73	7.52	-
FeY	25.83	10.72	7.71	1.80
CoY	25.82	10.36	6.80	3.12
NiY	24.37	10.47	6.72	1.88
CuY	25.63	10.82	7.21	3.46

The unit cell formula of FeY, CoY, NiY and CuY are given in the Table II.3a.2. Si/Al ratio remains almost the same in almost all the metal exchanged zeolites indicating that the zeolite framework is kept intact and dealumination has not taken place as a result of ion exchange. The degree of ion exchange, which is the percentage of Na^+ ions replaced by metal ions from the total amount of Na equivalent to Al content of the zeolite, is also given in the Table.

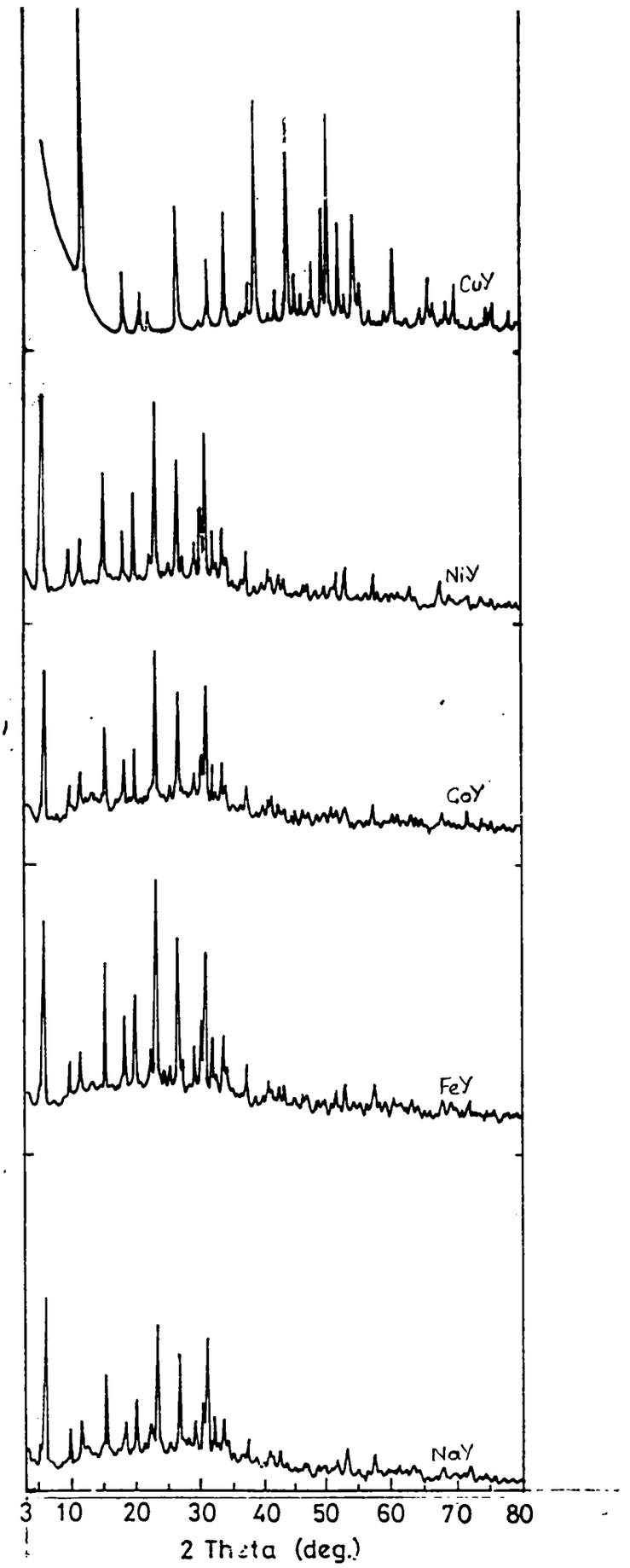

Figure II.c.1 XRD pattern of NaY and metal exchanged zeolites

Table II.3a.2
Composition of the metal exchanged zeolites

Sample	Degree of ion exchange(%)	Unit cell formula
NaY	-	$Na_{56}(AlO_2)_{56}(SiO_2)_{136}.nH_2O$
FeY	24.35	$Na_{42.36}Fe_{4.54}(AlO_2)_{56}(SiO_2)_{136}.nH_2O$
CoY	27.59	$Na_{40.54}Co_{7.7}(AlO_2)_{56}(SiO_2)_{136}.nH_2O$
NiY	16.52	$Na_{46.75}Ni_{4.62}(AlO_2)_{56}(SiO_2)_{136}.nH_2O$
CuY	27.17	$Na_{40.78}Cu_{7.61}(AlO_2)_{56}(SiO_2)_{136}.nH_2O$

II.3a.2.2 X-ray diffraction pattern.

X-ray diffraction is one of the best known techniques for finding out information about the structure and composition of crystalline materials. X-ray powder diffraction is one of the most used technique in the study of zeolites, to (i) identify the zeolite structure (finger print of individual zeolites)[2] (ii) check its phase purity, (iii) find out the crystallinity and(iv) estimate the unit cell parameters[3].

XRD patters of the parent zeolite HY and the metal exchanged zeolites are given in the Fig II.3a.1. It is found that the crystalline structure is retained in the metal exchanged zeolites. Similar observations have been made by various workers earlier[4-6]. However, it has been observed that the zeolite framework collapses[7] if the pH is less than 4.

II.3a.2.3 Surface area and Pore volume.

Surface area and Pore volume of the zeolite NaY as well as the metal exchanged zeolites (estimated by the low temperature nitrogen adsorption at relative pressure P/P0~0.9) are given in the Table II.3a.3.

Table II.3a.3
Surface area and pore volume data of metal exchanged zeolite Y

Sample	Surface are m^2/g	Pore volume ml/g
NaY	550	0.3045
FeY	540	0.2033
CoY	535	0.1913
NiY	530	0.2008
CuY	540	0.1924

There is a slight reduction in the values for the metal exchanged zeolites. This also is an indication of the retention of the zeolite crystalline structure. Pore volume (P/P_0~0.9) varies in between 0.0924-0.1013 ml/g

II.3a.2.4 IR spectra.

The IR spectra give information on the nature of the ligands (4000-1200 cm^{-1}) and on the interaction of the ions with the framework (1000-400 cm^{-1}). In ths region occurs the internal vibrations of the SiO_4 and AlO_4 groups and the external vibrations between these tetrahedra[8,9].

These vibrations are not specifically assigned to SiO_4 and AlO_4 groups but to $(Si/Al)O_4$ groups designated as TO_4. In zeolite Y, the asymmetric and symmetric stretching vibrations of the TO_4 units are respectively at 1150 and 1030 cm^{-1} and at 795 and 745 cm^{-1}. The TO_4 deformation modes are observed at 460 cm^{-1} and the deformation of the rings of 6 TO_4 units at 570 cm^{-1}.

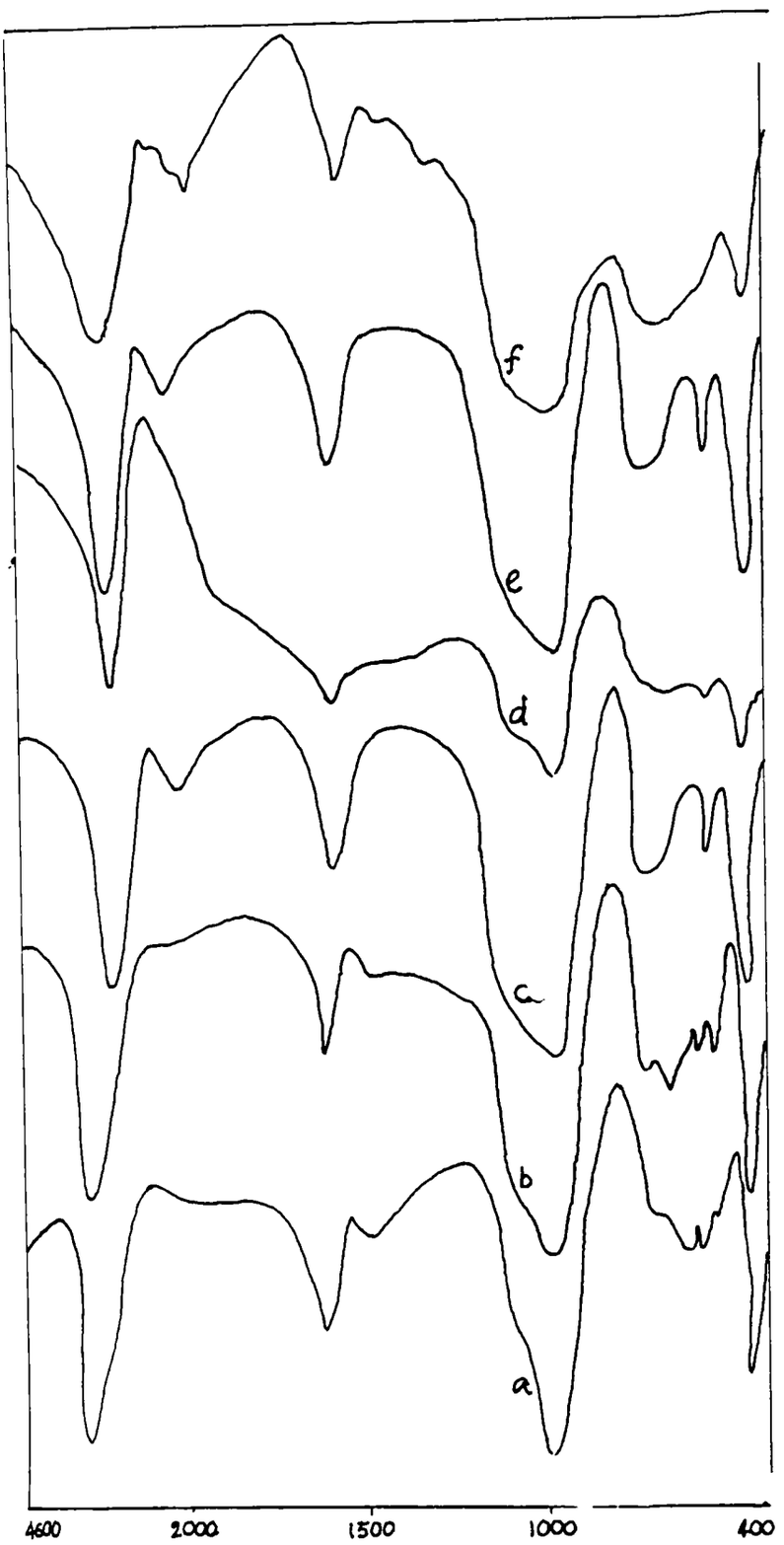

Figure II.3a.2 IR Spectra of a) HY b)NaY c)FeY d) CoY e) NiY and f)CuY

The metal exchanged zeolites and the parent zeolite give IR spectra in which bands are almost alike (Fig II.3a.2). This supports the fact that the zeolite framework is not disturbed on metal exchange with a very low concentration of metal salt solution.

II.3b Zeolite encapsulated APAcAc complexes.

II.3b.1 Experimental

Flexible ligand method[10] was used for synthesizing zeolite encapsulated APAcAc complexes of Fe(III), Co(II), Ni(II) and Cu(II). In this method a preformed ligand was allowed to react with the transition metal previously introduced into the zeolite cages. Based on the metal content in the metal exchanged zeolite, the amount of ligand was taken so as to keep the ligand to metal ratio approximately 3. The mixture was taken in an ampule, sealed and heated for 12h. The temperature was maintained at 115°C to effect complexation. A slight colour change was observed in all the cases as an indication of complexation. After complexation the zeolite is purified by soxhlet extraction with methanol. Washing is continued for another 24h even after the extracting solvent becomes colourless to ensure complete removal of the surface species. The uncomplexed metal ions are removed by further stirring with NaCl solution (0.1M, 500ml) for 24h. It was filtered washed until free of chloride ions and finally dried in an air oven (100°C) for 2h.

II.3b.2 Results and discussion

II.3b.2.1 Chemical analysis.

The analytical data of the complexes in zeolite are given in the Table II.3b.1 In all the cases Si/Al ratio is found to be 2.4. This shows that the zeolite framework is retained without any damage even after encapsulation. From the carbon, hydrogen and nitrogen percentage it is confirmed that encapsulation had taken place.

Table.II.3b.1
Analytical data of zeolite encapsulated APAcAc complexes.

Sample	%Metal	%Si	%Al	%C	%N
Fe(APAcAc)Y	0.07	26.30	10.91	0.70	0.15
Co(APAcAc)Y	0.46	20.44	8.48	1.82	0.39
Ni(APAcAc)Y	0.41	24.32	10.09	1.77	0.38
Cu(APAcAc)Y	0.30	26.33	10.93	0.49	0.10

The analytical data suggest that the empirical formulae of the encapsulated APAcAc complexes are FeL, CoL, NiL and CuL respectively.

II.3b.2.2 Scanning electron micrograph.

Scanning electron micrograph (SEM) of Fe(APAcAc)Y, before and after soxhlet extraction was taken and given in the Fig.II.3b.1 SEM taken before soxhlet extraction shows aggregates of ligand species formed on the surface, but in the SEM taken after soxhlet extraction the surface is found to be clean. During the soxhlet extraction procedures, the extraction is continued further for 24h even after the

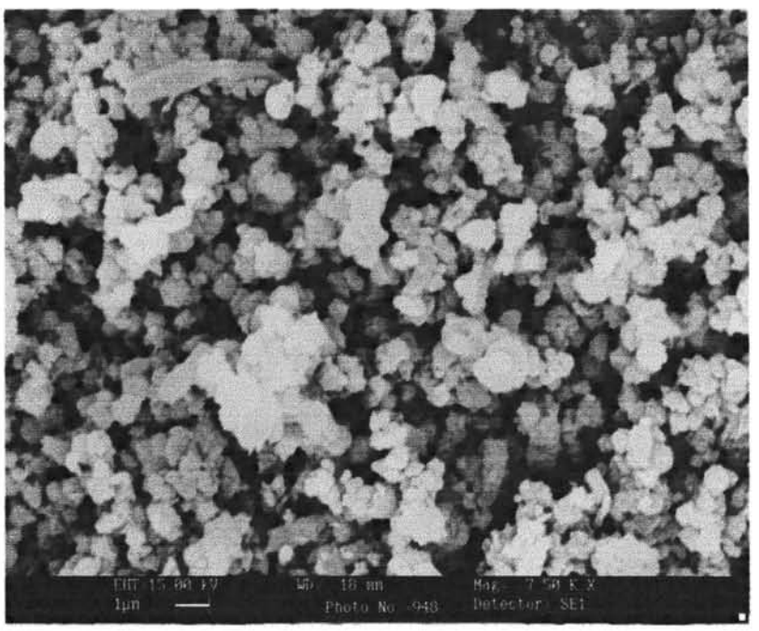

(a)

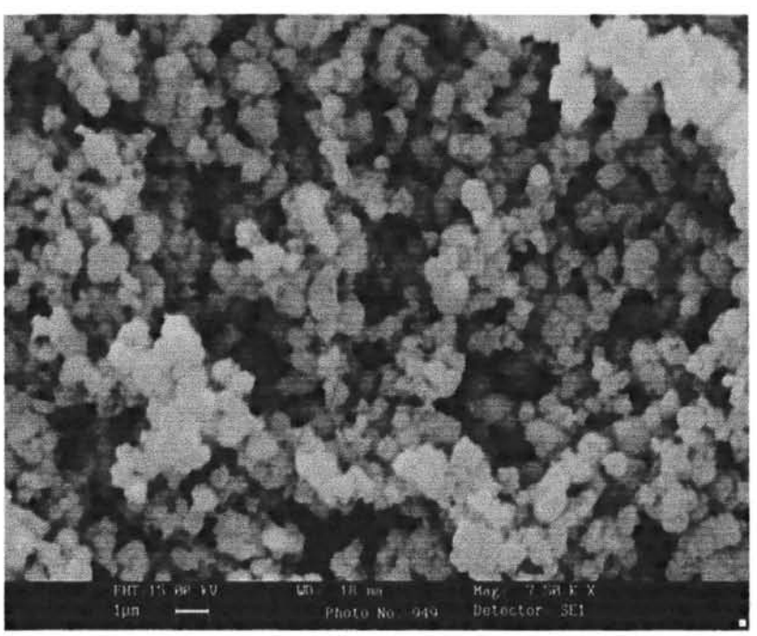

(b)

Figure II.3b.1 Scanning Electron Micrograph of Fe(APAcAc)Y
(a) before and (b) after soxhlet extraction

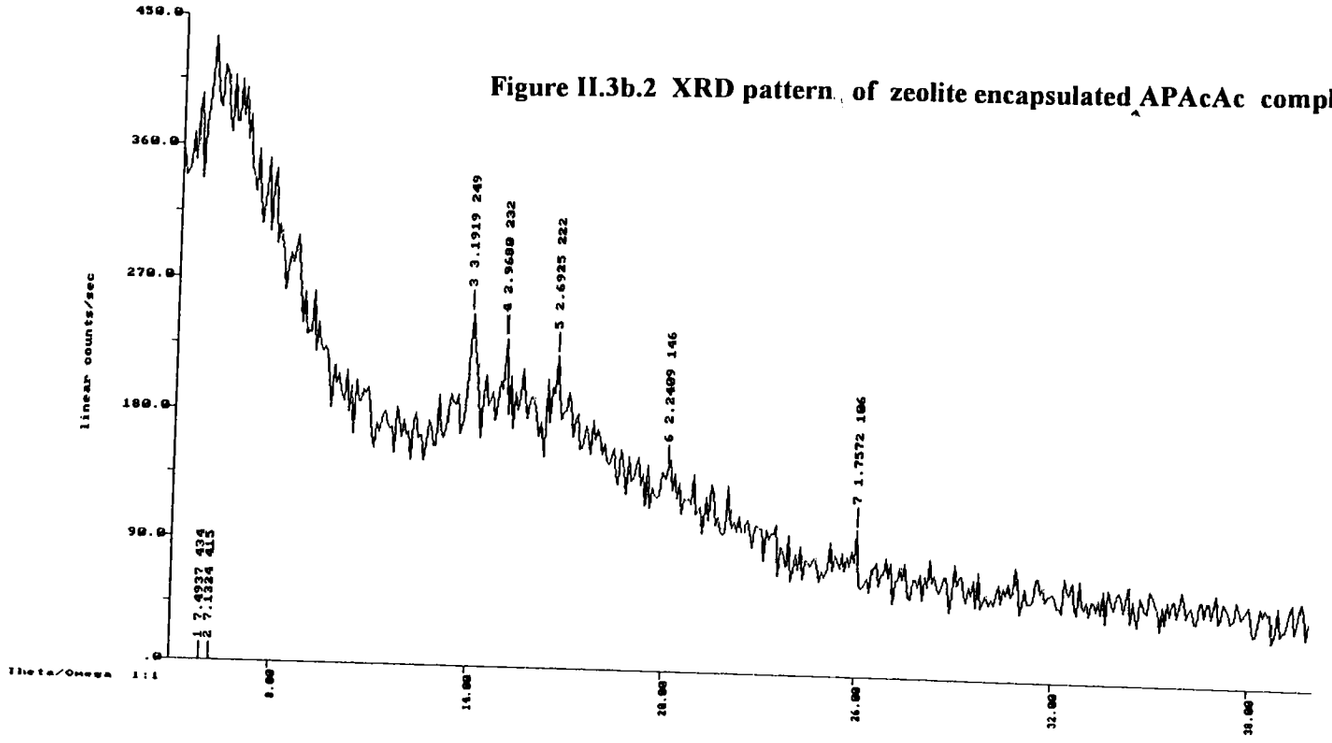

Figure II.3b.2 XRD pattern of zeolite encapsulated APAcAc complex of Fe

solvent becomes colourless. From the SEM taken after soxhlet extraction it is evident that the surface is clean by the extended extraction procedures.

II.3b.2.3 XRD patterns.

XRD pattern of Fe(APAcAc)Y, is given in the Fig II.3b.2 When compared with the XRD pattern of the corresponding metal exchanged zeolites it is found to be more or less similar. Various reports show that zeolite framework structure is retained even after the encapsulation as is evident from the XRD patterns[11]. The peaks of M(APAcAc) were not observed in the XRD patterns of the encapsulated complexes since its percentage in zeolite is very less and is well dispersed inside the cages.

II.3b.2.4 Surface area and Pore volume.

Surface area and Pore volume of the encapsulated complexes of APAcAc was given in the Table II.3b.2.

Table.II.3b.2
Surface area and Pore volume data

Sample	Surface area			Pore volume		
	MY	M(APAcAc)Y	% loss	MY	M(APAcAc)Y	% loss
Fe(APAcAc)Y	540	390	27.77	0.2033	0.1346	33.79
Co(APAcAc)Y	535	380	28.97	0.1913	0.1382	27.75
NiAPAcAc)Y	530	230	56.60	0.2008	0.1562	22.22
Cu(APAcAc)Y	540	330	38.88	0.1924	0.1466	23.81

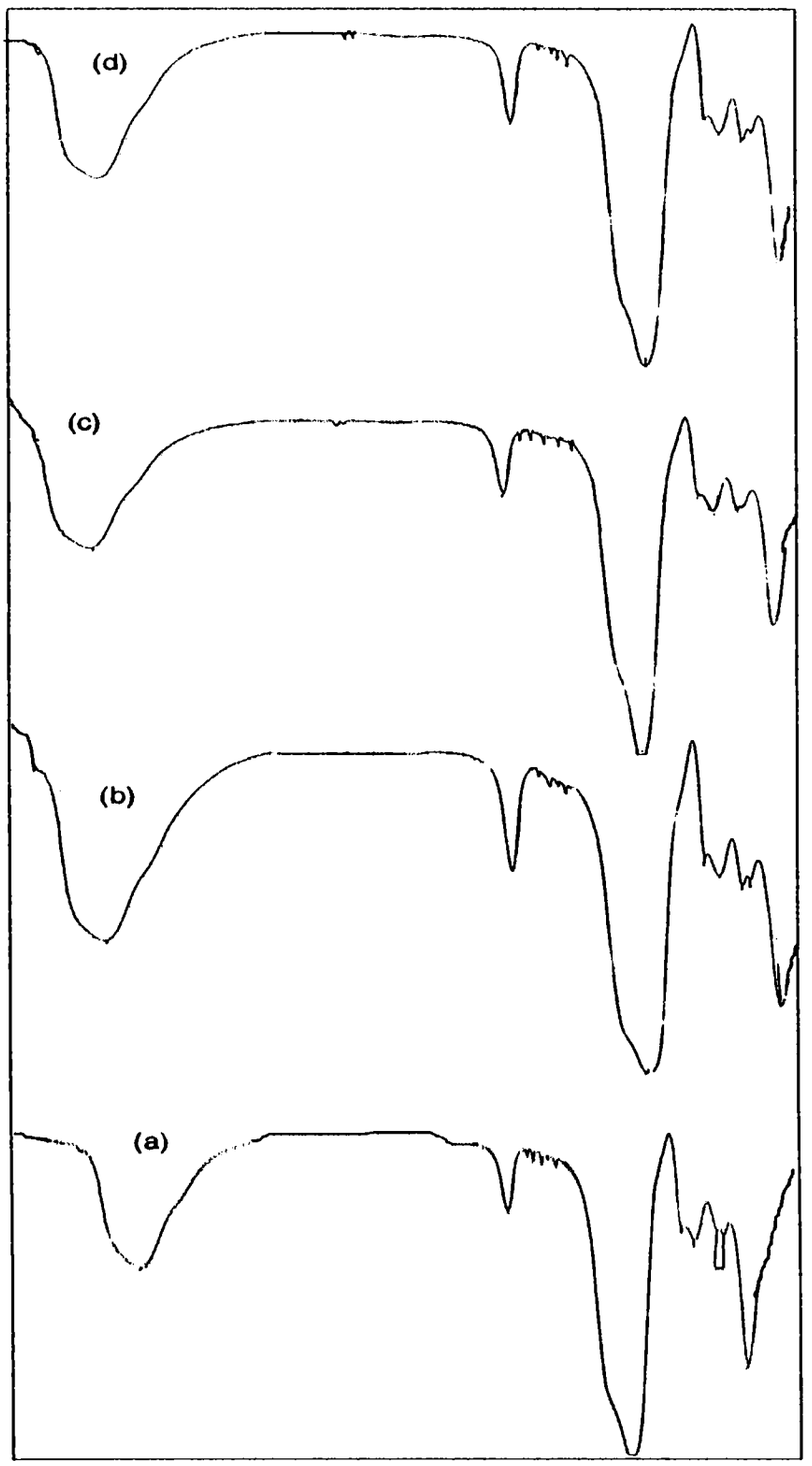

Figure II.3b.3. IR Spectra of (a) Fe(APAcAc)Y, (b)Co(APAcAc)Y
(c) Ni(APAcAc)Y (d) Cu(APAcAc)Y

Eventhough there is not much difference in the surface area of the parent zeolite HY, and the metal exchanged zeolite MY, the surface area of the zeolite encapsulated complexes decreases significantly. This is an indication of the encapsulation of the complexes in the cavities.

II.3b.2.5 IR spectra.

IR spectrum of the encapsulated APAcAc complexes are taken by KBr pellet technique in the region 400-1400 cm^{-1}.

IR spectra of APAcAc and their Fe(III), Co(II), Ni(II) and Cu(II) complexes have been characterized in part I, chapter III. In the case of the IR spectra of zeolite encapsulated (APAcAc) complexes most of the significant bands of the ligand are expected where prominent zeolite bands occur. Therefore the ligand bands are obscured by the broad zeolite bands.

In pure complexes OH stretch of the ligand is absent and ν_{NH} is retained. In this region there is a broad intense band of the zeolite and therefore this band could not be identified. Similarly the regions in which $\nu_{C=O}$ and ν_{NH} are expected (1500-1650 cm^{-1}) contain strong zeolite bands making it difficult to identify the shift in these vibrations. However, there are weak signals due to ligand in the spectrum of the encapsulated complexes in other regions. The spectrum is presented in the Fig.II.3b.4.

II.3b.2.6 Electronic spectra.

The electronic spectra of all the encapsulated complexes were recorded using pure zeolite as the standard. The spectrum is given in Fig.II.3b.4. The spectra of Fe(III), Co(II), Ni(II) and Cu(II) complexes were given in part I, chapter III. The general features of the electronic spectra of the pure complexes and their zeolite encapsulated analogues are similar. However, the signals are much weaker in the case of encapsulated complexes. The spectrum of the encapsulated Cu(II) complex show entirely different nature from the spectrum of the pure complex. Eventhough the UV region shows similarity, the d-d bands observed in the case of pure complex is absent in the spectrum of encapsulated complex. This clearly shows a change in geometry from distorted octahedron on encapsulation of the pure complex. Since there are no bands in the region 500-800 nm suggest a square or tetrahedral configuration for the encapsulated Cu(II) complex.

II.3b.2.7 Magnetic measurements.

The magnetic moments of the encapsulated zeolite complexes determined using Gouy method at room temperature are given in Table.II.3b.5 The magnetic moments of the encapsulated complexes will be complicated due to contribution from possible impurities and zeolite support. However the magnetic moment values give some valuable information regarding the spin state of the metal ion present in the zeolite cavity.

The effective magnetic moment of the encapsulated Fe(III) complex is 5.78 BM. The value observed in the case of pure complex is 5.98 BM (part I, chapter III).

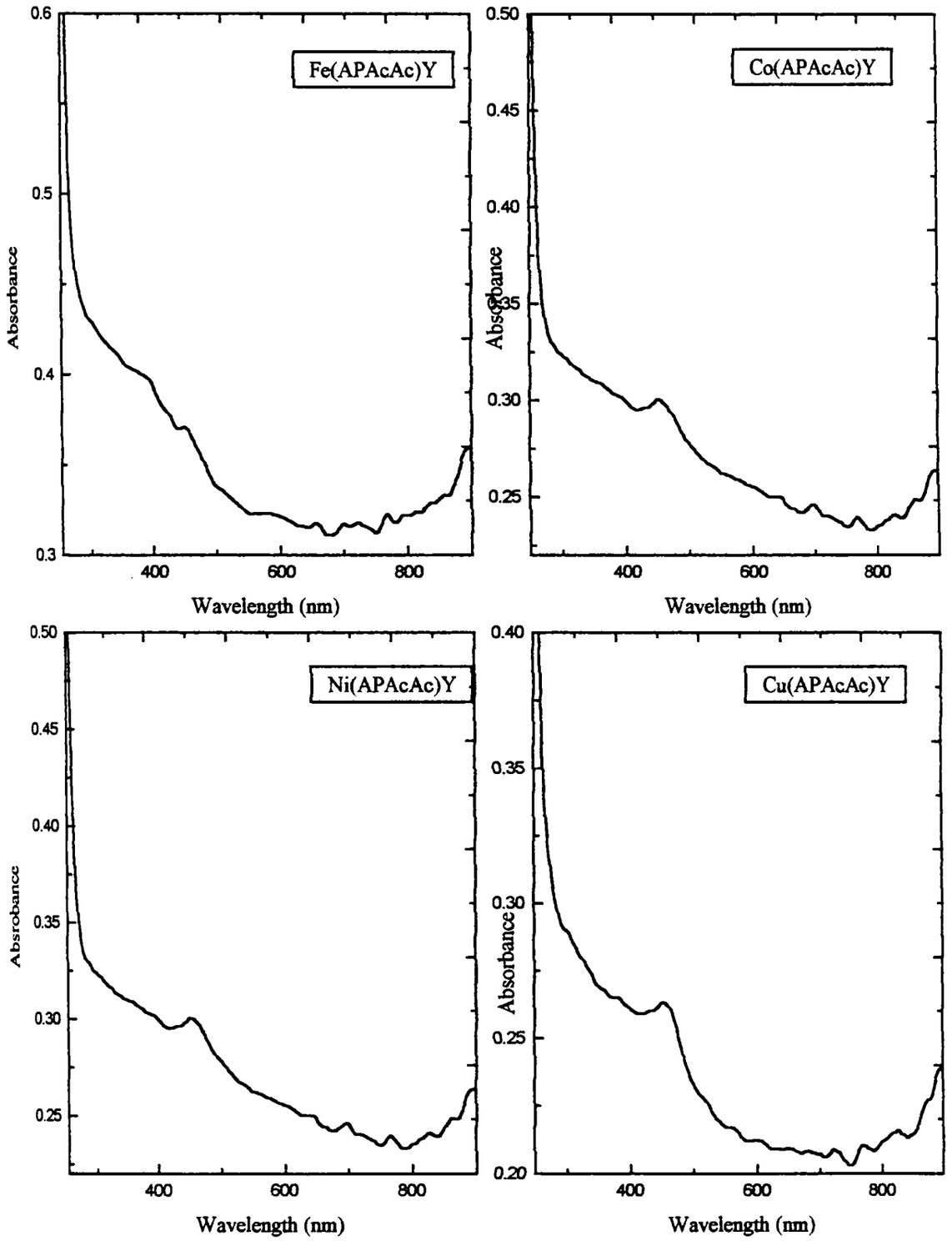

Figure II.3b.4 Electronic Spectra of zeolite encapsulated APAcAc complexes

The value observed for the encapsulated complex clearly shows the high spin nature of Fe(III) in the zeolite lattice. In the case of Fe(III) complexes the magnetic moment value is of no use to identify the geometry.

Table.II.3b.5
Magnetic moment data.

Complex	μ_{eff}
Fe(APAcAc)Y	5.78
Co(A PAcAc)Y	3.78
Ni(A PAcAc)Y	2.84
Cu(A PAcAc)Y	2.10

The magnetic moment measurements are useful in ascertaining the stereochemistry of Co(II) complexes[12]. The parent Co(II) complex found to show a magnetic moment value of 3.91 BM which is attributed to tetrahedral geometry for the complex. The magnetic moments observed in the present encapsulated complex (3.78 BM) is not much different from the values shown by the pure complex. This clearly shows that the encapsulation has not affected the geometry of the pure complex.

In the case of the encapsulated Ni(II) complex the magnetic moment values observed is 2.84BM, while the value observed for the pure complex was 2.78 BM. These values are nearer to the values expected for octahedral Ni(II). Thus in this case of Ni(II) complex also encapsulation has not altered the geometry as suggested by the magnetic moment.

The magnetic moment per copper atom in the encapsulated complex is 2.1BM. There is an increase of magnetic moment for the encapsulated Cu(II) complex compared to the magnetic moment observed for the pure complex (part I, chapter III). This is indicative of a change in the geometry on encapsulation of the pure Cu(II) complex in zeolite cavity.

In the case of encapsulated Co(II) and Ni(II) the geometry was found to be retained. However, it has to be noted that there is a change in the composition of the complex on encapsulation as suggested by the analytical data. The geometry of these complexes are not changed probably by satisfying the required coordination sites by the electron rich centres in the zeolite support.

II.3b.2.8 EPR

EPR spectroscopy is ideal to probe both molecular and electronic structural information of the paramagnetic ions and the effect of molecular confinement on the conformational geometry and mobility of the complexes inside the zeolite cages[13]. The X-band EPR spectrum of the encapsulated Cu(II) complex was analyzed at liquid nitrogen temperature (Fig.II.3b.5.) The parameters are given in Table.II.3b.6

Table II.3b.6
EPR data of Cu(APAcAc)Y

EPR parameter	Value for Cu(APAcAc)Y
$g_{\|\|}$	2.3776
$A_{\|\|}$	$162.54X10^{-4}$
$g_{\|\|}/A_{\|\|}$	146.28 cm
$g_{\perp}$	2.09

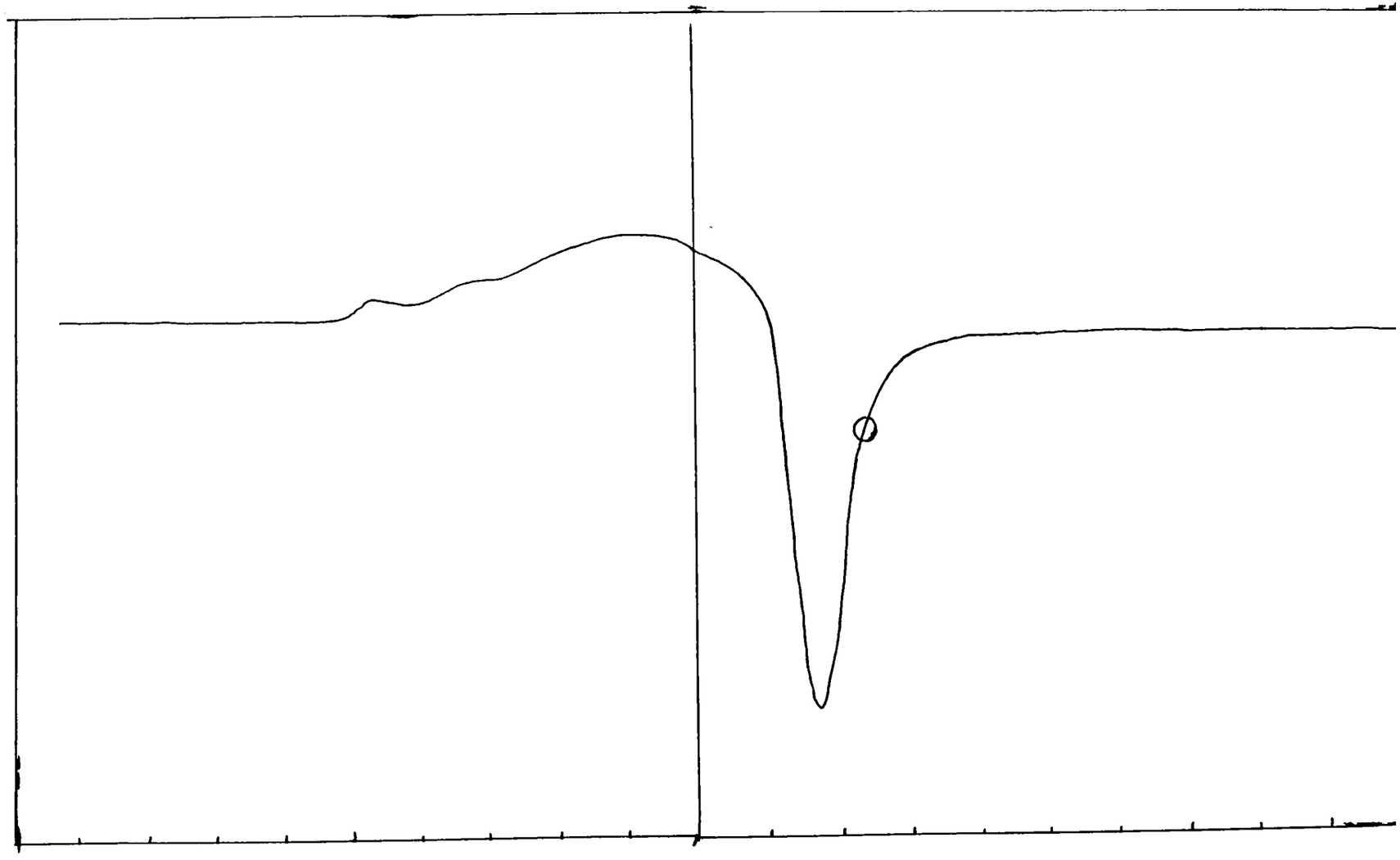

Figure II. 3b.5 EPR spectra of Cu(APAcAc)Y

The high $g_{\parallel}$ value observed for the encapsulated Cu complex can be attributed to a tetrahedrally distorted square planar complex. The $g_{\parallel}/A_{\parallel}$ value is greater than the value expected for a square planar complex and is very much close to a flattened tetrahedral structure.

II.3b.2.9 Thermal Studies

TG curves of zeolite encapsulated APAcAc complexes are given in Fig. and the thermal data are given in Table II.3b.7 The TG patterns for all the four complexes are found to be the same. In all the four complexes decomposition starts from the ambient temperature. The first stage in all the cases is due to loss of intrazeolite and co-ordinated water molecules[14]. The subsequent loss can be due to the decomposition of encapsulated complex.

Table II.3b.7
TG data of for zeolite encapsulated APAcAc complexes

Complex	Stability (°C)	Decomposition range	Total weight loss (%)
Fe(APAcAc)Y	Ambient	Ambient-105 105-283 283-603 603-799	13.04
Co(APAcAc)Y	Ambient	Ambient-105 105-255 255-602 602-798	18.76
Ni(APAcAc)Y	Ambient	Ambient-105 105-281 281-554 554-798	15.91
Cu(APAcAc)Y	Ambient	Ambient-105 105-362 362-583 583-799	15.33

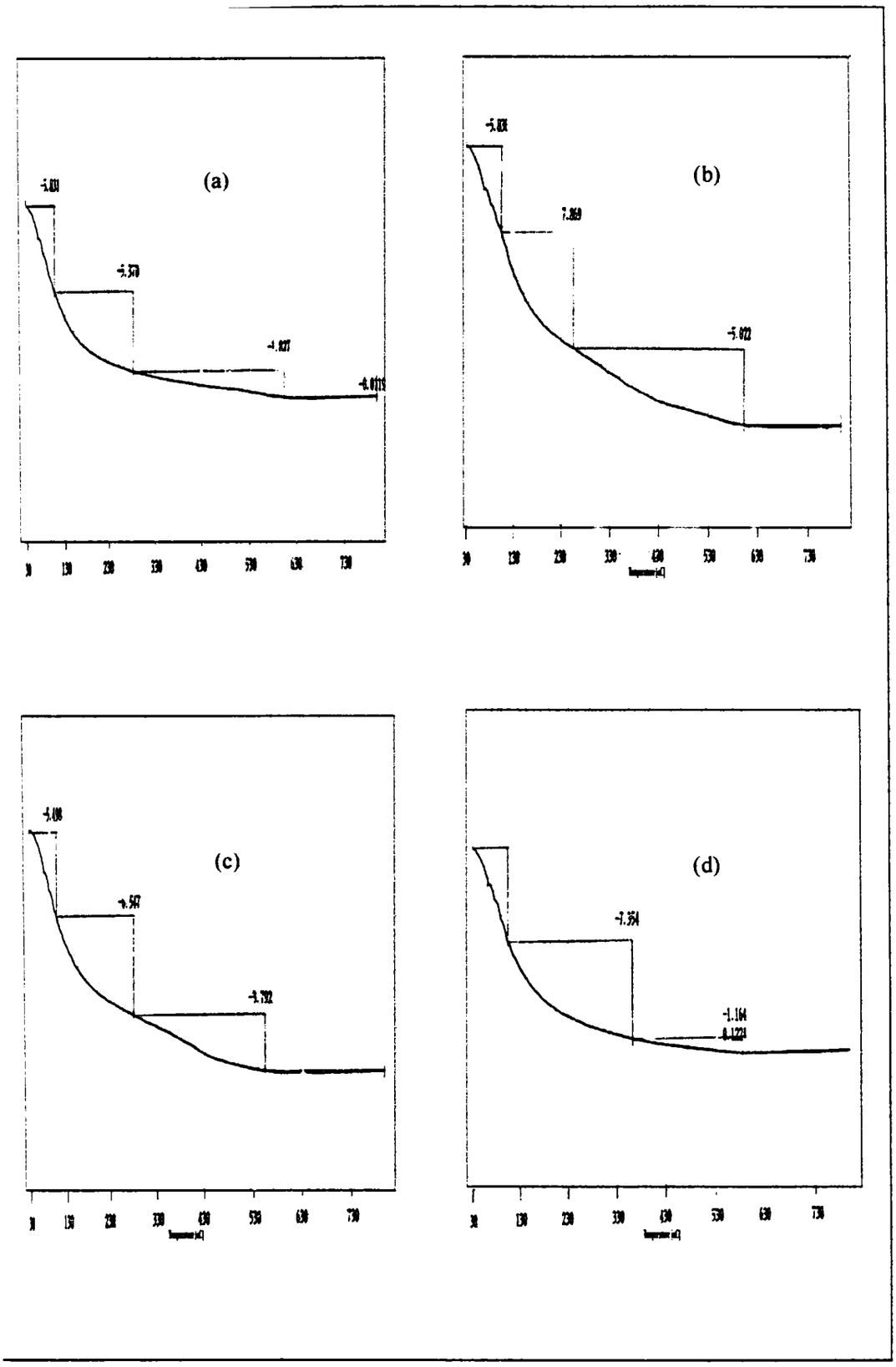

Figure Ii.3b.6 T.G. Curves of (a) Fe(APAcAc)Y (b) Co(APAcAc)Y
(c) Ni (APAcAc)Y (d) Cu (APAcAc)Y

The compound is stable only upto room temperature. The decomposition starts around 31°C and the major decomposition occurs in between 31°C and 603°C. The total mass loss observed for Fe(III) complex is 13.04%. The Co(II) complex also shows the mass loss from 31°C onwards and decomposes in four stages. Here also the major decomposition completes before 602°C. The total mass loss in this case is 18.76%. The Ni(II) complex is stable upto 30°C. The total mass loss is 15.91%. In Cu(II) complex total mass loss is 15.33%. Here the major mass loss occurs before 583°C. The TG curves are presented in Fig. II.3b.6.

II.3c Zeolite encapsulated APAcAcA complexes.

II.3c.1. Experimental

The encapsulated Fe(III), Co(II), Ni(II) and Cu(II) of APAcAcA were prepared as described earlier using flexible ligand method. The uncomplexed ligand and the surface complexes were removed by soxhlet extraction with methanol. The uncomplexed metal ions were removed by ion exchange with NaCl solution. All the steps were repeated as explained in the general methods of preparation described in Part II, Chapter II. Details regarding the analytical techniques and procedural details employed for the characterization are given in Part II, Chapter II.

II.3c.2 Results and discussion.

II.3c.2.1 Chemical analysis

Analytical data of the zeolite encapsulated complexes of APAcAcA are given in Table.II.3c.1

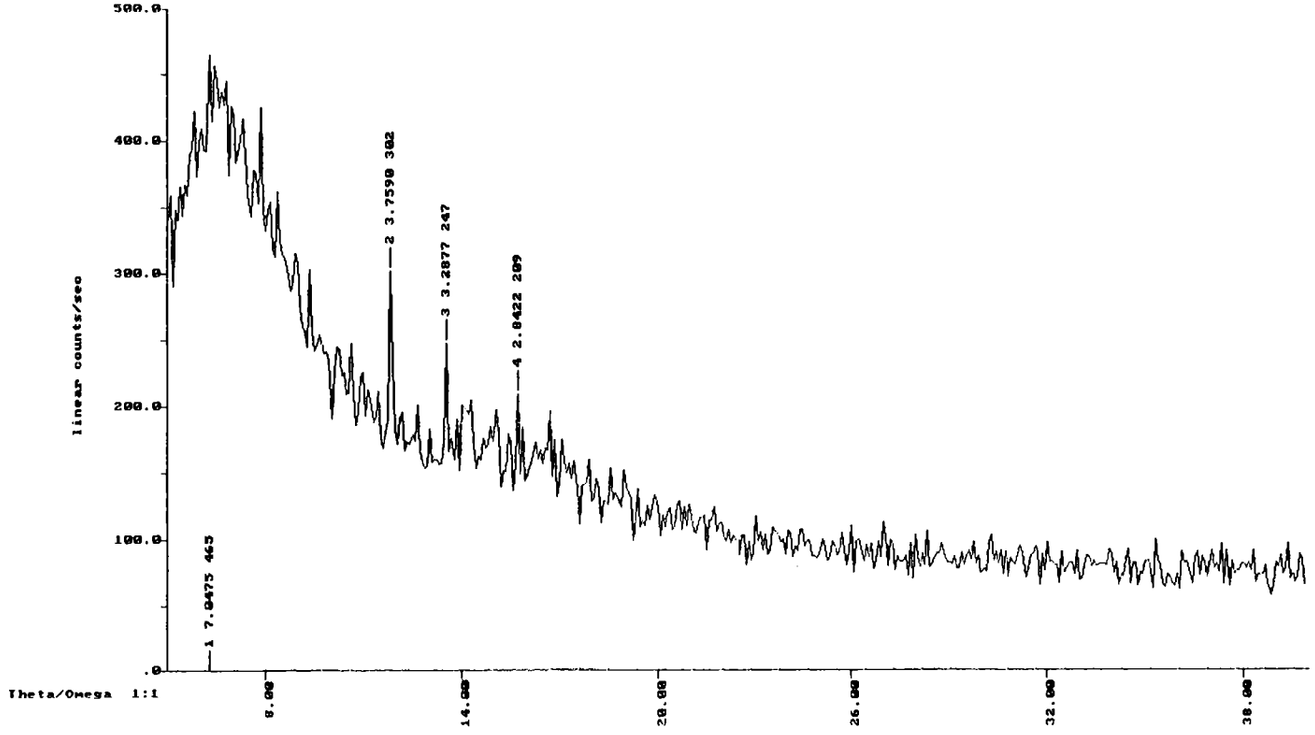

Figure II.c.1 XRD pattern of zeolite encapsulated APAcAcA complex of Co

The analytic data reveal that the encapsulated complexes have the compositions FeL, CoL, NiL and CuL (where L is APAcAcA). The analytic data shows the presence of 1:1 metal to ligand ratio for the complexes inside the cavity. Data also reveal the possibility of the existence of traces of metal ions occluded even after the final Na exchange.

Table.II.3c.1
Analytical data

Sample	Metal %	Si %	Al %	C %	N %
Fe(APAcAcA)Y	0.07	21.21	8.80	3.99	0.87
Co(APAcAcA)Y	1.24	21.07	8.74	4.22	0.92
Ni(APAcAcA)Y	0.39	24.08	9.99	2.49	0.54
Cu(APAcAcA)Y	0.48	28.06	11.64	0.83	0.18

II.3c.2.2 XRD Patterns.

The XRD patterns of the zeolite encapsulated Co(II) complex of APAcAcA are shown in Fig II.c.1. The XRD patterns are similar to those obtained for the metal exchanged zeolites. This clearly shows that the zeolite frame work structure is retained even after the encapsulation of the metal complexes.

II.3c.2.3 Surface area and Pore volume.

The details of the determination of the surface area and pore volume are given in Part II, Chapter II and the data obtained are presented in Table.II.3c.2. The data indicate the encapsulation of the complexes in the zeolite cavities

Table II.3c.2.
Surface area and Pore volume data of encapsulated APAcAcA complexes.

Sample	Surface area			Pore volume		
	MY	M(APAcAcA)Y	% loss	MY	M(APAcAcA)Y	% loss
Fe(APAcAcA)Y	540	391	27.64	.2033	0.1260	38.04
Co(APAcAcA)Y	535	373	30.21	0.1913	0.1545	19.24
NiAPAcAcA)Y	530	227	57.35	0.2008	0.0861	57.14
Cu(APAcAcA)Y	540	364	32.62	0.1924	0.1371	28.78

II.3c.2.4 IR Spectra.

A broad band observed around 3500 cm^{-1} due to phenolic OH and two NH groups for the free ligand is retained in the spectrum of the pure complexes without much change. There is a prominent band for zeolite at 3456 cm^{-1}. The other bands observed for zeolite are at 1633, 1029 and 729 cm^{-1}. In the free ligand two C=O frequencies, one due to free C=O group at 1634 cm^{-1} and the other at 1600 cm^{-1} due to H-bonded C=O are observed. From the shift of the C=O stretching frequency at 1634 cm^{-1} , it was concluded that free C=O is one of the donor sites in the pure complexes. In these complexes the H-bonded $\nu_{C=O}$ and ν_{CN} at 1513 cm^{-1} do not show any change indicating that these groups are not involved in coordination. In the spectra of the encapsulated complexes the C=O stretching frequency region is masked by the strong zeolite band and therefore the coordination through these groups could not be ascertained. However, the spectra of the encapsulated APAcAcA complexes do not suggest any change in the coordination pattern on encapsulation. Shift due to ν_{N-N} of the ligand is masked by broad zeolite band at 1029cm^{-1}.

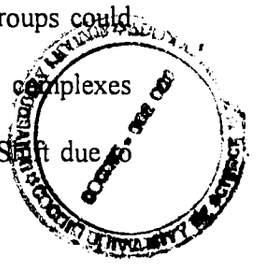

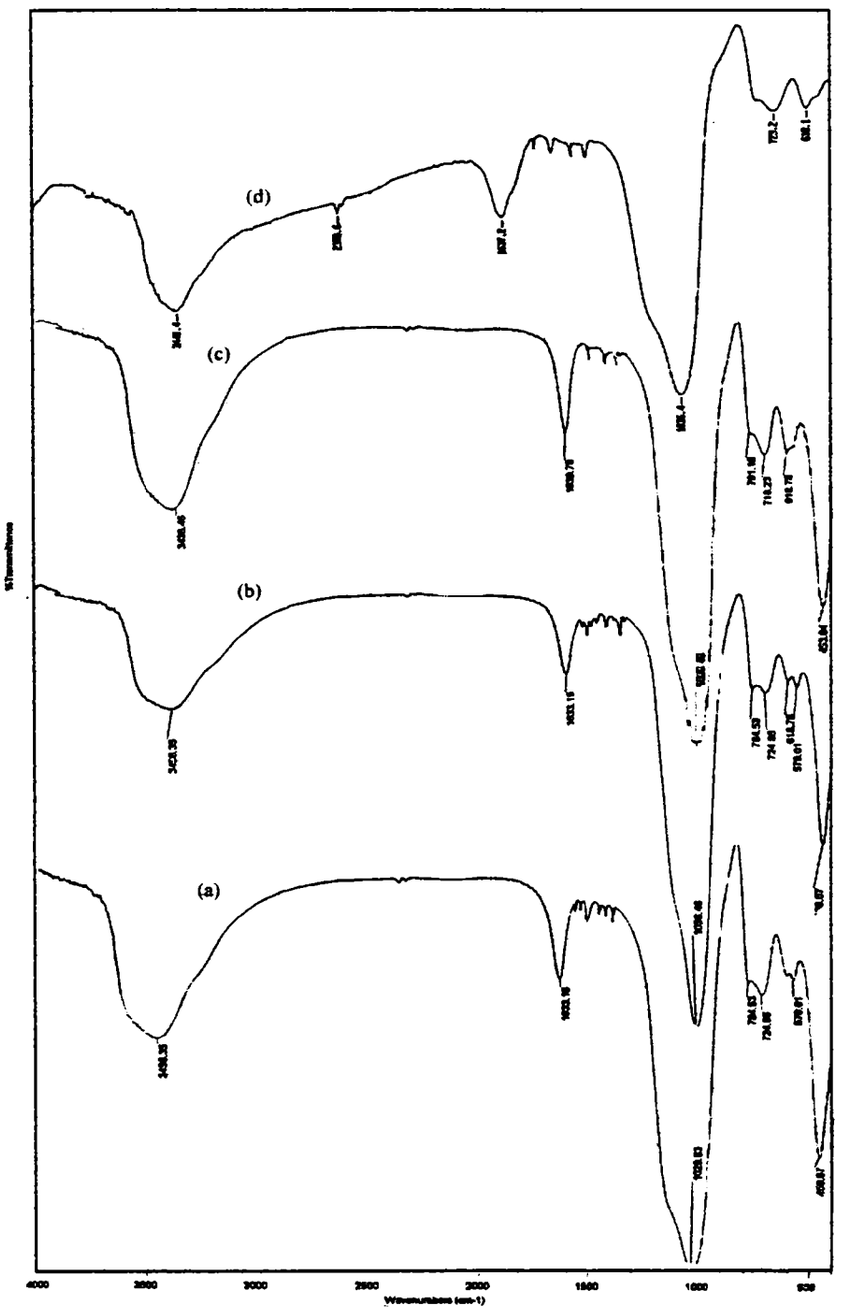

Figure II.3c.2 IR Spectra of (a) Fe(APAcAcA)Y (b) Co(APAcAcA)Y
(c) Ni(APAcAcA)Y (d) Cu (APAcAcA)Y

II.3c.2.5 Electronic Spectra.

It is not possible to assign any particular geometry for Fe(III) complexes as all the d-d transitions are spin and Laporte forbidden. The electronic spectrum of the encapsulated Fe(III) complex is similar to that of the pure complex which shows only ligand and charge transfer bands. The pure complexes of Co(II) and Ni(II) were assigned tetrahedral geometry on the basis of electronic spectral evidence. This assignment was supported by the magnetic data also. In the case of the encapsulated Co(II) and Ni(II) complexes, the electronic spectra are similar to their pure counter parts with much decreased resolution and intensity. Therefore, it can be concluded that the geometries have not altered on encapsulation. In the case of the encapsulated Cu(II) complex, the spectrum is entirely different from that of the pure complex. The band around 700nm is not found in the spectrum of the encapsulated complex. The absence of a d-d band in the visible region is a clear indication of tetrahedral geometry for the Cu complex, probably a tetrahedrally distorted square planar geometry. The magnetic data and EPR parameters are also in support of this structure.

II.3c.2.6 Magnetic Data.

The magnetic moment calculated from the susceptibilities determined by Gouy method are given in Table.II.3c.3. The magnetic moment values of the encapsulated complexes are almost similar to the values observed for the pure complex. The magnetic moment values of Fe(III) and Cu(II) complexes are of not much use in a structural context. However, they give information about the presence of magnetic interactions. The magnetic moment values of the present encapsulated

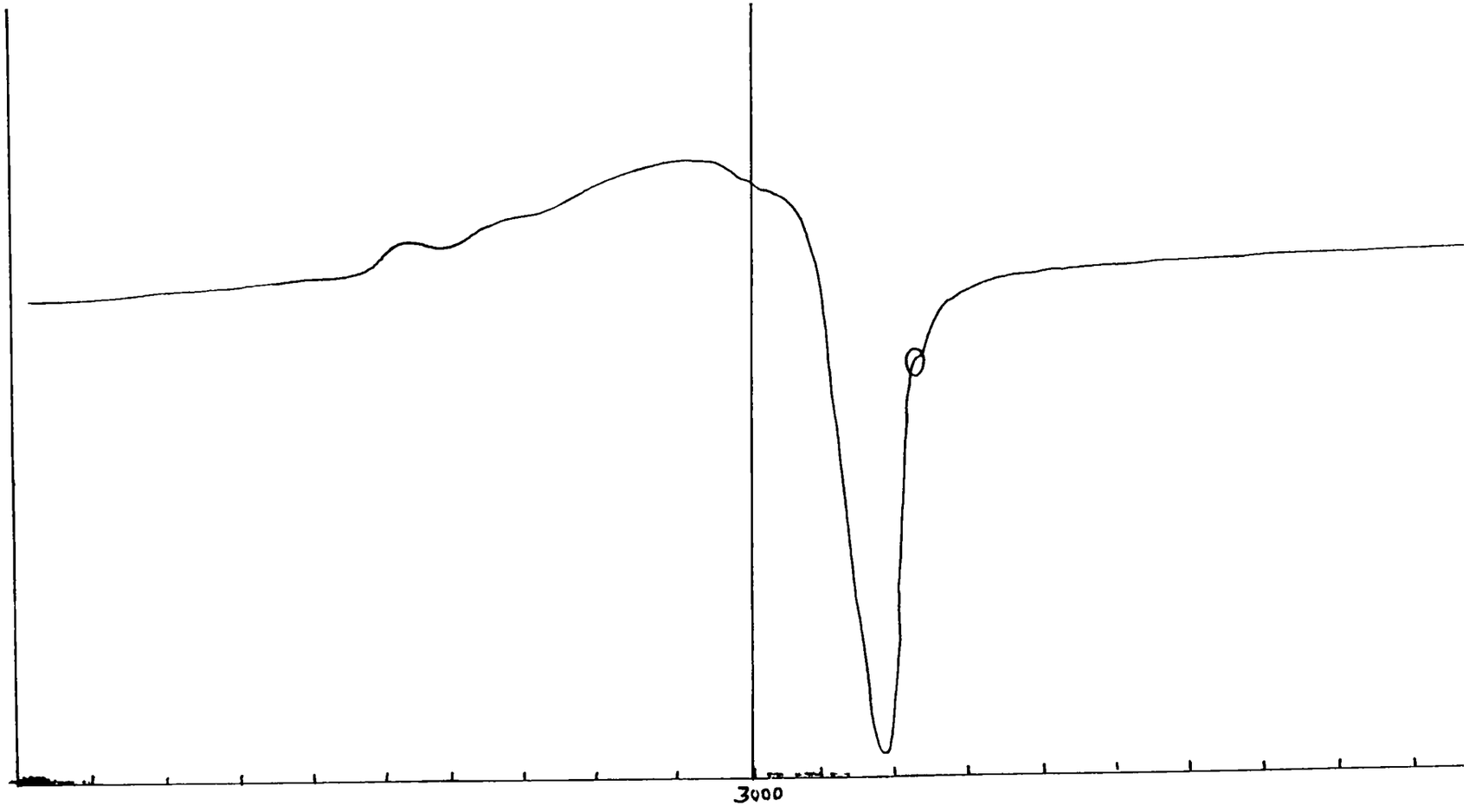

Figure II. c.3 EPR spectra of Cu(APAcAcA)Y

Fe(III) and Cu(II) complex reveal the absence of any metal-metal interactions which is not unexpected in the case of metal ions complexed in zeolite cavities. The Co(II) and Ni(II) complexes are tetrahedral as the values exhibited by them are in the range expected for tetrahedral complexes of these metal ions.

Table.II.3c.3
Magnetic data of encapsulated APAcAcA complexes.

Complex	μ_{eff} BM
Fe(APAcAcA)Y	5.80
Co(APAcAcA)Y	3.48
Ni(APAcAcA)Y	3.60
Cu(APAcAcA)Y	1.79

II.3c.2.7 EPR

The X-band EPR spectrum of the encapsulated Cu(II) complex of APAcAcA is given in the Fig.II.3c.3 and the data are given in the Table.II.3c.4.

Table.II.3c.4
EPR data of Cu(APAcAcA)Y

EPR parameter	Values for Cu(APAcAcA)
$g_{\|}$	2.37
$A_{\|}$	$169.73X10^{-4}$
$g_{\|} / A_{\|}$	139.43cm
$g_{\perp}$	2.09

The α^2 value observed is close to unity which indicates the covalent nature of bonding between the metal and the ligand orbitals.The $g_{\parallel}$ /$A_{\parallel}$ value shows that the complex has a tetrahedrally distorted square planar structure.

II.3c.2.8 Thermal studies

The TG curves for the decomposition of APAcAcA complexes are given in Fig. II.3c.4. The data are summarized in Table II.3c.6

Table II.3c.6.
TG data for zeolite encapsulated APAcAcA complexes

Complex	Stability (°C)	Decomposition range	Total weight loss (%)
Fe(APAcAcA)Y	Ambient	Ambient-105 105-316 316-616 616-799	15.54
Co(APAcAcA)Y	Ambient	Ambient-105 105-229 229-611 611-798	15.63
Ni(APAcAcA)Y	Ambient	Ambient-105 105-376 376-577 577-798	16.55
Cu(APAcAcA)Y	Ambient	Ambient-101 101-210 210-555 555-798	19.22

All the complexes are stable only upto ambient temperature and decomposes in four stages. Eventhough the decomposition starts at room temperature, the decomposition at the initial stage are due to the loss of intra zeolite and coordinated water molecules and are not due to the decomposition of the metal complexes. The

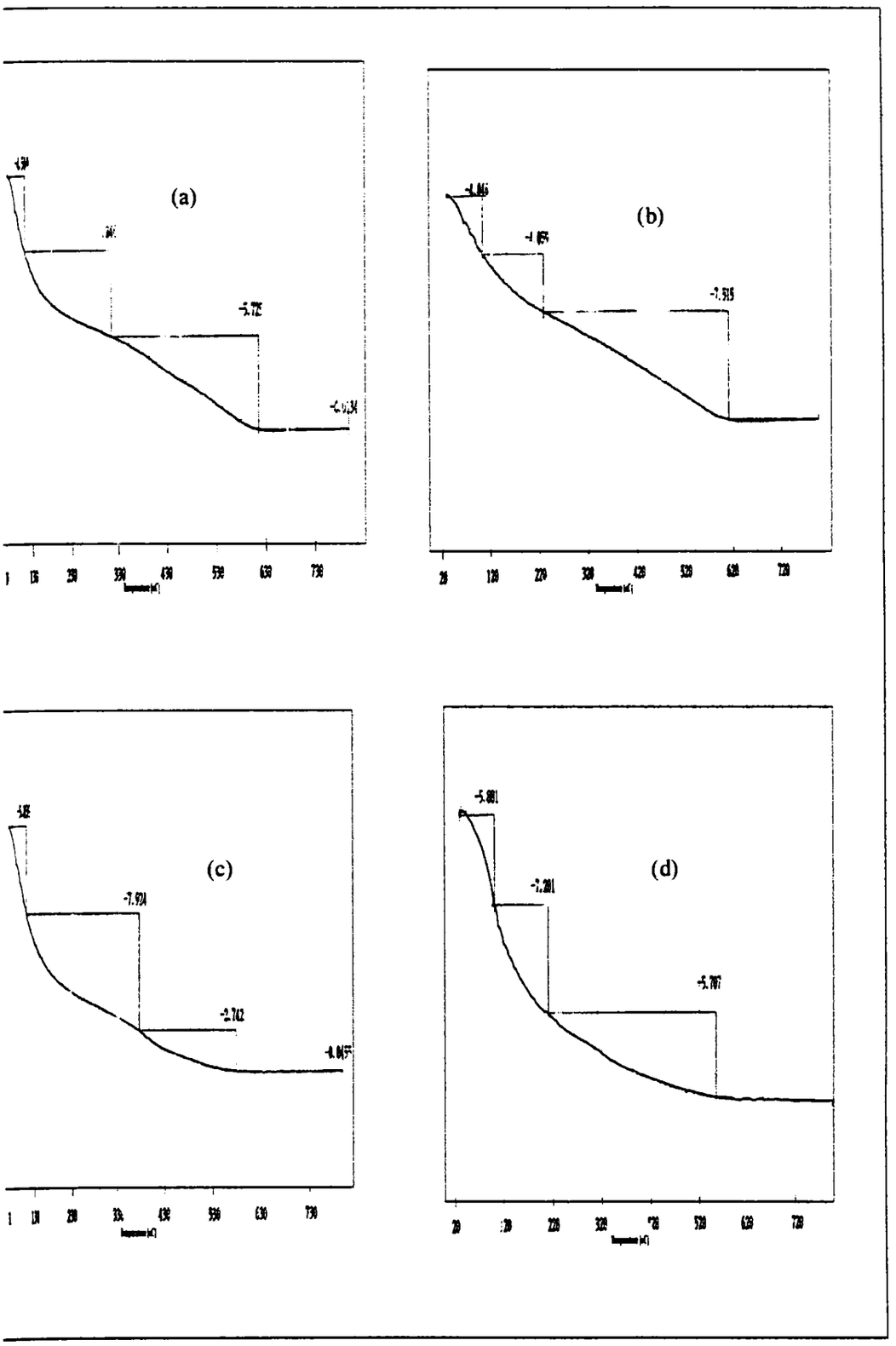

Figure II.3c.2 T.G Curves of (a) Fe(APAcAcA)Y (b) Co(APAcAcA)Y
(c) Ni(APAcAcA)Y (d) Cu(APAcAcA)Y

total mass loss observed for zeolite encapsulated Fe(III), Co(II), Ni(II) and Cu(II) complexes are 15.54, 15.63, 16.55 and 19.22% respectively. The TG curves are given in Fig. II.3c.5

II.3d Zeolite encapsulated AUAcAcA complexes.

II.3d.1 Experimental

The zeolite encapsulated Fe(III), Co(II), Ni(II) and Cu(II) complexes of AUAcAcA were synthesized using flexible ligand method. The preparative details are given earlier. The analytical methods and characterization techniques are given in PartII, ChapterII.

II.3d.2 Results and discussion.

II.3d.2.1 Chemical analysis

The analytical data of the zeolite encapsulated Fe(III), Co(II), Ni(II) and Cu(II) complexes of AUAcAcA are given in Table.II.3d.1.

Table.II.3d.1
Analytical data of M(AUAcAcA)Y complexes.

Sample	Metal %	Si %	Al %	C %	N %
Fe(AuAcAcA)Y	0.42	27.85	11.56	1.58	0.66
Co(AuAcAcA)Y	0.51	26.08	10.82	1.02	0.43
Ni(AuAcAcA)Y	0.94	27.52	11.41	0.20	0.08
Cu(AuAcAcA)Y	0.77	27.22	11.29	1.53	0.65

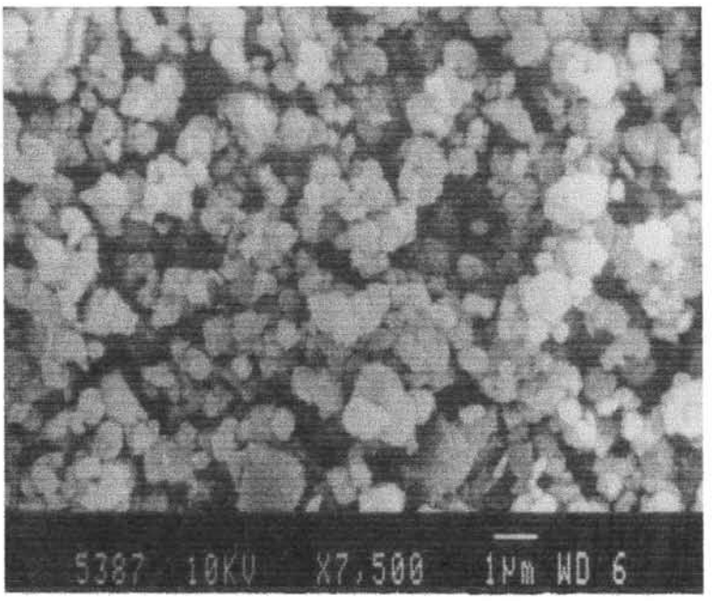

(a)

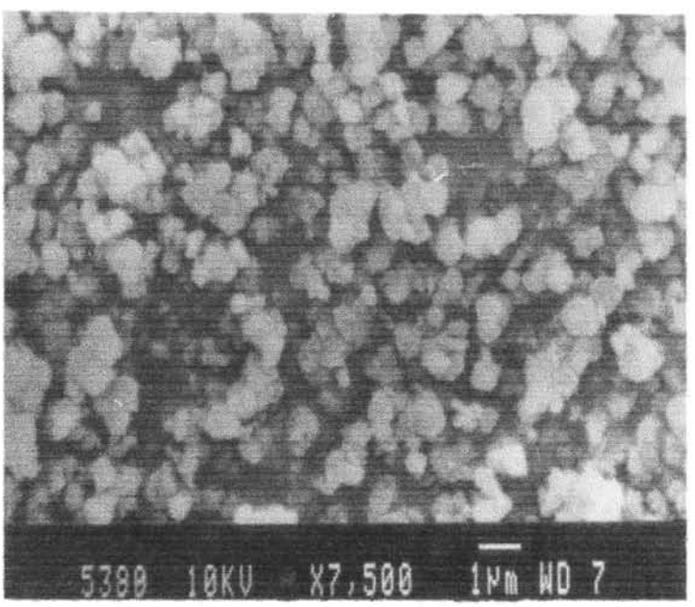

(b)

Figure II.3d.1 Scanning Electron Micrograph of Fe(AUAcAc)Y (a) before and (b) after soxhlet extraction

The analytical data suggest 1:1 ligand to metal stoichiometry for the encapsulated complexes of AUAcAcA.

II.3d.2.2 Scanning electron micrograph.

Scanning electron micrograph (SEM) of the Fe(APAcAc)Y, before and after soxhlet extraction was taken and given in the Fig.II.3d.1 SEM taken before soxhlet extraction shows aggregates of ligand species formed on the surface, but in the SEM taken after soxhlet extraction the surface is found to be clean. During the soxhlet extraction procedures, the extraction is continued further for 24h even after the solvent becomes colourless. From the SEM taken after soxhlet extraction it is evident that the surface is clean by the extended extraction procedures.

II.3d.2.3 XRD patterns.

XRD pattern of Ni(AUAcAcA)Y is given in the Fig.II.3d.2. . When compared with the XRD pattern of the corresponding metal exchanged zeolites, the patterns for the complexes are found to be more or less similar. Zeolite framework structure is retained even after the encapsulation as is evident from the XRD patterns. The peaks of M(AUAcAcA) were not observed in the XRD patterns of the encapsulated complexes since its percentage in zeolite is very less and is well dispersed inside the cages.

II.3d.2.4 Surface area and Pore volume.

Surface area and pore volume of the encapsulated complexes of AUAcAcA was given in theTable.II.3d.2. Eventhough there is not much difference in the surface area of the parent zeolite HY, and the metal exchanged zeolite MY, the surface area

Figure II.3d.2 XRD pattern of zeolite encapsulated AUAcAcA complex of Ni

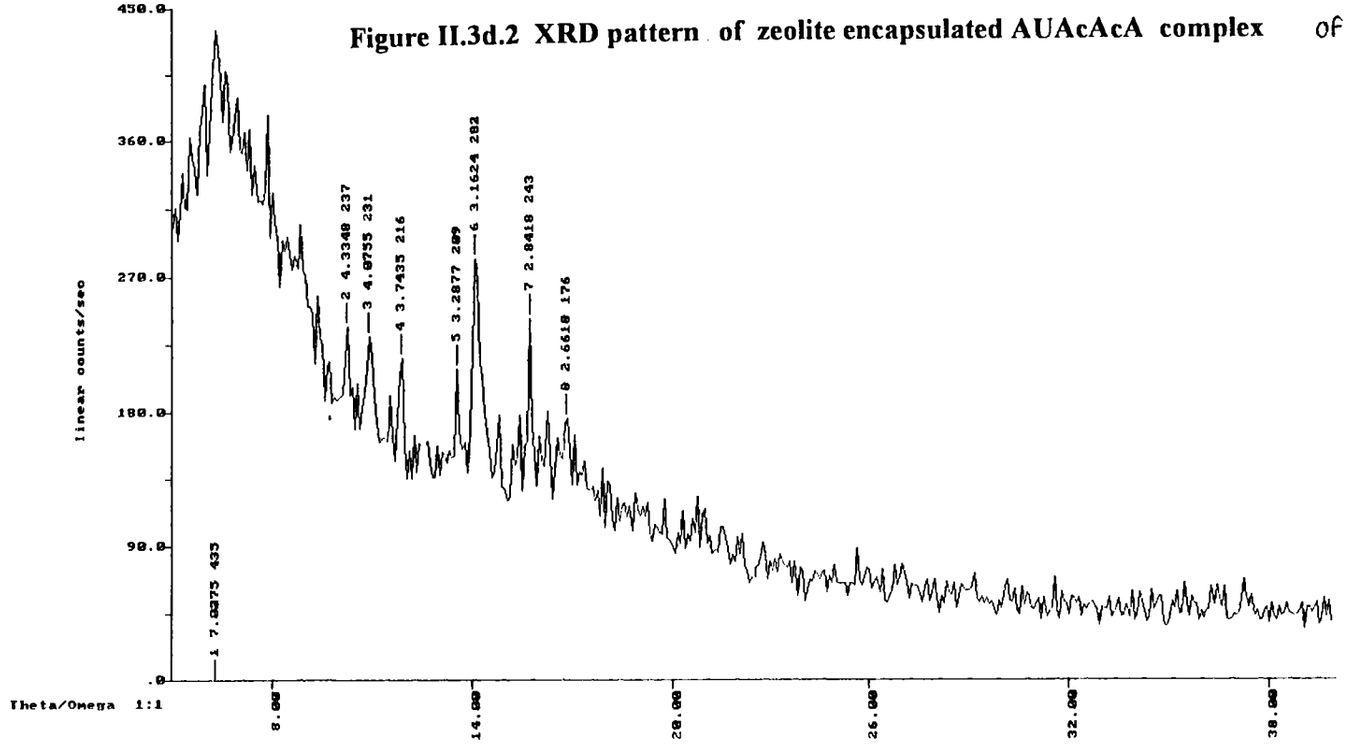

of the zeolite encapsulated complexes decreases significantly. This is an indication of the encapsulation of the complexes in the cavities.

Table.II.3d.2
Surface area and Pore volume data

Sample	Surface area			Pore volume		
	MY	M(AUAcAcA)Y	% loss	MY	M(AUAcAcA)Y	% loss
Fe(AUAcAcA)Y	540	386	28.57	0.2033	0.1185	42.34
Co(AUAcAcA)Y	535	370	30.02	0.1913	0.1403	26.65
Ni(AUAcAcA)Y	530	224	57.92	0.2008	0.0675	66.36
Cu(AUAcAcA)Y	540	361	33.20	0.1924	0.1360	29.35

II.3d.2.5 IR Spectra.

A band around 3460 cm^{-1} in the spectrum of the free ligand is attributed to the NH and OH stretching frequencies. In the spectra of the complexes this region does not show any significant change. However based on the analytic data it was suggested that one of the NH groups is deprotonated and bonded to the metal in the complexes. In the spectra of the encapsulated complexes the 3450 cm^{-1}region is similar to that found in the spectra of the pure complexes. Therefore, any change in the bonding pattern through NH cannot be expected. In the spectrum of the free ligand there is a band at 1713cm^{-1} assignable to free C=O group. This band is found to shift to around 1670 cm^{-1} on complexation suggesting the participation of free C=O in bonding. Similarly, the ν_{CN} observed at 1600 cm^{-1} in the spectrum of the free ligand is shifted to lower energy region (~ 1550 cm^{-1}) in the spectra of the complexes. This shows that azomethine nitrogen is involved in bonding. The H-bonded C=O

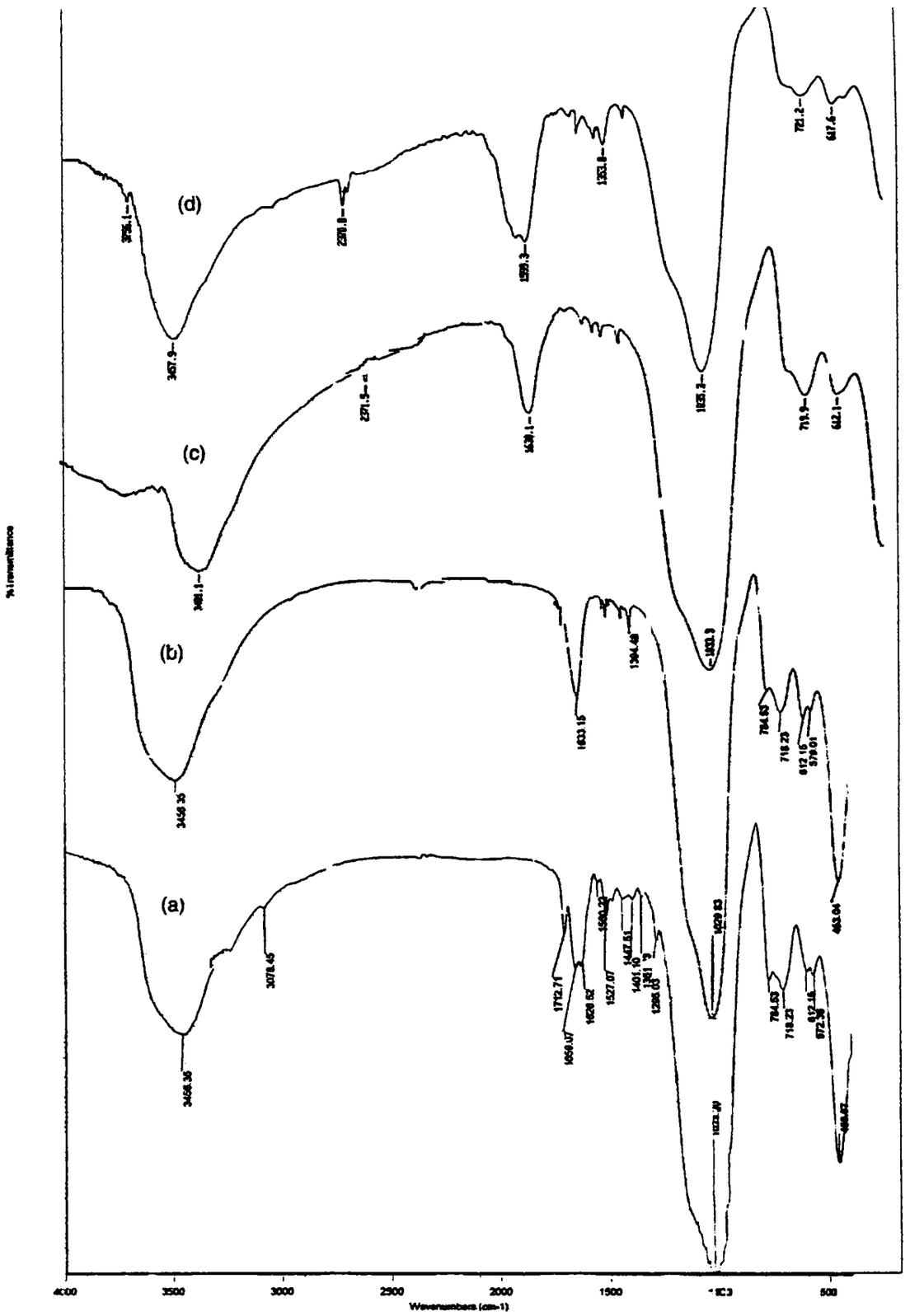

Figure II.3d.3 IR Spectra of (a) Fe(AUAcAcA)Y (b) Co(AUAcAcA)Y
(c) Ni(AUAc AcA)Y (d) Cu(AUAcAcA)Y

stretching frequency at 1650 cm^{-1} and the ring νC=O at 1633 cm^{-1} do not show any change in the spectra of the pure complexes. Therefore these groups are not involved in coordination. In the spectrum of the encapsulated complexes, the region 1600-1700 cm^{-1} contains strong zeolite band. Since the ligand bands in this region overlap with the zeolite band, the identification of the donor sites on the basis of frequency shifts in this region is difficult. Band due to ν_{N-N} band of the ligand is also masked by the broad zeolite band in the region 1030cm^{-1}. IR spectra of AUAcAcA complexes are given in Fig. II.3d.3.

II.3d.2.6 Electronic Spectra.

The electronic spectrum of the encapsulated Fe(III) complex is similar to that of the pure complex and shows only the ligand and charge transfer bands. The electronic spectrum of the encapsulated Co(II) complex suggest tetrahedral geometry probably distorted due to steric factors. The electronic spectrum of the Ni(II) complex suggests octahedral geometry. The spectrum of the encapsulated Cu(II) complex shows significant change from the spectrum of the pure complex. The spectrum suggests that the geometry has undergone a change on encapsulation from distorted octahedral to tetrahedral flattening towards planarity. This is also in conformity with the ESR parameters.

II.3d.2.7 Magnetic Data.

The magnetic data obtained for encapsulated complexes of AUAcAcA are given in Table.II.3d.3 The magnetic data cannot give any indication about the exact geometry of Fe(III) and Cu(II) complexes . However, the magnetic data can give

evidence for the presence of metal-metal interaction if any. The magnetic moment values of the present encapsulated complexes of Fe(III) and Cu(II) show the absence of any antiferromagnetic coupling. The magnetic data of the encapsulated Cu(II) complex suggests square planar or flattened tetrahedral geometry while that of the Ni(II) complex indicate octahedral environment around Ni(II).

Table.II.3d.3
Magnetic data of zeolite encapsulated AUAcAcA complexes.

Complex	μ_{eff} BM
Fe(AUAcAcA)Y	5.70
Co(AUAcAcA)Y	4.68
Ni(AUAcAcA)Y	2.81
Cu(AUAcAcA)Y	1.90

II.3d.2.8 EPR

The X-band EPR spectral data of the encapsulated Cu(II) complex of AUAcAcA are given in Table.II.3d.4 And spectrum is given in Fig II.3d.4. The g_{II}/A_{II} value observed suggests a flattened tetrahedral structure for the encapsulated complex. The α^2 value of the present complex shows that the Cu^{2+} ion is in an ionic environment.

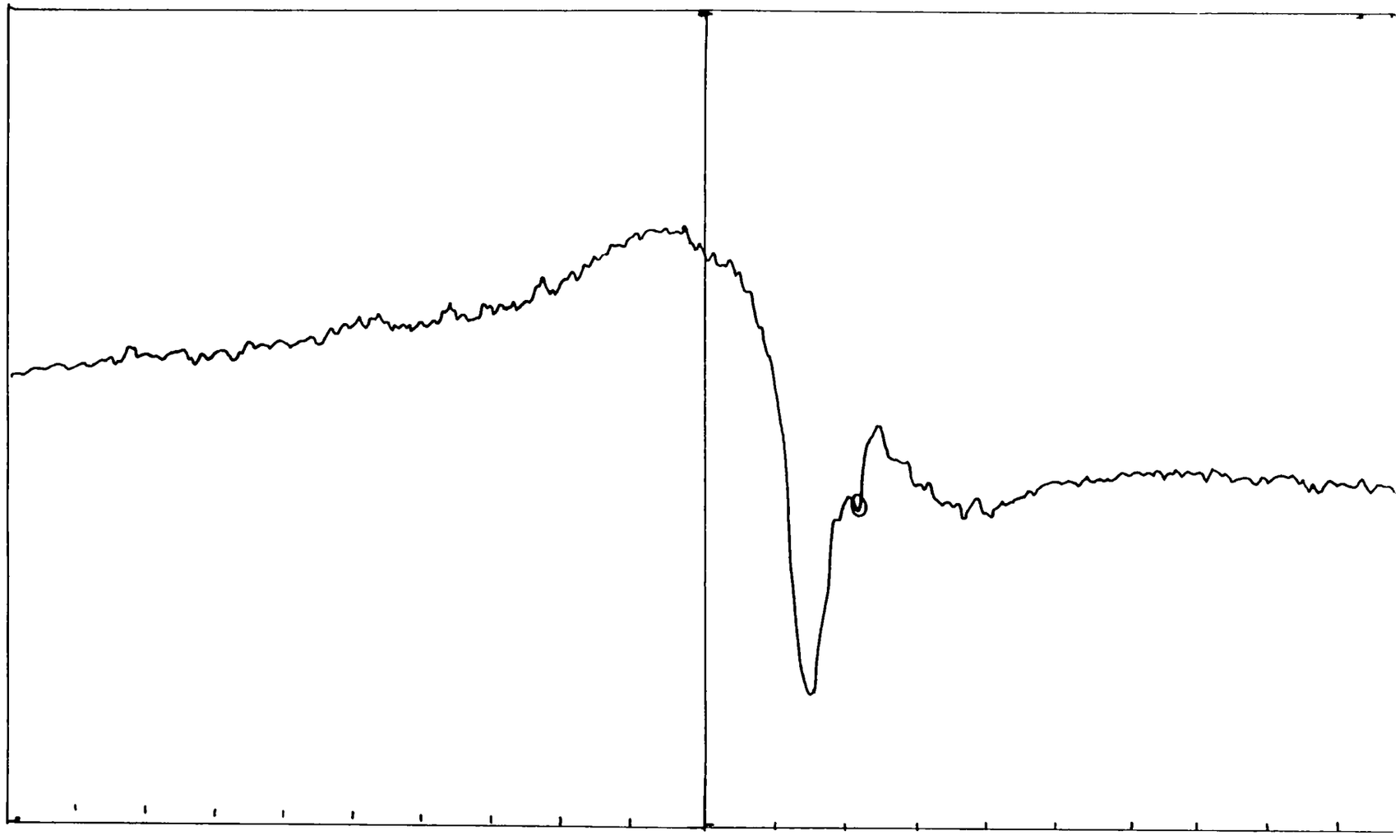

Figure II. 3d.4 EPR spectra of Cu(AUAcAcA)Y

Table.II.3d.4
EPR data of Cu(AUAcAcA)Y

EPR parameter	Values for Cu(AUAcAcA)Y
$g_{\|\|}$	2.3826
$A_{\|\|}$	$163.22X10^{-4}$
$g_{\|\|}/A_{\|\|}$	145.97cm
$g_{\perp}$	2.0183
$A_{\perp}$	$9.423X10^{-4}$
α^2	0.88
μ_{eff}	1.85

II.3d.29 Thermal studies

The TG curves are given in the Fig. II.3d.5 And the thermal decomposition data are presented Table II.3d.5. All the complexes starts decomposing from ambient temperature. There are four stages of decomposition. The first two stages may corresponds to the removal of the intra zeoalite and coordinated water. The total mass loss after the complete decomposition for the Fe(III), Co(II), Ni(II) and Cu(II) complexes are 14.48, 15.92, 16.01 and 19.97% respectively.

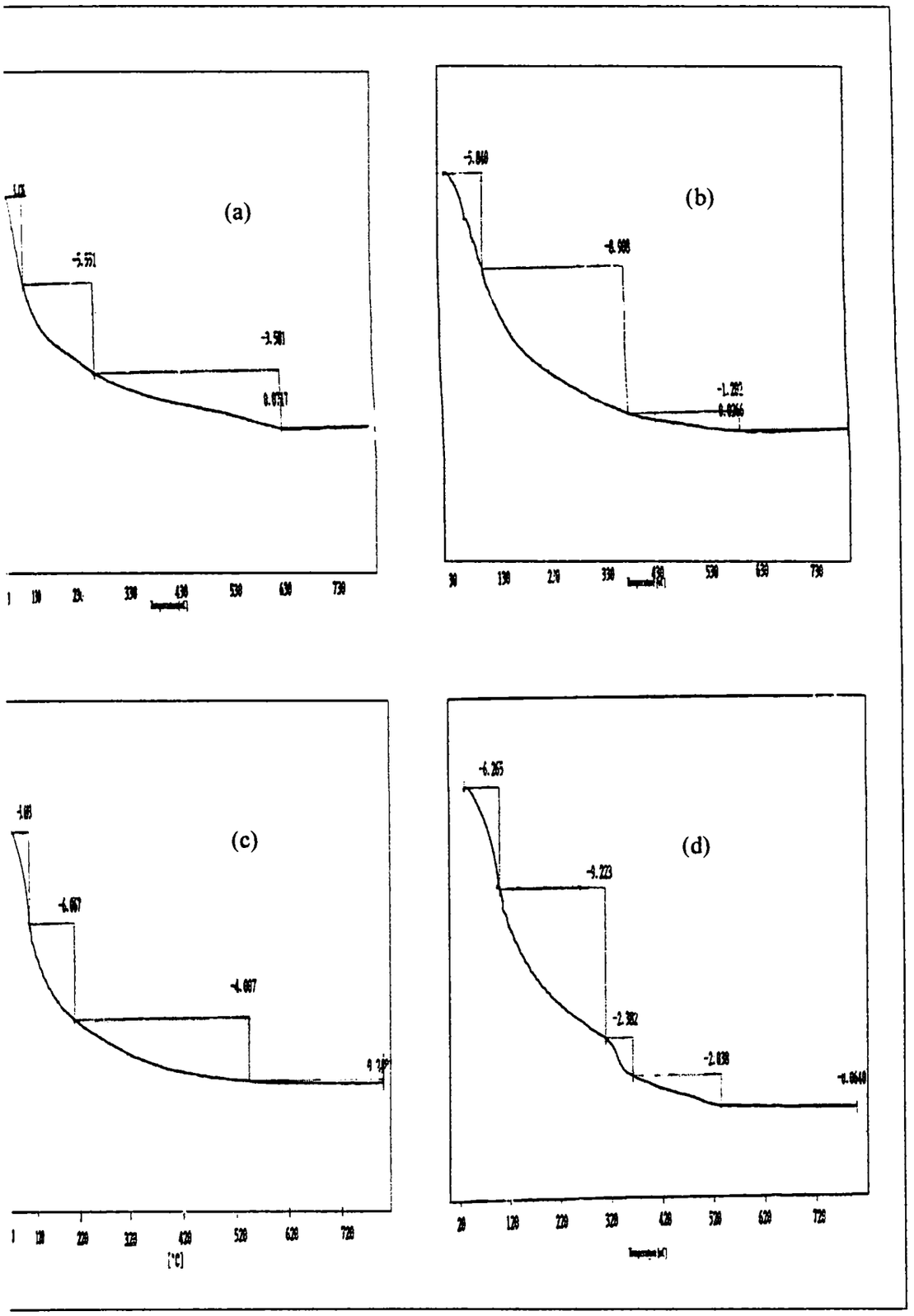

Figure II.3c.5 T.G Curves of (a) Fe(AUAcAcA)Y (b) Co(AUAcAcA)Y
(C) Ni(AUAcAcA)Y (d) Cu(AUAcAcA)Y

Table II.3d.5
TG data for zeolite encapsulated AUAcAcA complexes

Complex	Stability (°C)	Decomposition range	Total weight loss (%)
Fe(AUAcAcA)Y	Ambient	Ambient-105 105-269 269-625 625-798	14.48
Co(AUAcAcA)Y	Ambient	Ambient-105 105-377 377-591 591-799	15.92
Ni(AUAcAcA)Y	Ambient	Ambient-101 101-209 209-543 543-799	16.01
Cu(AUAcAcA)Y	Ambient	Ambient-101 101-308 308-361 361-534 534-799	19.97

References

1. C.Tollman, H.Herron, Symposium on Hydroc. Oxidation, 194th National Meeting of the Am. Chem. Soc, New Orleans, LA, Aug.30-Sept.4 (1987)
2. R.Van Ballmoos, *Collection of simulated XRD powder patterns for zeolites*, Butterworths, London(1984)
3. R. Szostak, *Molecular Sieves :Principles of Synthesis and Identification* (Van Nostrand Reinhold), NewYork (1989) 83
4. G.Meyer, Wohrle.D, M. Mohl, G. Schulz-Ekloff, *Zeolites*, 4(1984)30
5. K.L.N.Phani, S.Pitchumani, S.Ravichandran, *Langmuir*, 9 (1993) 2455
6. K.O.Xavier, J.Chacko, K.K.Mohammed Yusuff, *J. Mol.Catal.A:Chemical*, 178 (2002) 275
7. P.G.menon, *Lectures on Catalysis*, 41st Ann. Meeting, Ind. Acad. Sci (Ed: S.Ramasheshan).,(1975)
8. E.M.Flaningen, H.Khatani, H.A.Szymanski, *Adv. Chem. Ser.*, 101(1971) 201
9. E.M.Flaningen, *Zeolite Chemistry and Catalysis* (Ed:J.A.Rabo), A.C.S.Monograph., 171 (1976) 80
10. N.Herron, *Inorg. Chem.*, 25 (1986) 4714.
11. N.Herron, G.D.Stucky, C.A.Tolman, *J. Chem. Soc, Chem. Commun.*, (1986) 1521.
12. A,Abragam, M.H.L.Pryce, *Proc. Roy. Soc.*, A206, 173 (1951)
13. T.H.Bennur, D. Srinivas, P.Ratnasamy, *Microporous and Mesoporous Materials.*, 48 (2001) 111.
14. S. Seelan, A. K. Sinha, D. Sreenivas. S. Sivasankar, *J. Mol. Catal., A: Chemical*, 157 (2000) 163.

Chapter IV

CATALYSIS BY ZEOLITE ENCAPSULATED METAL COMPLEXES

II.4.1 Introduction

Zeolite encapsulated metal complexes offer several advantages in catalytic reactions due to their ruggedness, protection against deactivation by dimer and cluster formation during catalysis and ease of separation from the reaction products[1]. Applications of such complexes have been reported in reactions like vapour phase carbonylation of methanol or aromatic compounds and hydroformylation reaction using zeolite entrapped Rh/Ir mono and polynuclear carbonyl compounds[2-6] hydrogenation using zeolite encapsulated Pd(Salen)[7], and toluene oxidation using VO(Salen)Y complex[8].

The oxidation of organic compounds is of importance both in synthetic organic chemistry and in large scale industrial production[9-11]. The choice of the oxidants for this purpose has to be based on the environmental protection and energy saving factors. Even though molecular oxygen and air are cheap and environmentally safe, they are not preferred for want of elevated temperature and pressure. On the non-biochemical front, it was reported that controlled partial oxidation is easier to effect with sacrificial oxidants[12], such as hydrogen peroxide[13-15], or alkylhydroperoxides[16,17], than with molecular oxygen or air. These sacrificial oxidants have been used in catalytic systems involving tailored transition-metal complexes or metal substituted polyoxometalates either in a homogeneous state[18], encapsulated in molecular sieves[19-21] or anchored to the inner surfaces of mesoporous silica.

The cyclohexanol oxidation with H_2O_2 using Cu(Salen)Y has been studied and a conversion of 50% with 90% selectivity was reported earlier[22]. Cyclohexanol oxidation is an industrially important reaction. Even though a mixture of cyclohexanone and cyclohexanol is acceptable for nylon production, cyclohexanone is desirable as the sole oxidation product in a variety of fine chemical syntheses[23,24].

Tert-butylhydroperoxide (TBHP) is an environmentally friendly and cheap oxidant[25]. Excellent catalytic conversions were obtained for the epoxidation of olefins and alcohol oxidation using $[Cu(His)_2]Y$ (His=histidine) catalyst at relatively low temperatures in the presence of peroxides[26]. This oxidant is stable upto 75°C and is soluble in organic solvents. It is used as a catalyst in polymerization reactions, to introduce peroxy group into organic molecules and in radical substitution reaction. There are reports on the liquid phase oxidation reaction of ethylbenzene with TBHP as oxidant and chlorobenzene as solvent at 393K[27]. Hence it appears that under certain reaction conditions the stability of the oxidant, TBHP can be increased above the reported 75°C.

During the present study the cyclohexanol oxidation with TBHP in the presence of pure metal complexes of acetylacetone- 2-hydroxyphenylhydrazone (APAcAc), acetoacetanilide- 2-hydroxyphenylhydrazone (APAcAcA) and acetoacetanilide-3,5-dihydro-2,4-dione pyrimidylhydrazone (AUAcAcA) and their zeolite encapsulated analogues was investigated. The results of the present study are given below.

II.4.2 Experimental

II.4.2.1 Materials used

Synthesis and characterization of the pure complexes (part I, chapter II), metal exchanged zeolites (part II, chapter III) and zeolite encapsulated metal complexes (part II, Chapter III) have been described earlier.

II.4.2.2 Experimental set up

The schematic diagram of the experimental set up is given in Fig. II. 4.1.

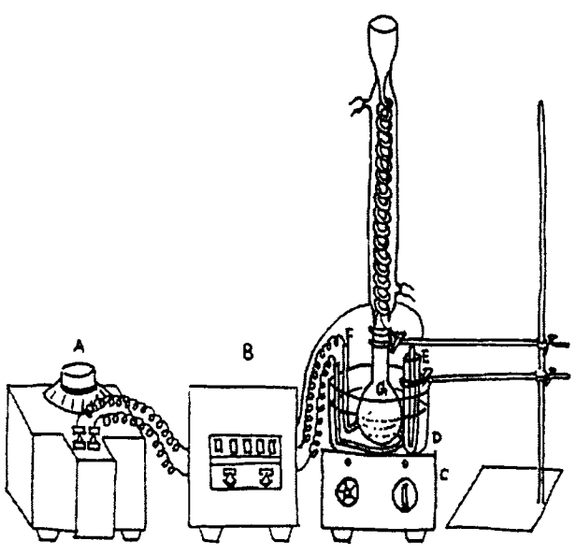

A. Dimmerstat
B. Temperature controller
C. Magnetic stirrer
D. Oil bath
E. Thermocouple
F. Heating element
G. Reaction flask

Figure II.4.1 Experimental set up for Oxidation reaction

The required amount of the substrate was taken in a suitable solvent. Then the specified amount of the catalyst sample as well as the oxidant was added. The reaction mixture was stirred magnetically for the required time. After the experiment, the flask was cooled. The traces of the catalyst were separated by filtration. The product and the unreacted substrate were analyzed using gas chromatograph.

II.4.2.3 Reaction Procedure

The catalytic activity was tested for the liquid phase oxidation reaction of cyclohexanol with 70% TBHP as oxidant and chlorobenzene as solvent at 383K. The reaction was also followed by varying the temperature, solvent and amount of the catalysts. The product formed *viz.* cyclohexanone were analysed by GC employing a carbowax column.

II.4.2.4 Recycling studies

In order to check the leaching of metal ions (under reaction conditions) recycling experiment was carried out on the washed catalyst. The recycle experiment was done as per the following procedure. The catalyst that was separated from the reaction mixture was washed with acetone several times and was dried at 110°C for 6h. The reaction was then carried out using the recycled catalyst.

II.4.3 Results and discussion

Among the zeolite encapsulated metal complexes, the Cu complexes are the most extensively studied and they are the most active catalysts in many organic reactions. Therefore, during the present study Cu(APAcAc)Y was chosen to find the optimum temperature, duration, oxidant-substrate mole ratio, amount of catalyst etc.

II.4.3.1 Choice of solvent

Initially the catalytic activity of Cu(APAcAc)Y was studied in toluene, toluene/water, water, methanol and chlorobenzene with a view to finding out the most suitable solvent. The results are given in Table II.4.1. From the data given in the table, it can be seen that of all the solvents studied chlorobenzene was found to be the most suitable solvent. Therefore, all the further studies were carried out using chlorobenzene as solvent.

Table II.4.1
Activity for cyclohexanol oxidation using Cu(APAcAc)Y in different solvents

Solvent used	Water	Toluene	Toluene/Water	Chlorobenzene	Methanol
Conversion of cyclohexanol (%)	47.17	2.78	0.46	57.78	9.2

Reaction conditions:
Oxidant/Substrate=2; Temperature=90°C; Time=3h; Catalyst amount=0.02g

II.4.3.2 Choice of temperature

In order to find out the optimum temperature for this oxidation reaction, the reaction was performed at 30°, 70°, 90° and 110°C. The results are presented in Table II.4.2

TableII.4.2
Activity for cyclohexanol oxidation using Cu(APAcAc)Y at different temperatures

Temperature (°C)	30	70	90	110
Conversion of cyclohexanol (%)	5.19	32.68	57.78	61.08

Reaction conditions:
Oxidant/Substrate=2; Solvent=chlorobenzene; Time=3h; Catalyst amount=0.02g

The increase of temperature enhanced the conversion upto 110°C. The maximum conversion was found to be at 110°C. However, the temperatures higher than 110°C was not tried as the oxidant will decompose at higher temperatures. So 110°C was chosen as the temperature for all the further studies.

II.4.3.3 Choice of oxidant to substrate mole ratio.

The results for different oxidant/substrate ratio are given in Table II.4.3

TableII.4.3
Cyclohexanol oxidation using Cu(APAcAc)Y at different oxidant/substrate mole ratios

Oxidant/Substrate	0.25	0.50	1	2	3
Conversion of cyclohexanol %	1.74	16.48	23.25	57.78	57.89

Reaction conditions:
Solvent=chlorobenzene; Time=3h; Catalyst amount=0.02g

The conversion was found to increase substantially when the oxidant/substrate ratio was increased from 0.25 to 2. However, there was no significant increase in the conversion when the ratio was increased from 2 to 3. Therefore, the mole ratio 2 was taken as the optimum and this was used for further investigations.

II.4.4 Cyclohexanol oxidation using zeolite Y and metal exchanged zeolites

Under the optimum conditions determined, the catalytic activities of zeolite Y, metal exchanged zeolites, pure metal-hydrazone complexes and the zeolite encapsulated metal-hydrazone complexes were investigated. The results of these studies using zeolite Y and metal exchanged zeolites are given in Table II.4.4. The results are represented as a bar chart in Fig.II.4.2. The results clearly show that the catalytic activity is due to the presence of metal ions inside the cavity as evidenced by the absence of any activity for zeolite Y. Among the metal ions the most active metal ion is Cu eventhough, the other metal ions show considerable activity.

Table II.4.4
Activity for cyclohexanol oxidation using zeolite Y and metal exchanged zeolites

Sample	NaY	FeY	CoY	NiY	CuY
Conversion %	Nil	28.47	39.78	28.89	55.72

Reaction conditions:
Temperature=110°C; Oxidant=1ml; Substrate=0.5ml;
Solvent=chlorobenzene(3.5ml); Time=3h; Catalyst amount=0.03g

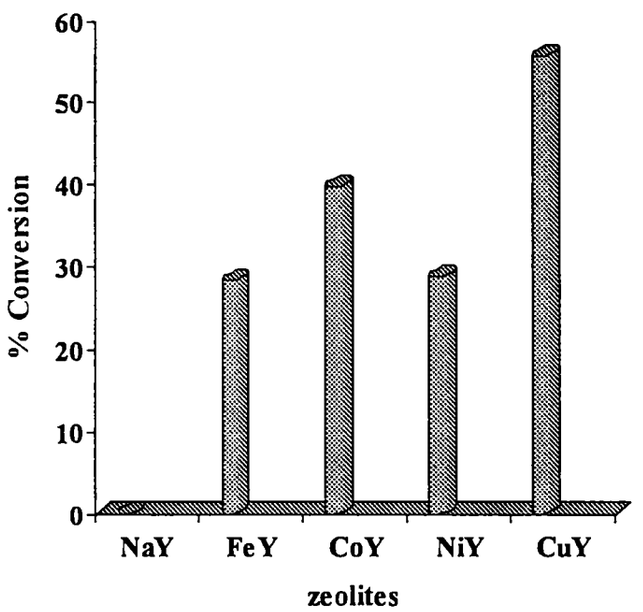

FigureII.4. 2 Cyclohexanol oxidation using metal exchanged zeolite Y

II.4.5 Cyclohexanol oxidation using zeolite encapsulated Fe(III), Co(II), Ni(II) and Cu(II) complexes of APAcAc .

Catalytic activity for the oxidation reaction was determined using the four metal encapsulated complexes with a view to comparing the relative activities of different encapsulated complexes. The results are summarized in Table IV.5.

Table II.4.5
Activities for cyclohexanol oxidation using M(APAcAc)Y complexes

Complex	Fe(APAcAc)Y	Co(APAcAc)Y	Ni(APAcAc)Y	Cu(APAcAc)Y
Conversion %	6.04	57.67	33.27	64.88

Reaction conditions:
Temperature=110°C; Oxidant=1ml; Substrate=0.5ml;
Solvent=chlorobenzene(3.5ml); Time=3h; Catalyst amount=0.03g

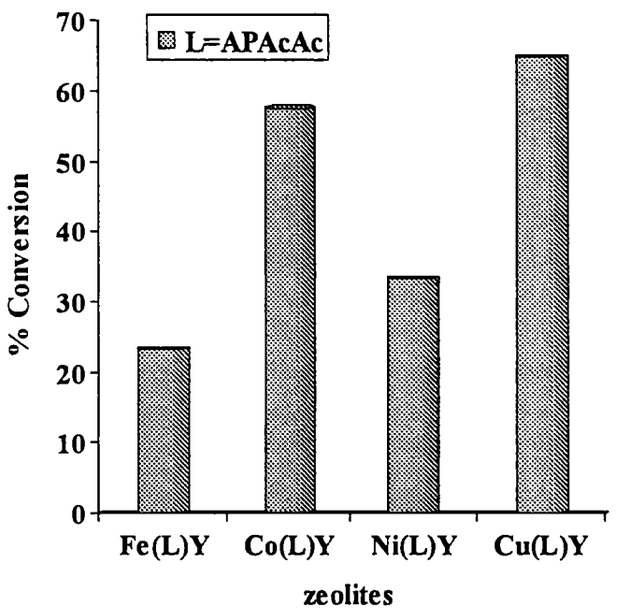

Figure II.4. 3 Cyclohexanol oxidation using zeolite Y encapsulated APAcAc complexes

Among the four complexes investigated, Cu(APAcAc)Y is showing maximum activity. The activities of the other complexes follow the order Co(APAcAc)Y> Ni(APAcAc)Y> Fe(APAcAc)Y. The electronic spectrum and EPR parameters suggest a tetrahedrally distorted square planar geometry for the Cu complex. This change in molecular geometry arising out of encapsulation and the consequent

availability of vacant sites can be the probable cause for the higher catalytic activity of the Cu complex. The Co complex also shows significant activity which can be attributed to some sort of distortion in molecular geometry on encapsulation. The magnetic and electronic properties indicate a tetrahedral structure for the Co(II) complex. The Co(II) tetrahedral complexes may flip over to square pyramidal complexes on interaction with the substrate/ligand which might be the reason for the increased activity. The octahedral symmetry of Ni complex renders them weakly active. Not much increase in the percentage of conversion was observed for the complexes, when compared to the Fe and Ni exchanged zeolites. Significant increase in the conversion rate is seen for Co(II) and Cu(II) complexes.

II.4.6 Cyclohexanol oxidation using zeolite encapsulated Fe(III), Co(II), Ni(II) and Cu(II) complexes of APAcAcA .

The results of the activity studies of the encapsulated APAcAcA complexes are given in Table II.4.6 For these complexes also the activity is higher for Cu(APAcAcA)Y complex. But in the case of Co(II) and Ni(II) complexes, the trend in activities is reversed compared to that of the encapsulated APAcAc complexes. The activity order for this series of complexes is as follows: Cu(APAcAcA)> Ni(APAcAcA)Y>Co(APAcAcA)Y> Fe(APAcAcA)Y. In this case also the higher activity of Cu complex can be attributed to a tetrahedrally distorted square planar geometry. A significantly higher activity of the Ni complex can be due to its tetrahedral structure. The spectral and magnetic properties of this complex clearly indicate a tetrahedral structure. The lower activity of the Co complex is due to its tetrahedral geometry. In this series also the Fe complex is the least active.

TableII.4.6
Activities for cyclohexanol oxidation using M(APAcAcA)Y complexes.

Complex	Fe(APAcAcA)Y	Co(APAcAcA)Y	Ni(APAcAcA)Y	Cu(APAcAcA)Y
Conversion %	23.72	35.38	58.92	60.53

Reaction conditions:
Temperature=110°C; Oxidant=1ml; Substrate=0.5ml;
Solvent=chlorobenzene(3.5ml); Time=3h; Catalyst amount=0.03g

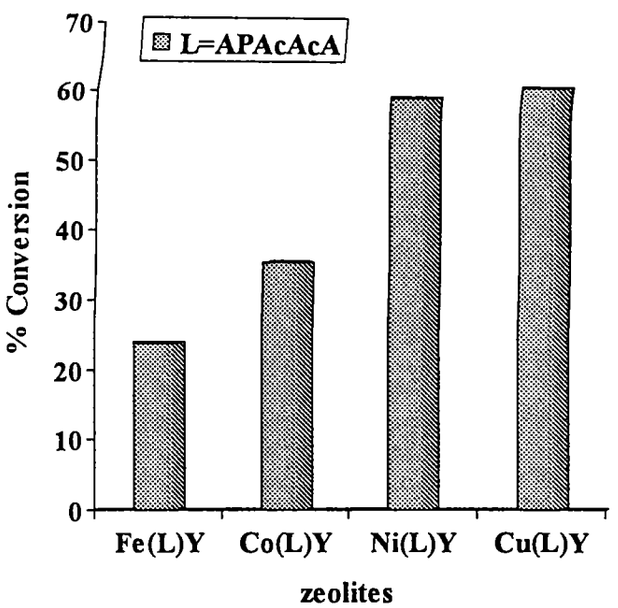

Figure II.4. 4 Cyclohexanol oxidation using zeolite Y encapsulated APAcAcA complexes

II.4.7 Cyclohexanol oxidation using zeolite encapsulated Fe(III), Co(II), Ni(II) and Cu(II) complexes of AUAcAcA .

The activity studies of the encapsulated AUAcAcA complexes were carried out under similar conditions as those used for the other two series. The results of the activity studies of the encapsulated AUAcAcA complexes are given in Table II.4.7.

TableII.4.7
Activities for cyclohexanol oxidation using M(AUAcAcA)Y complexes

Complex	Fe(AUAcAcA)Y	Co(AUAcAcA)Y	Ni(AUAcAcA)Y	Cu(AUAcAcA)Y
Conversion %	30.98	56.73	32.42	64.38

Reaction conditions:
Temperature=110°C; Oxidant=1ml; Substrate=0.5ml;
Solvent=chlorobenzene(3.5ml); Time=3h; Catalyst amount=0.03g

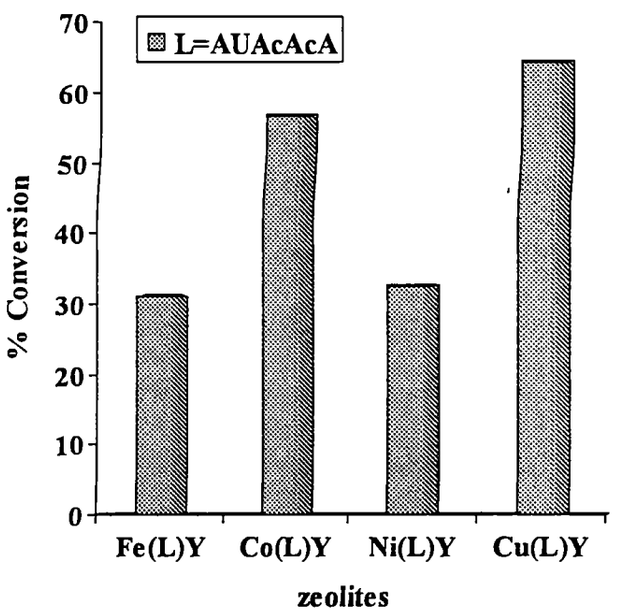

Figure II.4. 5 Cyclohexanol oxidation using zeolite Y encapsulated AUAcAcA complexes

The activity is found to be the maximum for the Cu(AUAcAcA)Y complex. *The trend in the activities for the other complexes is similar to that of APAcAc* complexes in zeolite Y cavity. They follow the order: Cu(AUAcAcA)Y > Co(AUAcAcA)Y > Ni(AUAcAcA)Y > Fe(AUAcAcA)Y. The reason for the

occurrence of this order may be the structural features of these complexes as explained earlier for the APAcAc complexes.

Recycling studies

The recycle experiment was done using Cu(APAcAc)Y complex which showed the maximum activity in all the test reactions. After the reaction, the catalyst was separated from the reaction mixture, washed with acetone several times and was dried at 80°C. The reaction was then carried out using the recycled catalyst. The catalyst thus recycled showed an activity of 38%.

II.4.8 Cyclohexanol oxidation using pure Fe(III), Co(II), Ni(II) and Cu(II) complexes of APAcAc, APAcAcA and AUAcAcA.

To compare the relative activities of the pure complexes and their encapsulated analogues, the oxidation studies were carried out with pure complexes as catalysts under the conditions employed for the encapsulated complexes. The results are presented in the TableII.4.8. It can be seen from the table that for the pure complexes of APAcAc, APAcAcA and AUAcAcA, the activities are negligible except in a few cases. In all the cases Cu(II) complexes show significant activity. Of all the other complexes only the Fe(III) complex of AUAcAcA shows fairly good activity. Eventhough copper(II) and iron(III) has got distorted octahedral symmetry, due to interaction between the metal centres, these interactions may be removed on dissolution resulting in vacant coordination sites. This might be the reason for the increased catalytic activity of these complexes. The increased activities for the encapsulated analogues can be tentatively attributed to a change in geometry of the complexes on encapsulation

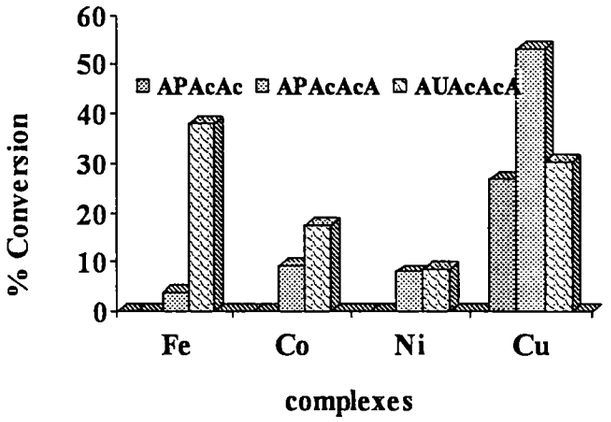

Figure II.4. 6 Cyclohexanol oxidation using pure complexes

Table II.4.8
Activity studies of pure complexes of Fe(III), Co(II), Ni(II) and Cu(II) with APAcAc, APAcAcA, and AUAcAcA

Complex	Conversion %
$Fe(APAcAc)_3$	Negligible
Co(APAcAc)Cl	Negligible
$Ni_2(APAcAc)_3Cl$	Negligible
Cu(APAcAc)Cl	26.79
$Fe(APAcAcA)_3$	4.06
$Co(APAcAcA)_2$	9.41
Ni $(APAcAcA)_2$	8.09
$Cu(APAcAcA)_2$	53.2
Fe(AUAcAcA)ClOH	38.25
Co(AUAcAcA)Cl	17.59
Ni(AUAcAcA)Cl	8.74
Cu(AUAcAcA)Cl	30.37

References:

1. C. Ratnasamy, A. Murugkar, S.Padhye, *Ind. J. Chem.*, 35A (1996) 1
2. P. Gellin, C.Naccache, Y.B.Taarit, *Pure Appl. Chem.*, 8(1988)1315
3. P.A. Jacobs, R. Chantillon, P. Delaet., J. Verdouck, M. Tielen, *ACS Symp. Ser.*, 218 (1983) 439
4. A. Auroux, V. Bolis, P. Wierzchowski, P. Grzvelle, J. Vedrine., *J. Chem. Soc. Faraday Trans.*, (1979)2544
5. M. Iwamoto, H. Kusano, S. Kagawa, *Inorg. Chem.*, 22(1983) 3366
6. E. Mantooani., N. Palldino, A. Zarrobi., *J. Mol. Catal.*, 3 (1977) 285
7. [S. Kowalak., R.C. Weiss, K. Balkus.J.Jr., *J. Chem. Soc. Chem. Commun.*, (1991) 57
8. N. Ulagappan., Proceedings of the 31st annual convention of chemists, Varanasi (1994) F1
9. A.H.Haines, *Methods for the oxidation of organic compounds*, Academic Press, London, Ist part (1985)2nd part (1988)
10. R.A.Sheldon, J.K.Kochi, *Metal-Catalysed oxidation of organic compounds,* Academic Press, Newyork(1981)
11. G.W.Parshall, *Homogeneous Catalysis* Wiley-Interscience, NewYork(1980)
12. J. M. Thomas, R. Raja, G. Sankar, R. G. Bell, *Acc.Chem.Res.*,34 (2001)191-200
13. T. Tatsumi., K. Yanagisawa., K. Asano., M. Nakamura., H. Tominaga., *Zeolites Microporous Crystals.*, 83 (1994) 417
14. J.M. Thomas., *New microcrystalline catalysts. Philos.Trans.R.Soc.*,333 (1990) 173
15. T. Okuhara, N. Mizuno., *Adv.Catal.*, 41 (1996) 113
16. T. Maschmeyer, J.M. Thomas, G. Sankar, R.D. Olyroyd, I.J. Shannon., J.A. Kleptko, A.F. Masters, J.K. Beattle, C.R.A. Catlow, *Angew. Chem., Int. Ed. Engl.*, 36 (1997) 1639
17. J.Y. Wang., G.G. Xia, Y.G. Yin, S.L.O. Suib, *J. Catal.*, 176 (1998) 275
18. T. Hayashi, A. Kishida, N. Mizuno, *Chem.Commun.*, (2000) 381
19. N. Herron., C.A. Tolman., *J.Am.Chem.Soc.*, 109 (1987) 2837
20. R. Raja, P. Ratnasamy, *U.S.Patent.*, 5, 767, 320 (1998)
21. R. Raja, P. Ratnasamy, *Stud. Surf. Sci. Catal.*, (1996)101, 181
22. C. Ratnasamy, A. Murugkar, S. Padhye, *Ind. J. Chem.*, 35A (1996) 1-3
23. *Catalytic oxidation, Principles and Applications*, R.A. Sheldon, R.A. van Santen, Eds, World Scientific Publishing, Singapore (1995)

24. H.H. Szmant., *Organic Building Blocks of the Chemical Industry*, Wiley: NewYork (1989)

25. K.B.Sharpless, T.R.Verhoeven, *Aldrichimica Acta.*, 12 (1979) 63.

26. B. M.Wekhuysen, A. A. Verberchmoes, I..P.Vannijvel, J. A. Pelgrims, P. L. Buskens, P. A. Jacobs, R. A. Schoonheydt, *Angew.Chem.Int.Ed.Engl.*, 34 (1995)23,24

27. A. Sakthivel, S. E. Dapurkar, P. Selvam, *Catalysis Letters*, 77 (2001) 1

SUMMARY AND CONCLUSION

The thesis deals with the synthesis, characterization and catalytic activity studies of some new Fe(III), Co(II), Ni(II) and Cu(II) complexes of hydrazones and their zeolite encapsulated analogues. Hydrazones have diverse applications in biological, non-biological and biochemical front. For convenience, the thesis is divided into two parts. Part I deals with the synthesis of twelve new transition metal complexes and their characterization. Part II contains the method of encapsulation of these complexes in zoelite cavities and their characterization. A comparative account of the catalytic activities of the pure and encapsulated complexes is also given in this part.

Chapter I of part I of the thesis is a general introduction to the chemistry of hydrazones and their metal complexes: Hydrazones have the triatomic grouping C-N=N. It can be considered as Schiff bases derived from acid hydrazides or from a coupled product of a diazonium salt with a reactive methylene group of a β-carbonyl compound. At the end of the chapter, the scope of the present work is given justifying the choice and significance of the work undertaken along with relevant references.

Chapter II of this part presents the details regarding the materials employed for the synthesis of the ligands and their metal complexes. The techniques employed for the characterization of the ligand and metal complexes are also described in this chapter. The hydrazones used in the present study were prepared by diazotising a primary amine and

coupling with compounds containing active methylene group. Primary amines used were *o*-aminophenol and 5-aminouracil. Acetyl acetone and acetoacetanilide are the compounds containing active methylene group. Three ligands have been successfully synthesized namely acetylacetone-2-hydroxyphenylhydrazone (APAcAc), acetoacetanilide-2-hydroxyphenyl hydrazone (APAcAcA) and acetoacetanilide-3,5-dihydro-2,4-dionepyrimidylhydrazone respectively. The purity of the compounds was tested by TLC. They were characterized on the basis of analytical and spectral data. The functional groups in the ligand were identified with the help of FTIR spectra. $^1H_1$ NMR spectra are in conformity with proposed structures. The electron spray mass spectra (ESMS) were taken to show the fragmentation pattern of the ligand. The mass spectra clearly suggest the existence of the ligands in the hydrazone form

Chapter III of Part I of the thesis is on the synthesis and characterization of Fe(III), Co(II), Ni(II) and Cu(II) complexes of APAcAc, APAcAcA and AUAcAc. This chapter is again divided into three parts: Part A, Part B and Part C. Part A deals with the complexes of APAcAc. The complexes are all stable and non-electrolytes in methanol. The molecular formula of the complexes are $Fe(APAcAc)_3$, Co(APAcAc)Cl, $Ni_2(APAcAc)_3Cl$ and Cu(APAcAc)Cl. IR spectral data suggest that APAcAc acts as a monoanionic bidentate ligand coordinating through the phenolic oxygen and the azomethine nitrogen in all the complexes. Magnetic measurement and electronic spectral data indicate octahedral geometry for the Fe(III) and Ni(II) complex, tetrahedral geometry for the Co(II) complex and tetragonally distorted octahedral geometry for the Cu(II) complex. EPR data also favour such a structure for the Cu(II) complex. TG of all

the complexes have been recorded and the TG data suggest the following stability order for the complex $Fe(APAcAc)_3 < Ni_2(APAcAc)_3Cl > Cu(APAcAc)Cl$.

Part B of this chapter is the synthesis and characterization of complexes of APAcAcA. The Fe(III) complex has the molecular formulae $Fe(APAcAcA)_3$ and the Co(II), Ni(II) and Cu(II) complexes have the formula ML_2 (L= APAcAcA). The complexes are all non electrolytes. The APAcAcA acts as monoanionic bidentate ligands coordinating through the carbonyl and nitrogen of the –NH group of the ligand. Magnetic measurement and electronic spectral data are in favour of octahedral structure for the Fe(III) complex, tetragonally distorted octahedral structure for the Cu(II) and tetrahedral structure for the Ni(II) and Co(II) complexes. The complexes are all stable below 200°C. Part C of this chapter deals with the complexes of AUAcAcA. The complexes are stable and nonelectrolytes in methanol. IR spectral data suggest AUAcAcA as a monovalent tridentate ligand co-ordinating through the free carbonyl, the azomethine group and the -NH group of the ligand. From magnetic and electronic spectral data, an octahedral structure can be assumed for the Fe(III) and Co(II) complexes and a distorted tetrahedral structure for Ni(II) complex and a tetrahedrally distorted octahedral structure for the Cu(II) complex. The attainment of octahedral structure for Fe(III) and Co(II) complex may be due to the interaction of two molecular species of the complex. The TG data reveal the following stability order for the complex Fe<Co<Ni>Cu.

Part II of the thesis deals with the zeolite encapsulated Fe(III), Co(II), Ni(II) and Cu(II) complexes of these ligands. This part is divided into four chapters.

Chapter I of this part presents a general discussion on the zeolite encapsulated metal complex system and the catalytic activity of the systems. Chapter II includes details regarding materials used for the synthesis of zeolite encapsulated metal complexes and techniques involving their synthesis and characterization. The zeolite Y having silica alumina ratio of 2.4 and surface area of $546m^2/gm$ was used in the study. Details regarding the technique used for characterization such as AAS, Scanning Electron Micrograph (SEM), Surface area, pore volume, XRD and TG measurements and FTIR, and diffuse reflectance UV-Vis Spectroscopy are presented in this chapter..

Chapter III of this part deals with the synthesis and characterization of zeolite encapsulated Fe(III), Co(II), Ni(II) and Cu(II) complexes of APAcAc, APAcAcA, and AUAcAcA. The complexes were encapsulated in zeolite cages by refluxing the metal exchanged zeolite with the ligand or by heating the exchanged zeolite with ligand in a sealed ampoule. The complexes were purified by Soxhlet extraction and finally exchanged with sodium ions to remove the excess metal ions. The complexes were characterized by using AAS, SEM, XRD, FTIR, and diffuse reflectance UV-Vis Spectroscopy. Scanning electron micrographs of the encapsulated complexes before and after the Soxhlet extraction indicate the absence of surface adsorbed complexes. XRD patterns and silica alumina ratio reveal the retention of zeolite Y framework even after the encapsulation procedures. Lower surface area of the encapsulated complexes compared to that of the corresponding metal exchanged zeolite suggests encapsulation of the metal complexes inside the zeolite cages. FTIR spectra of the encapsulated complexes were compared with the bands of the corresponding complexes to ascertain any change in the coordination behavior. The magnetic and electronic spectra indicate

that all the encapsulated Fe(III) complexes, Ni(APAcAcA)Y and Ni(AUAcAcA)Y have octahedral geometry, Co(APAcAc)Y Co(APAcAcA)Y, Ni(APAcAc)Y, Co(AUAcAcA)Y have tetrahedral geometry and Cu(II) complexes have either tetrahedrally distorted octahedral or flattened tetrahedral geometry.

Chapter IV of Part II describes our studies on the catalytic activity of zeolite Y encapsulated complexes in the oxidation of cylcohexanol with *tert*-butyl hyrdrogen peroxide as the oxidant to cyclohexanone. The reaction was studied in different solvents like water, toluene, chlorobenzene, methanol etc. Chlorobenzene was found to be the most suitable solvent for this oxidation reaction and maximum conversion occurs at 110°C. Zeolite encapsulated copper(II) complex alone have considerable activity towards the cyclohexanol oxidation in all the three series of complexes. Co(II) complex of APAcAc and AUAcAcA shows significant activity while the Ni(II) complex of APAcAc is promising as a heterogeneous catalyst. The activity of the Cu(II) complexes has been attributed to the availability of vacant donor sites and decreased electron density at the metal center due to their tetrahedrally distorted square planar structure. To compare the catalytic activity of the encapsulated complexes with those of the pure complexes, the oxidation of cyclohexanol reaction was studied in presence of pure metal complexes under the same reaction condition employed for the encapsulated complexes. In most of the cases pure complexes of Fe(III), Co(II) and Ni(II) showed negligible activity while Cu(II) complexes show considerable activity.